

AN ABSTRACT OF THE THESIS OF

Robert W. Smith for the degree of Doctor of Philosophy in  
Chemistry presented on 5 October 1989 .

Title: Structure and Properties of New, Complex Copper and Zinc  
Borates

Redacted for Privacy

Abstract approved: \_\_\_\_\_

✓ Douglas A. Keszler \_\_\_\_\_

Eight new complex copper and zinc borates have been prepared and characterized. The alkaline-earth copper borates were identified from analyses of the phase systems  $\text{SrO-CuO-B}_2\text{O}_3$  and  $\text{BaO-CuO-B}_2\text{O}_3$ . The complex zinc borates were identified from efforts to prepare the Zn analog of the compound  $\text{BaCuB}_2\text{O}_5$ . Structural features of these compounds have been determined by X-ray diffraction methods.

The polymorphic compound  $\text{Sr}_2\text{Cu}(\text{BO}_3)_2$  crystallizes in a low-temperature monoclinic structure and a high-temperature orthorhombic form; the transition temperature is  $800^\circ\text{C}$ . The low-temperature  $\alpha$ -form is isostructural to the compound  $\text{Na}_2\text{Cu}(\text{CO}_3)_2$  and the high-temperature  $\beta$ -form is a new type that exhibits the polynuclear unit  $\text{Cu}_2(\text{BO}_3)_4$ . The compound  $\text{Ba}_2\text{Cu}(\text{BO}_3)_2$  is isostructural to  $\beta$ - $\text{Sr}_2\text{Cu}(\text{BO}_3)_2$ . The orthoborate  $\text{SrCu}_2(\text{BO}_3)_2$  crystallizes in a unique

tetragonal structure that exhibits infinite, two-dimensional sheets of edge- and vertex-sharing  $\text{CuO}_4$  rectangles and  $\text{BO}_3$  triangles that are interleaved by Sr atoms. This compound decomposes to finely divided CuO above  $970^\circ\text{C}$ . The magnetic moment is reduced from the expected value by Cu-Cu antiferromagnetic coupling. The acentric pyroborate  $\text{BaCuB}_2\text{O}_5$  crystallizes in a unique monoclinic structure that exhibits infinite, two-dimensional sheets of edge- and vertex-sharing  $\text{CuO}_4$  and  $\text{B}_2\text{O}_5$  groups that are interleaved by Ba atoms. The effect of the orientation of the  $\text{B}_2\text{O}_5$  groups on optical second harmonic generation is discussed.

Efforts to prepare the Zn analog of  $\text{BaCuB}_2\text{O}_5$  resulted in the preparation of the acentric orthoborate  $\text{BaZn}_2(\text{BO}_3)_2$  which crystallizes in an orthorhombic cell. The efficiency of second harmonic generation by this material is discussed. The framework alkali zinc orthoborates  $\text{AZn}_4(\text{BO}_3)_3$  where A = K, Rb, and Cs crystallize in a structure built from vertex-sharing  $\text{ZnO}_4$  and  $\text{BO}_3$  groups; the alkali metals occupy a site in the rectangular channels formed by the framework. Ion-exchange reactions of the K analog are discussed.

The pentaborate  $\text{Ba}_2\text{LiB}_5\text{O}_{10}$  crystallizes in a monoclinic cell exhibiting a unique one-dimensional polyborate anion built from two distinct  $\text{BO}_3$  groups and one distinct  $\text{BO}_4$  group that share vertices.

Structure and Properties of  
New, Complex Copper and Zinc Borates

by

Robert W. Smith

A THESIS

submitted to

Oregon State University

in partial fulfillment of  
the requirements for the  
degree of

Doctor of Philosophy

Completed 5 October 1989

Commencement June 1990

APPROVED:

Redacted for Privacy

\_\_\_\_\_  
Professor of Chemistry in charge of major

Redacted for Privacy

\_\_\_\_\_  
Head of Department of Chemistry

Redacted for Privacy

\_\_\_\_\_  
Dean of Graduate School

Date thesis is presented 5 October 1989

## ACKNOWLEDGEMENTS

Proverbs 15:22 says, "For lack of advice plans go wrong, but with many counsellors they are accomplished." So it is with this work.

For their help, as both friends and colleagues, I am indebted to Hongxing Sun, Paul Thompson, Yaobo Yin, Kathleen Schaffers, Jinfan Huang, Ted Alekel, Jim Cox, and Jeanne Luce who've helped me through the good and the not so good times. Thanks to them, I've never had to go too long without a good laugh.

Additional thanks must go to the inorganic chemistry faculty of Oregon State University, John Yoke, Carroll DeKock, and Jim Kreuger, for the advice and particularly for the excellent instruction they gave to me. It is because of professors such as them that my study of chemistry has been so enjoyable.

Most of all, I must acknowledge the enormous debt I owe to my major professor, Doug Keszler. It has been both an honor and a privilege to work under Doug's supervision. Indeed, I have heard envy expressed from all parts of the Chemistry Department at my good fortune.

For all these people and the good mind, the felicitous circumstances, and the fascinating world that the good Lord has placed before me, I am truly blest.

## CONTRIBUTION OF AUTHORS

Jeanne L. Luce performed the syntheses and ion-exchange experiments described in Chapter 7.

## TABLE OF CONTENTS

CHAPTER 1: INTRODUCTION .....	1
Structural Chemistry of Copper and Zinc Borates .....	4
Solid-State Copper Catalysts .....	8
Phase Diagrams and Synthesis Studies .....	11
Optical Frequency Conversion .....	13
References .....	16
 CHAPTER 2: SYNTHESSES AND CRYSTAL STRUCTURES OF THE $\alpha$ - AND $\beta$ - FORMS OF THE ORTHOBORATE $\text{Sr}_2\text{Cu}(\text{BO}_3)_2$ .....	18
Abstract .....	19
Introduction .....	20
Experimental .....	21
Results .....	26
Discussion .....	38
Acknowledgements .....	41
References .....	42
 CHAPTER 3: STRUCTURE OF $\text{Ba}_2\text{Cu}(\text{BO}_3)_2$ .....	44
Abstract .....	45
Introduction .....	46
Experimental .....	47
Discussion .....	50
Acknowledgements .....	56
References .....	57
 CHAPTER 4: SYNTHESIS, STRUCTURE, AND PROPERTIES OF THE ORTHOBORATE $\text{SrCu}_2(\text{BO}_3)_2$ .....	58
Abstract .....	59
Introduction .....	60
Experimental .....	61
Results and Discussion .....	65
Acknowledgements .....	75
References .....	76
 CHAPTER 5: SYNTHESIS, STRUCTURE, AND PROPERTIES OF THE ACENTRIC PYROBORATE $\text{BaCuB}_2\text{O}_5$ .....	77
Abstract .....	78
Introduction .....	79
Experimental .....	80
Results .....	85
Discussion .....	94
Acknowledgements .....	97
References .....	98
 CHAPTER 6: SYNTHESIS, STRUCTURE, AND PROPERTIES OF THE ACENTRIC ORTHOBORATE $\text{BaZn}_2(\text{BO}_3)_2$ .....	100
Abstract .....	101
Introduction .....	102

Experimental .....	103
Results .....	108
Discussion .....	117
Acknowledgements .....	122
References .....	123
CHAPTER 7: THE FRAMEWORK ALKALI ZINC ORTHOBORATES	
AZn <sub>4</sub> (BO <sub>3</sub> ) <sub>3</sub> , A = K, Rb, and Cs .....	124
Abstract .....	125
Introduction .....	126
Experimental .....	127
Results and Discussion .....	130
Acknowledgements .....	144
References .....	145
CHAPTER 8: THE PENTABORATE Ba <sub>2</sub> LiB <sub>5</sub> O <sub>10</sub> .....	
Abstract .....	147
Introduction .....	148
Experimental .....	149
Discussion .....	152
Acknowledgements .....	159
References .....	160
BIBLIOGRAPHY .....	161
APPENDIX A: MOLECULAR ORBITALS OF THE ORTHOBORATE AND PYROBORATE ANIONS .....	
	166

## LIST OF FIGURES

<u>Figure</u>	<u>page</u>
1.1 Borate groups.	5
1.2 Phase diagrams of Sr-Cu-B-O and Ba-Cu-B-O.	12
2.1 Sketch of the unit cell of the structure of $\alpha$ - $\text{Sr}_2\text{Cu}(\text{BO}_3)_2$ viewed down the $\underline{b}$ axis.	29
2.2 Sketches of the copper borate network in $\alpha$ - $\text{Sr}_2\text{Cu}(\text{BO}_3)_2$ .	30
2.3 Sketch of the unit cell of $\beta$ - $\text{Sr}_2\text{Cu}(\text{BO}_3)_2$ viewed down the $\underline{a}$ axis.	34
2.4 Sketches of the $\text{Cu}_2(\text{BO}_3)_4$ unit in $\beta$ - $\text{Sr}_2\text{Cu}(\text{BO}_3)_2$ .	36
2.5 Sketches of the Sr environments for $\beta$ - $\text{Sr}_2\text{Cu}(\text{BO}_3)_2$ .	37
3.1 Labeled sketch of the unit cell for $\text{Ba}_2\text{Cu}(\text{BO}_3)_2$ .	51
3.2 Sketches of the $\text{Cu}_2(\text{BO}_3)_4$ unit.	53
3.3 Sketches of Ba environments in $\text{Ba}_2\text{Cu}(\text{BO}_3)_2$ .	55
4.1 Sketch of the unit cell viewed down [001].	68
4.2 Sketch of the unit cell viewed down $\langle 100 \rangle$ .	69
4.3 Sketch of a portion of the infinite Cu-B-O network parallel to the (001) plane.	70
4.4 Sr environment in $\text{SrCu}_2(\text{BO}_3)_2$ .	72
5.1 Schematic diagram of the apparatus used for SHG measurements.	84
5.2 Labeled sketch of the unit cell viewed along the $\underline{c}$ axis.	88
5.3 Sketch of a portion of the Cu-B-O network viewed along the $\underline{c}$ axis.	89
5.4 Sketches of the $\text{CuO}_4$ and $\text{B}_2\text{O}_5$ groups.	91
5.5 Coordination environment of Ba.	92
6.1 Schematic diagram of the apparatus used for SHG measurements.	107
6.2 Labeled sketch of the unit cell viewed along the $\underline{c}$ axis.	111
6.3 Sketch of a portion of the zinc borate network viewed along the $\underline{a}$ axis.	112

6.4	One-dimensional zinc oxide sublattice viewed along the $\underline{b}$ axis.	113
6.5	Sketches of six-membered $\text{Zn}_2\text{BO}_8$ ring and eight-membered $\text{Zn}_2\text{B}_2\text{O}_9$ ring.	114
6.6	Coordination environment of the Ba atom.	116
6.7	A single $\text{BO}_3$ group in a cartesian coordinate system.	119
6.8	Two sets of $\text{BO}_3$ groups in the compound $\text{BaZn}_2(\text{BO}_3)_2$ .	120
7.1	Labeled sketch of the unit cell of $\text{KZn}_4(\text{BO}_3)_3$ viewed along the $\underline{b}$ axis.	133
7.2	Sketch of the vertex-sharing $\text{ZnO}_4$ band extending in the $\underline{b}$ - $\underline{c}$ plane.	134
7.3	Sketch of the zinc borate network viewed along the $\underline{b}$ axis.	135
7.4	Coordination environment of K.	137
8.1	Drawing of the structure of $\text{Ba}_2\text{LiB}_5\text{O}_{10}$ .	153
8.2	Double strands of $\text{BO}_3$ and $\text{BO}_4$ groups in the anion $[\text{B}_5\text{O}_{10}]^{5-}$ .	154
8.3	The polyanion $[\text{B}_5\text{O}_{10}]^{5-}$ bridged by Li atoms.	155
A.1	Energy level diagram for the orthoborate anion.	168
A.2	Correlation diagram of selected MO's between $D_{2h}$ , $C_{2v}$ , and $C_2$ $[\text{B}_2\text{O}_5]^{4-}$ geometries.	172
A.3	Sketches of idealized $\pi$ system MO's in $C_{2v}$ and $C_2$ symmetry.	173

## LIST OF TABLES

<u>Table</u>	<u>page</u>
2.1 Crystal data and experimental conditions for $\alpha$ - and $\beta$ - $\text{Sr}_2\text{Cu}(\text{BO}_3)_2$ .	24
2.2 Final atomic coordinates and temperature factors for $\alpha$ - $\text{Sr}_2\text{Cu}(\text{BO}_3)_2$ .	27
2.3 Selected distances (Å) and angles (°) for $\alpha$ - $\text{Sr}_2\text{Cu}(\text{BO}_3)_2$ .	28
2.4 Final atomic coordinates and temperature factors for $\beta$ - $\text{Sr}_2\text{Cu}(\text{BO}_3)_2$ .	32
2.5 Selected distances (Å) and angles (°) for $\beta$ - $\text{Sr}_2\text{Cu}(\text{BO}_3)_2$ .	33
3.1 Final atomic coordinates for $\text{Ba}_2\text{Cu}(\text{BO}_3)_2$ .	48
3.2 Selected distances (Å) and angles (°) for $\text{Ba}_2\text{Cu}(\text{BO}_3)_2$ .	50
4.1 Crystal data and experimental conditions for $\text{SrCu}_2(\text{BO}_3)_2$ .	63
4.2 Final atomic coordinates and temperature factors for $\text{SrCu}_2(\text{BO}_3)_2$ .	66
4.3 Selected distances (Å) and angles (°) for $\text{SrCu}_2(\text{BO}_3)_2$ .	67
5.1 Crystal data and experimental conditions for $\text{BaCuB}_2\text{O}_5$ .	82
5.2 Final atomic coordinates and temperature factors for $\text{BaCuB}_2\text{O}_5$ .	86
5.3 Selected distances (Å) and angles (°) for $\text{BaCuB}_2\text{O}_5$ .	87
6.1 Crystal data and experimental conditions for $\text{BaZn}_2(\text{BO}_3)_2$ .	105
6.2 Final atomic coordinates and temperature factors for $\text{BaZn}_2(\text{BO}_3)_2$ .	109
6.3 Selected distances (Å) and angles (°) for $\text{BaZn}_2(\text{BO}_3)_2$ .	110
7.1 Crystal data for $\text{KZn}_4(\text{BO}_3)_3$ .	131
7.2 Selected distances (Å) and angles (°) for $\text{KZn}_4(\text{BO}_3)_3$ .	132
7.3 Oxygen centered angles (°) for $\text{KZn}_4(\text{BO}_3)_3$ .	136
7.4 Crystal data for $\text{RbZn}_4(\text{BO}_3)_3$ .	139
7.5 Selected distances (Å) and angles (°) for $\text{RbZn}_4(\text{BO}_3)_3$ .	140
7.6 Cell parameters refined from powder data.	142
8.1 Crystal data for $\text{Ba}_2\text{LiB}_5\text{O}_{10}$ .	151

8.2	Selected distances (Å) and angles (°) for Ba <sub>2</sub> LiB <sub>5</sub> O <sub>10</sub> .	156
A.1	Extended Hückel parameters.	167
A.2	Molecular orbital energies (eV).	167

# STRUCTURE AND PROPERTIES OF NEW, COMPLEX COPPER AND ZINC BORATES

## CHAPTER 1

### INTRODUCTION

Inorganic solid-state compounds containing copper have a wide range of useful chemical and physical properties. These include both solid-state copper catalysts and the recently discovered high  $T_c$  superconductors. Among the former materials are a  $\text{CuO/ZnO/Al}_2\text{O}_3$  catalyst used in the production of methanol from synthesis gas (1), copper metal used in the hydration of acrylonitrile to acrylamide (2), and  $\text{Cu}_2\text{Al}_6\text{B}_4\text{O}_{17}$  used in the oxidative dehydrogenation of a variety of organic substrates (3). Among the latter compounds are  $\text{Sr}_x\text{La}_{2-x}\text{CuO}_4$  ( $x \approx 0.15$ ) (4),  $\text{Ba}_2\text{YCu}_3\text{O}_7$  (5), and  $\text{Ba}_2\text{Tl}_2\text{Ca}_{n-1}\text{Cu}_n\text{O}_{2n+4}$  ( $n = 1-3$ ) (6,7,8) which have superconducting transition temperatures ( $T_c$ ) of up to 122 K.

Inorganic borates comprise another family of compounds whose utility is indicated by their large number of applications. For example, alkali borates are used extensively as cleansing agents, zinc borates are added to various paints as antifungal and anti-corrosive agents, and borosilicate glass (Pyrex) is familiar to every freshman chemistry student.

Viewed from the structural aspects of their chemistry, complex

copper borates containing alkali or alkaline-earth ions present potentially unique structural types because of the nature of the chemical bonding of the  $\text{Cu}^{2+}$  ion. Its  $d^9$  electron configuration makes it susceptible to Jahn-Teller effects that result in tetragonally distorted octahedra or square-planar geometries where the distortion is severe. The structures of borates include triangular planar or tetrahedral orthoborate anions, double-triangular pyroborate anions, and a wide range of condensed borate chains, rings, and networks. Group IA and IIA metals also exist in varied coordination environments, ranging from four- to ten-coordinate sites. Thus, incorporation of alkali- or alkaline-earth-centered polyhedra into matrices containing  $\text{Cu}^{2+}$  cations and various borate anions should produce a host of materials with new and unique structural features.

There are few reports of complex copper borates, and transition-metal borates in general. Among alkali copper borates only the lithium compounds  $\text{Li}_2\text{CuB}_4\text{O}_8$ ,  $\text{Li}_4\text{Cu}(\text{BO}_3)_2$ , and  $\text{Li}_2\text{Cu}_2(\text{BO}_3)_2$  (9) are known. No alkaline-earth copper borate has been reported prior to this work.

Because of the catalytic ability of copper compounds, the potential for finding new and unique structural types, and the underdeveloped state of complex copper borate chemistry, I have elected to synthesize and characterize new alkaline-earth copper borates. The phase studies that I describe here should also be useful for those researchers examining the use of borate fluxes for the crystal growth of the high  $T_c$  superconducting copper oxides.

From consideration of the structural characteristics of some of the new compounds that were discovered in the course of this work, additional derivatives were proposed to exist. For example, the  $\text{Cu}^{2+}$  site in the compound  $\text{BaCuB}_2\text{O}_5$  exhibits a tetrahedral distortion. It seemed likely that a derivative with a  $\text{Zn}^{2+}$  ion substituted for the  $\text{Cu}^{2+}$  ion could be prepared. From attempts to prepare such derivatives, four new alkali and alkaline-earth zinc borates were discovered; their structures and properties have been investigated.

In this chapter, I present additional general background on the characteristics of relevant copper and zinc borates. In Chapter 2, I describe the syntheses, structures, and phase transition of the polymorphic compound,  $\text{Sr}_2\text{Cu}(\text{BO}_3)_2$ . In Chapter 3, I describe the structure of the compound  $\text{Ba}_2\text{Cu}(\text{BO}_3)_2$  which is isostructural to the high temperature,  $\beta$ -form of  $\text{Sr}_2\text{Cu}(\text{BO}_3)_2$ . In Chapter 4, the synthesis, structure, and physical properties of the new orthoborate  $\text{SrCu}_2(\text{BO}_3)_2$  are presented. In Chapters 5 and 6, I describe the synthesis, structure, and optical properties of the new pyroborate  $\text{BaCuB}_2\text{O}_5$  and the new orthoborate  $\text{BaZn}_2(\text{BO}_3)_2$ , respectively. In Chapter 7, I describe the syntheses, structures, and properties of the new family of alkali zinc orthoborates  $\text{AZn}_4(\text{BO}_3)_3$ ,  $\text{A} = \text{K}, \text{Rb},$  and  $\text{Cs}$ . In Chapter 8, I discuss the structure of the polyborate  $\text{Ba}_2\text{LiB}_5\text{O}_{10}$ . In the appendix, I present molecular orbital diagrams for the orthoborate anion and various geometries of the pyroborate anion,  $[\text{B}_2\text{O}_5]^{4-}$ .

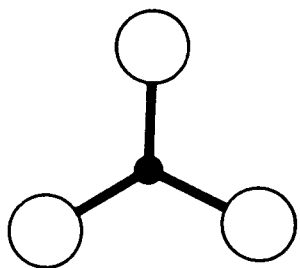
## Structural Chemistry of Copper and Zinc Borates

Copper and zinc borates occur in a wide range of three-dimensional structures that typify the diversity of borate chemistry in general. While borate structural types have been reviewed elsewhere (10), it is useful to illustrate a few copper and zinc borates to explain the factors that control the structural features of these compounds and to explain how these factors may be manipulated.

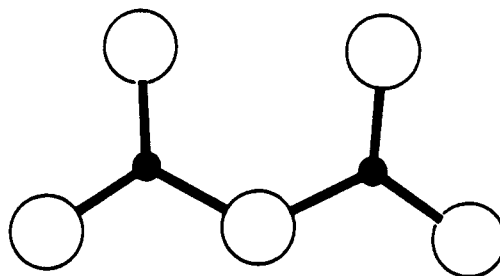
The formula  $\text{Cu}_3\text{B}_2\text{O}_6$  suggests that it is a simple orthoborate exhibiting the trigonal  $[\text{BO}_3]^{3-}$  anion shown in Figure 1.1a. However, its formula is more descriptively written as  $\text{Cu}_{15}[(\text{B}_2\text{O}_5)_2(\text{BO}_3)_6\text{O}_2]$ , the anions being two pyroborate groups (Figure 1.1b), six orthoborate groups, and two oxide anions (11). The structure is built from B atoms in triangular planes and Cu atoms in rectangular planes of O atoms. Some of the  $\text{BO}_3$  groups condense into  $\text{B}_2\text{O}_5$  groups through shared O vertices and some of the Cu atoms have one or two long Cu-O bonds that afford either square-pyramidal or tetragonally distorted octahedral geometries. All borate anions are isolated from each other by the intervening Cu polyhedra.

The other compound reported in the  $\text{CuO-B}_2\text{O}_3$  binary system is the metaborate  $\text{CuB}_2\text{O}_4$  (12). Its structural features include  $\text{CuO}_4$  squares and  $\text{B}_3\text{O}_9$  rings; the metaborate ring consists of vertex-sharing  $\text{BO}_4$  tetrahedra (Figure 1.1c). Each of the six peripheral O atoms of the ring shares a vertex with another ring to afford the network  $\frac{3}{2}[\text{B}_3\text{O}_6]^{3-}$ . Cu atoms occupy fourfold positions in channels created by the borate network. The metaborate anion of  $\text{CuB}_2\text{O}_4$  may be

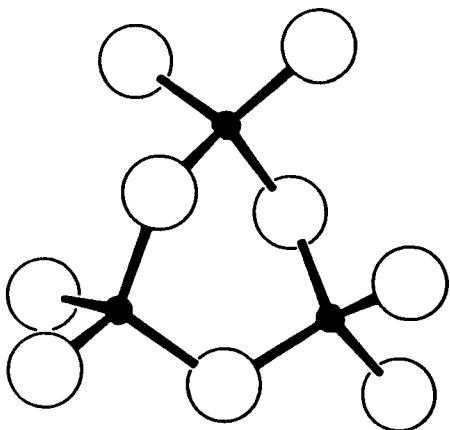
a)



b)



c)



d)

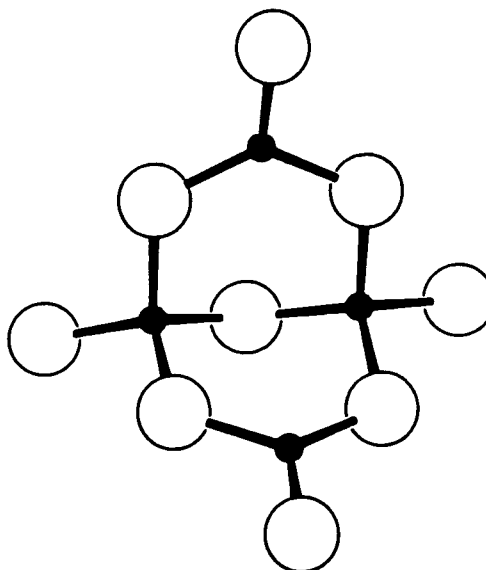


Figure 1.1 Borate groups.

a) orthoborate    b) pyroborate    c) metaborate ring    d) tetraborate

compared to other metaborate anions of formula  $[\text{BO}_2]_n^{n-}$ . Most metaborates form with discrete  $[\text{B}_3\text{O}_6]^{3-}$  rings composed of condensed  $\text{BO}_3$  triangles or as infinite one-dimensional chains of vertex-sharing  $\text{BO}_3$  groups. Thus, structural information of the borate anion cannot be obtained from knowledge of the formula alone.

Polyborates exist as various chains, rings, or three-dimensional frameworks of  $\text{BO}_4$  tetrahedra or  $\text{BO}_4$  and  $\text{BO}_3$  polyhedra fused by sharing O vertices. The tetraborate  $\text{ZnB}_4\text{O}_7$  is such a compound (13). It is composed of  $\text{BO}_4$ ,  $\text{BO}_3$ , and  $\text{ZnO}_4$  polyhedra linked through O vertices into a three-dimensional network. The  ${}^3[\text{B}_4\text{O}_7]^{2-}$  anion is comprised of two  $\text{BO}_3$  triangles and two  $\text{BO}_4$  tetrahedra (Figure 1.1d). Neighboring units are connected through the terminal O atom of a  $\text{BO}_3$  triangle to a terminal O atom of a  $\text{BO}_4$  tetrahedron. Several divalent metals may be substituted into this network, including Mg, Mn, Fe, and Cd. Another  $[\text{B}_4\text{O}_7]^{2-}$  anion consists solely of  $\text{BO}_4$  tetrahedra linked into a three-dimensional framework. Atoms Sr and Pb form compounds with this type of anion (14,15).

Finally, simple orthoborates such as  $\text{Zn}_3(\text{BO}_3)_2$  are very common. This compound has a unique structure comprised of edge- and vertex-sharing  $\text{ZnO}_4$  tetrahedra and  $\text{BO}_3$  triangles (16,17).

The type of borate anion that forms is primarily a function of the electron density that is available to support the  $\pi$ -electron system of the orthoborate anion,  $[\text{BO}_3]^{3-}$ . In compounds with a higher ratio of Lewis base to the Lewis acid boron, the simple orthoborate anion,  $[\text{BO}_3]^{3-}$  will form. This is seen in  $\text{Zn}_3(\text{BO}_3)_2$  where electron density is donated by the Zn atom. In contrast,  $\text{ZnB}_4\text{O}_7$  is boron-

rich, less electron density is available to support the  $\pi$ -system, and half the boron exists in a tetrahedral environment. Consequently, the structural features of borates may be controlled to a large extent by the stoichiometry and nature of the associated cations. The compounds described in this work contain simple orthoborate or condensed pyroborate anions because of the electropositive nature of the alkali and alkaline-earth metals that coordinate to the borate groups. The exception is the boron-rich pentaborate  $\text{Ba}_2\text{LiB}_5\text{O}_{10}$  in which one quarter of the B atoms occupy tetrahedra.

## Solid-State Copper Catalysts

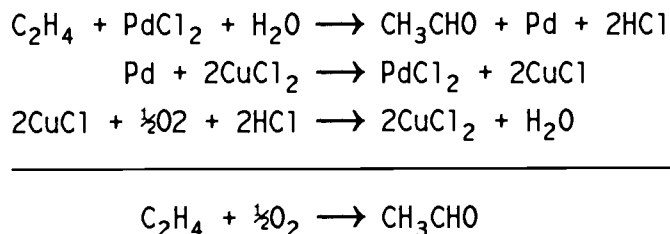
Copper is the active ingredient in several catalysts involving heterogeneous, homogeneous, gas phase, and solution reactions. The properties of some copper catalysts have been reviewed (18). Some examples of solid-state copper catalysts in heterogeneous and homogeneous reactions follow.

1) A  $\text{CuO/ZnO/Al}_2\text{O}_3$  catalyst is used in the low-temperature production of methanol from synthesis gas containing carbon monoxide, carbon dioxide, and dihydrogen. Methanol is used primarily in the production of formaldehyde and in feed stocks or fuels. Prior to the development of the copper-based catalysts, iron and chromium oxides were used, though the latter required more extreme reaction conditions because of their poor activity.

2) Chrysanthemate esters are produced from the cyclopropanation reaction of alkyldiazoacetates with 2,5-dimethyl-2,4-hexadiene in the presence of a copper bronze (19); these esters are potent pesticides. The copper bronze catalyst allows production of the esters in a continuous process that minimizes exposure of workers to the explosive diazoacetate intermediate.

3) Ethylene is oxidized to acetaldehyde in the Wacker process with the reagents  $\text{PdCl}_2$  and  $\text{CuCl}_2$ . This process replaced various other inefficient methods in the early 1960's, only a few years after its initial development.  $\text{PdCl}_2$  is the active ingredient in the catalyst, oxidizing ethylene in the initial reaction to form acetaldehyde and is reoxidized by the  $\text{CuCl}_2$  which is itself reoxidized by

dioxygen (see below).



The ability of the Cu species to oxidize the reactants and then be reoxidized itself by  $\text{O}_2$  is important in each of the processes described above.  $\text{Cu}^{2+}$  is most likely the oxidant in reactions involving copper catalysis. The standard reduction potentials of  $\text{Cu}^{2+}$  to  $\text{Cu}^+$  and  $\text{Cu}^+$  to Cu are 0.158 V and 0.522 V, respectively. This allows for facile redox reactions as in the Wacker process where the oxidant is a metal cation and  $\text{O}_2$  is merely present to reoxidize the  $\text{Cu}^+$  cation.

Two important characteristics of heterogeneous copper catalysis are the dispersion of the active site and the choice of the support. The former property is achieved by maximizing the surface area of the active component of the catalyst. Copper catalysts are commonly obtained by coprecipitation of suitable compounds, impregnation of a support with the active component, sol-gel techniques, or thermal treatment of a precursor. Each of the above treatments is designed to produce finely divided copper species, having particle sizes of approximately 50 nm. Surface areas of these catalysts in industrial applications typically range from 80-120  $\text{m}^2/\text{g}$  of Cu. Methanol synthesis catalysts, for example, are produced in their simplest form by coprecipitation of copper, zinc, and aluminum nitrates by sodium

carbonate followed by filtration, washing, drying, and calcination (20).

Supported catalysts are usually preferable over pure catalysts because of the mechanical properties they give the catalyst and the greater chemical activity they produce. Porosity, thermal stability, heat transfer ability, and mechanical strength are among the factors considered in choosing a support. A review of support properties has been given elsewhere (21).

One avenue of research in developing new catalysts is to combine in a single compound the active properties of the copper metal with the mechanical properties of an appropriate support. Through incongruent decomposition of the material both the active component and the support may be processed in a single step. Combining CuO with a basic alkaline earth oxide and acidic  $B_2O_3$  will leave CuO in an alkaline earth borate matrix upon decomposition. The acidity of the matrix can be controlled by either changing the stoichiometry of the complex copper borate or incorporating another acidic oxide such as  $Al_2O_3$  by synthesis of new materials. Incorporation of acidic oxides could enhance the incongruity to afford lower decomposition temperatures. Borates themselves may provide activity in addition to that of the Cu component. For example, supported  $Li_2B_4O_7$  has been reported to catalyze the production of ethane and ethylene from methane in the presence of dioxygen (22).

As a first step in studying the physical and chemical properties of these types of compounds the systems A-Cu-B-O, A = Ca, Sr, and Ba, have been investigated.

## Phase Diagrams and Synthesis Studies

The phase diagrams of the systems Ca-Cu-B-O, Sr-Cu-B-O, and Ba-Cu-B-O were fully investigated. Typically, a reaction mixture of the copper and alkaline earth nitrates and  $B_2O_3$  were ground together and then heated at  $600^\circ\text{C}$  to decompose the nitrates. Following a final sintering at  $800^\circ\text{C}$  for 18 hours the samples were analyzed by powder X-ray diffraction. New phases were identified from diffraction peaks that were not attributable to a known compound. The phase diagrams of the Sr-Cu-B-O and Ba-Cu-B-O systems are shown in Figure 1.2. No new compounds were identified in the system Ca-Cu-B-O.

Single crystals of new phases were obtained either by flux methods or from the melt. Generally, crystal growth from the melt is the preferred method because no potential impurities are introduced as is the case with the flux technique. However, if the compound melts incongruently or undergoes a phase transition the flux method is necessary. Thus, differential thermal analysis, to determine the melting characteristics, generally follows the identification of a new compound or phase. If a flux is used to grow single crystals, desirable features of the flux include 1) a melting point in the proper range, 2) an anion that is common to the solute and a cation that will not substitute into the lattice, and 3) solubility properties that are different from the solute, allowing the flux to be washed away without damaging the crystals.

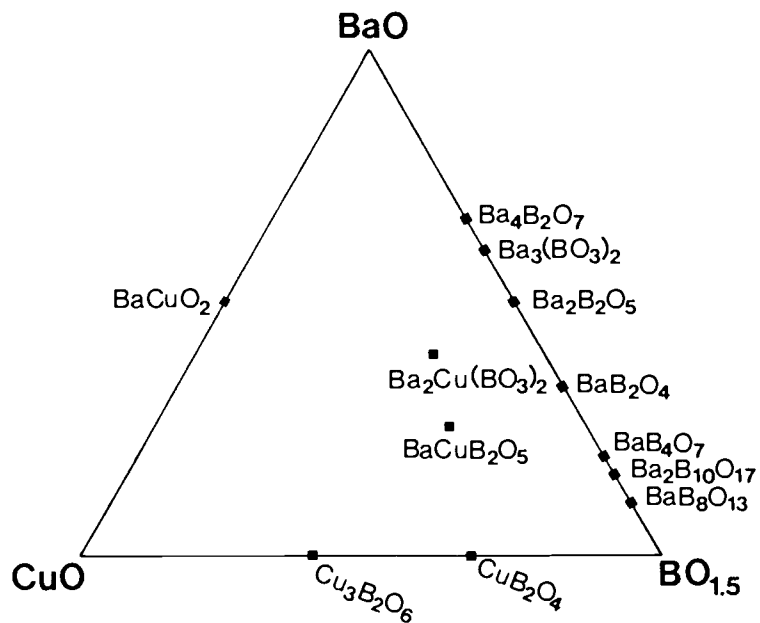
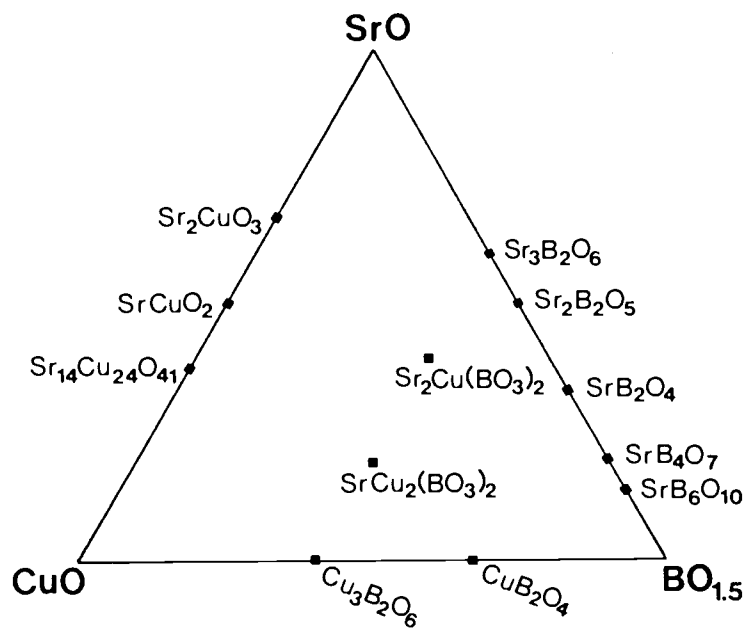


Figure 1.2 Phase diagrams of Sr-Cu-B-O and Ba-Cu-B-O.

## Optical Frequency Conversion

Interest in optical frequency conversion has grown tremendously in the past few years because of the need to tailor laser frequencies to specific values for specialized applications. They are especially useful for converting lasers with output in the infrared region, such as Nd<sup>3+</sup>:YAG, to frequencies in the visible or ultraviolet regions. Two borates have recently been developed with important capabilities as frequency converters. The borate  $\beta$ -BaB<sub>2</sub>O<sub>4</sub> (BBO) exhibits a wide transparency region and high birefringence that allow the production of the fifth harmonic of the Nd<sup>3+</sup>:YAG laser (23). The compound LiB<sub>3</sub>O<sub>5</sub> (LBO) exhibits a threshold for 50% power conversion that is nearly two orders of magnitude lower than that of the frequency converter KH<sub>2</sub>PO<sub>4</sub> (KDP) and an optical damage threshold that is the highest among all solid-state converters reported to date (24).

A review of optical frequency conversion has recently been published by Williams (25). Optical frequency conversion, or harmonic generation, occurs when an electromagnetic field induces a nonlinear polarization in a molecule or solid. In certain materials the induced polarization affords large nonlinear responses to the applied field. Equation [1]

$$P = \chi^{(1)}E + \chi^{(2)}E^2 + \chi^{(3)}E^3 + \dots \quad [1]$$

represents the polarization (P) of a material from the applied electric field (E); the coefficients  $\chi$  define the degree of the non-

linearity. Second harmonic generation (SHG) is illustrated by the second order polarization induced by an electric field that varies with time,  $E = E_0 \cos(\omega t)$ . Examination of the second order term upon substitution of  $E$  into Equation [1] results in Equation [2].

$$\begin{aligned}\chi^{(2)}E^2 &= \chi^{(2)}E_0^2 \cos^2(\omega t) \\ &= \frac{1}{2}\chi^{(2)}E_0^2 [1 + \cos(2\omega t)]\end{aligned}\quad [2]$$

Thus, for a  $\chi^{(2)} \neq 0$ , interaction of a photon with a nonlinear material can produce a photon with twice the frequency. It should be noted that centrosymmetric materials have  $\chi^{(2)} \equiv 0$  since every molecular contribution to  $\chi^{(2)}$  will have a corresponding contribution of opposite sign arising from arrangements related by the center of symmetry. Therefore, only an acentric material will afford SHG.

From the Anionic Group Theory (26) one predicts that the nature and arrangement of polyanions in a solid will control the SHG properties of a material because of the relevant electronic transitions associated with these groups. Examination of the structure of  $\text{BaCuB}_2\text{O}_5$  revealed characteristics suited for good SHG properties. The pyroborate anions in this compound are oriented such that polarization of individual anions will add constructively, a necessary requirement for extending the nonlinear properties from the microscopic to the macroscopic scale. However, the presence of  $\text{Cu}^{2+}$  cations with their unpaired d electrons affords absorption peaks in the visible region. Substitution of a metal with filled valence orbitals would eliminate this absorption. Because the Cu atoms in

$\text{BaCuB}_2\text{O}_5$  are tetrahedrally distorted from a square-planar geometry and the crystal radius of the atom Zn is similar to that of the Cu atom, I attempted to synthesize the Zn analog of  $\text{BaCuB}_2\text{O}_5$ . These efforts led to the discovery of the acentric orthoborate  $\text{BaZn}_2(\text{BO}_3)_2$  whose potential as an optical frequency converter is being investigated. The desire to produce new efficient frequency converters has led to the inclusion of complex zinc borates in this work.

I note, however, that the presence of absorption bands of the  $\text{Cu}^{2+}$  ion could afford large nonlinearities by increasing the hyperpolarizabilities,  $\beta$ , in a near resonance condition. Equation [3]

$$\beta_{ijk}(\omega, 2\omega) = \sum_{e, e'} \frac{\text{electronic transition moments}}{(\omega_e - \omega_g - 2\omega)(\omega_{e'} - \omega_g - \omega)} \quad [3]$$

is a simplified expression for the hyperpolarizability coefficients where  $\omega_e$  and  $\omega_g$  represent the energies of excited and ground electronic states of the solid and  $\omega$  and  $2\omega$  represent the energies of the incident and outgoing photons. Examination of Equation [3] suggests that large  $\beta$ 's may be realized for materials where the energies of  $\omega$  and  $2\omega$  are nearly in resonance with the absorption bands of the solid.

## References

1. G. C. Chinchon, P. J. Denny, D. G. Porter, G. D. Short, M. S. Spencer, K. C. Waugh, and D. A. Whan, Prepr. Pap.-Am. Chem. Soc., Div. Fuel Chem. **29**, 178 (1984).
2. E. Otsuka, T. Takahashi, N. Hashimoto, and F. Matsuda, Chem. Econ. Eng. Rev. **7** (4), 29 (1975).
3. A. Zletz (Amoco Corp.), U.S. Patent Application 709, 790, 11 March 1985.
4. J. G. Bednorz and K. A. Müller, Z. Phys. B **64**, 189 (1986).
5. M. K. Wu, J. R. Ashburn, C. J. Torng, P. H. Hor, R. L. Meng, L. Gao, Z. J. Huang, Y. Q. Wang, and C. W. Chu, Phys. Rev. Lett. **58**, 908 (1987).
6. Z. Z. Sheng and A. M. Hermann, Nature **332**, 55 (1988).
7. R. M. Hazen, L. W. Finger, R. J. Angel, C. T. Prewitt, N. L. Ross, C. G. Hadidacos, P. J. Heaney, D. R. Veblen, Z. Z. Sheng, A. El Ali, and A. M. Hermann, Phys. Rev. Lett. **60**, 1657 (1988).
8. C. C. Torardi, M. A. Subramanian, J. C. Calabrese, J. Gopalkrishnan, K. J. Morrissey, T. R. Askew, R. B. Flippen, U. Chowdhry, and A. W. Sleight, Science **240**, 631 (1988).
9. G. K. Abdullaev, P. F. Rza-Zade, and Kh. S. Mamedov, Zh. Neorgan. Khim. **27**, 1037 (1982).
10. G. Heller, Topics in Current Chemistry **131**, 39 (1986).
11. H. Behm, Acta Crystallogr., Sect. B **38**, 2781 (1982).
12. M. Martinez-Ripoll, S. Martinez-Carrera, and S. Garcia-Blanco, Acta Crystallogr., Sect. B **27**, 677 (1971).
13. M. Martinez-Ripoll, S. Martinez-Carrera, and S. Garcia-Blanco, Acta Crystallogr., Sect. B **27**, 672 (1971).
14. J. Krogh-Moe, Acta Chem. Scand. **18**, 2055 (1964).
15. A. Perloff and S. Block, Acta Crystallogr. **20**, 274 (1966).
16. S. Garcia-Blanco and J. Fayos, Z. Krist. **127**, 145 (1968).
17. W. H. Baur and E. Tillmanns, Z. Krist. **131**, 213 (1970).

18. O. A. Chaltykyan, "Copper Catalytic Reactions," Consultants Bureau, New York (1966).
19. Stauffer Chemical Company, British Patent 1,306,191.
20. G. C. Chinchin, P. J. Denny, J. R. Jennings, M. S. Spencer, and K. C. Waugh, Appl. Catal. 36, 1 (1988).
21. S. P. S. Andrew, "Catalyst Handbook," Wolfe Scientific Texts, New York (1970).
22. D. J. C. Yates, N. E. Zlotin, and J. A. McHenry, J. Catal. 117, 290 (1989).
23. C. Chen, Y. Fan, R. C. Eckardt, and R. L. Byer, SPIE Laser and Nonlinear Optical Materials 681, 12 (1986).
24. S. P. Velsko, Lawrence Livermore National Laboratory, private communication.
25. D. J. Williams, Angew. Chem. Int. Ed. Eng. 23, 690 (1984).
26. C. Chen and G. Liu, Ann. Rev. Mater. Sci. 16, 203 (1986).

## CHAPTER 2

SYNTHESES AND CRYSTAL STRUCTURES OF THE  $\alpha$ - AND  $\beta$ -FORMS  
OF THE ORTHOBORATE  $\text{Sr}_2\text{Cu}(\text{BO}_3)_2$ 

Robert W. Smith and Douglas A. Keszler

Department of Chemistry and Center for Advanced Materials Research

Oregon State University

Gilbert Hall 153

Corvallis, Oregon 97331-4003, USA

Journal of Solid State Chemistry 81, 305 (1989)

### Abstract

The low temperature  $\alpha$ -form and the high temperature  $\beta$ -form of the compound of formula  $\text{Sr}_2\text{Cu}(\text{BO}_3)_2$  have been synthesized and their structures established by single-crystal X-ray methods. The  $\alpha$ -phase crystallizes in a monoclinic cell of dimensions  $\underline{a} = 5.707(1)$ ,  $\underline{b} = 8.796(2)$ ,  $\underline{c} = 6.027(1)$  Å, and  $\beta = 116.98(1)^\circ$  with  $Z = 2$ ; the space group is  $P2_1/c$ . The structure was determined from 1039 independent reflections and refined to the final residuals  $R = 0.037$  and  $R_w = 0.051$ . It is composed of sheets of isolated  $\text{CuO}_4$  square planes that are rotated out of the  $\underline{b}$ - $\underline{c}$  plane and connected by  $\text{BO}_3$  and  $\text{SrO}_7$  units; it is isomorphous to  $\text{Na}_2\text{Cu}(\text{CO}_3)_2$ . The  $\beta$ -phase crystallizes in an orthorhombic cell of dimensions  $\underline{a} = 7.612(3)$ ,  $\underline{b} = 10.854(7)$ , and  $\underline{c} = 13.503(4)$  Å with  $Z = 8$ ; the space group is  $Pnma$ . The structure was determined from 1235 independent reflections and refined to the final residuals  $R = 0.030$  and  $R_w = 0.039$ . The structure exhibits isolated units of stoichiometry  $\text{Cu}_2(\text{BO}_3)_4$  that are built from  $\text{CuO}_4$  distorted square planes and triangular  $\text{BO}_3$  groups. These units are bridged by three crystallographically independent Sr atoms. The phase transition from the  $\alpha$ -phase to the  $\beta$ -phase occurs at  $800^\circ\text{C}$ . Considerable bond scission and reformation between the two phases indicate that the transition is first-order.

## Introduction

Only a limited number of anhydrous borates of the transition metals have been reported (1). Prompted, in part, by this state of underdevelopment and the characteristics of the compound  $\text{Cu}_2\text{Al}_6\text{B}_4\text{O}_{17}$  we have elected to synthesize new complex copper borates and their derivatives. The aforementioned borate has been reported to catalyze oxidative dehydrogenation of a variety of organic substrates and to be effective in the conversion of synthesis gas to alcohols (2); the solid solutions  $\text{Cu}_{2-x}\text{M}_x\text{Al}_6\text{B}_4\text{O}_{17}$  where  $\text{M} = \text{Zn}, \text{Co}, \text{Ni}, \text{or Mg}$  with  $0.01 \leq x \leq 0.8$  exhibit similar characteristics.

In this report we describe the preparation, crystal structure, phase transition, and magnetic moments of the polymorphic compound  $\text{Sr}_2\text{Cu}(\text{BO}_3)_2$  which is the first of a new family of alkaline earth copper(II) borates that we have discovered. Two phases, a low temperature  $\alpha$ -form and a high temperature  $\beta$ -form, are observed between  $25^\circ$  and  $1000^\circ\text{C}$  with a first-order phase transition at  $800^\circ\text{C}$ .

## Experimental

### Syntheses

The  $\alpha$ -phase was prepared by dissolving a stoichiometric ratio of the reagents CuO (99.999%, Johnson Matthey) and Sr(NO<sub>3</sub>)<sub>2</sub> (reagent grade, J.T. Baker) in dilute nitric acid and precipitating the cations with a 30% excess of oxalic acid dihydrate (reagent grade, J.T. Baker); the mixture was then dried. Powdered B<sub>2</sub>O<sub>3</sub> (99.99%, Morton Thiokol) was added and the mixture ground under hexane to a fine powder. This intimate mixture was heated in an alumina crucible at 700°C for 18 hours, cooled and ground again under hexane, and finally pressed into a pellet and sintered at 740°C for an additional 18 hours. Except for a few weak lines attributable to the phase Sr<sub>3</sub>B<sub>2</sub>O<sub>6</sub>, the powder X-ray trace of the product compares well to that calculated with the computer program LAZY-PULVERIX (3) from the results of the single-crystal structure analysis (vide infra).

Single crystals were grown with the compound LiBO<sub>2</sub> as a flux. A mixture with a sample:flux ratio by mass of 7:1 was heated in a Pt crucible to 875°C, cooled 6°/hour, then air-quenched. The resulting purple single crystals were physically separated from the crucible for the structure determination.

The  $\beta$ -phase was prepared by grinding a stoichiometric ratio of Sr(NO<sub>3</sub>)<sub>2</sub>, Cu(NO<sub>3</sub>)<sub>2</sub>·2½H<sub>2</sub>O (reagent grade, Mallinckrodt) and B<sub>2</sub>O<sub>3</sub> under hexane to a fine powder and calcining at 600°C for 30 minutes. A single phase resulted from subsequent sintering at 900°C for 18 hours. The powder X-ray trace for this powder compares well to that

calculated from the single-crystal X-ray data (vide infra). Lavender single crystals were obtained in a manner similar to that used for the growth of the  $\alpha$ -phase except the sample was heated to 950°C and subsequently quenched in air after cooling to 820°C.

### X-ray Work

Powder X-ray diffractograms were obtained from an automated Philips powder diffractometer equipped with a diffracted-beam monochromator set for Cu K $\alpha$  radiation.

A crystal of the  $\alpha$ -phase with dimensions 0.32 x 0.18 x 0.08 mm was chosen for the structure determination. Unit cell parameters were derived from a least-squares analysis of 22 reflections in the range  $19^\circ < 2\theta < 31^\circ$  that were automatically centered on a Rigaku AFC6R diffractometer using monochromatic Mo K $\alpha$  radiation. Intensity data in the range of indices  $0 \leq h \leq 9$ ,  $0 \leq k \leq 15$ , and  $-10 \leq l \leq 9$  were collected with the  $\omega$ - $2\theta$  scan technique at a scan speed of 16°/minute in  $\omega$  and a scan width  $\Delta\omega = (1.25 + 0.3 \tan\theta)^\circ$ . From 1504 reflections measured to  $2\theta = 75^\circ$ , 1039 unique data having  $F_0^2 \geq 3\sigma(F_0^2)$  were obtained.

Likewise, a crystal of the  $\beta$ -phase with dimensions 0.30 x 0.16 x 0.06 mm was studied. Lattice parameters were refined from 18 reflections in the range  $30^\circ < 2\theta < 40^\circ$ . From 1900 reflections measured in the range of indices  $0 \leq h \leq 10$ ,  $-14 \leq k \leq 15$ , and  $0 \leq l \leq 18$  to  $2\theta = 60^\circ$ , 1235 unique data having  $F_0^2 \geq 3\sigma(F_0^2)$  were obtained.

All calculations were performed on a microVax II computer with

programs from the TEXRAY crystallographic software package. The systematic absences  $h0l$  ( $l = 2n+1$ ) and  $0k0$  ( $k = 2n+1$ ) unambiguously define the space group  $P2_1/c$  for the  $\alpha$ -phase. The systematic absences  $0kl$  ( $k+l = 2n+1$ ) and  $hk0$  ( $h = 2n+1$ ) indicate that the  $\beta$ -phase crystallizes in the centric group  $Pnma$  or the acentric group  $Pn2_1a$ . We favor the centric group from the statistical analyses of the intensities (4) as well as the successful solution and refinement of the structure in this group. For each structure, the positional parameters for the Sr and Cu atoms were determined from the direct methods program MITHRIL (5) with the remaining atomic positions determined from analysis of subsequent difference electron density syntheses. Following refinement with isotropic thermal parameters the data were corrected for absorption with the computer program DIFABS (6); equivalent reflections were then averaged. Final least-squares refinement on  $F_o^2$  with data having  $F_o^2 \geq 3\sigma(F_o^2)$  and anisotropic thermal factors for each atom resulted in the residuals  $R = 0.037$  and  $R_w = 0.051$  for the  $\alpha$ -phase and  $R = 0.030$  and  $R_w = 0.039$  for the  $\beta$ -phase. The largest peaks in the final difference maps for the  $\alpha$ - and  $\beta$ -phases have heights of 0.742% and 0.628% of a Sr atom, respectively. Additional crystal data and experimental conditions are summarized in Table 2.1.

### Measurements

A Harrop model DT-726 differential thermal analyzer interfaced to a PC via a Metrabyte DAS-8 A/D converter and Series M1000 signal conditioner was used to obtain DTA data. The sample and reference

Table 2.1 Crystal data and experimental conditions for  $\alpha$ - and  $\beta$ -  
 $\text{Sr}_2\text{Cu}(\text{BO}_3)_2$ .

Crystal data	Experimental conditions	
	$\alpha$ -phase	$\beta$ -phase
Diffractometer	Rigaku AFC6R	
Radiation	Graphite monochromated Mo $K\alpha$ $(\lambda(K\alpha_1) = 0.70926 \text{ \AA})$	
Formula wt., amu	356.40	
$a$ , $\text{\AA}$	5.707(1)	7.612(3)
$b$ , $\text{\AA}$	8.796(2)	10.854(7)
$c$ , $\text{\AA}$	6.027(1)	13.503(4)
$\beta$ , deg.	116.98(1)	
$V$ , $\text{\AA}^3$	269.6(2)	1116(1)
Space group	$P2_1/c$	$Pnma$
$D_{\text{calc}}$ , $\text{g cm}^{-3}$	4.39	4.24
Crystal vol., $\text{mm}^3$	0.005	0.003
$F(000)$	326	1304
$Z$	2	8
Linear abs. coeff., $\text{cm}^{-1}$	230.07	222.44
$\mu$ factor	0.05	0.05
No. unique data with $F_0^2 >$ $3\sigma(F_0^2)$	1039	1235
$R_{\text{int}}$		0.027
$R(F)$	0.037	0.030
$R_w(F)$	0.051	0.039
Error in observation of unit wt., $e^2$	1.38	1.01

(Al<sub>2</sub>O<sub>3</sub>) were enclosed in Pt cups. A strong endothermic signal was observed with a heating rate of 10°/minute.

The effective magnetic moments were obtained at room temperature by the Guoy method. Measurements were made at a field strength of 5 kG, using an Alpha model AL 7500 water-cooled magnet with 4 inch pole faces and a 1.5 inch air gap. The Guoy tube was calibrated with HgCo(SCN)<sub>4</sub>. Diamagnetic corrections to molar susceptibilities were made from reported values (7) except for the Sr<sup>2+</sup> ion whose correction was determined by interpolation.

## Results

### Structure of $\alpha$ -phase

Final atomic coordinates and thermal parameters of the  $\alpha$ -form of the title compound are listed in Table 2.2. Selected interatomic distances and angles are given in Table 2.3. A drawing of the unit cell is given in Figure 2.1.

The structural features are square-planar  $\text{CuO}_4$  units, trigonal-planar  $\text{BO}_3$  groups, and tetragonal-base, trigonal-base  $\text{SrO}_7$  units. The square and trigonal planes share vertices to form a two-dimensional sheet  $\infty[\text{Cu}(\text{BO}_3)_2]$  extending parallel to the  $\underline{b}$ - $\underline{c}$  plane. The  $\text{CuO}_4$  planes of the sheet are rotated about the  $\text{O}(2)$ -Cu- $\text{O}(2)$  axes by approximately  $35^\circ$  out of the  $\underline{b}$ - $\underline{c}$  plane, affording the herringbone pattern, Figure 2.2a, when viewed along the  $\underline{c}$  axis. The B atoms bridge the isolated square planes, Figure 2.2b. The structure is completed by joining the successive sheets of Figure 2.2b by interleaving Sr atoms.

The average Cu-O distance of 1.930(6) Å is similar to values observed in other copper borates e.g., 1.95(1) Å for  $\text{Cu}_3\text{B}_2\text{O}_6$  (8) and 1.968 Å for  $\text{CuB}_2\text{O}_4$  (9). The square planes distort slightly to afford the angle  $\text{O}(1)$ -Cu- $\text{O}(2)$  of  $85.2(2)^\circ$ . The edge  $\text{O}(1)\cdots\text{O}(2)$  of this acute angle is shared by the Sr atom. The Sr atom is sevenfold coordinate, centering approximately a distorted tetragonal-base, trigonal-base polyhedron. An additional O atom,  $\text{O}(1)$ , is located 3.110(4) Å from the Sr atom. If this long distance were considered to be a weak bonding interaction, the environment could be described

Table 2.2 Final atomic coordinates and temperature factors for  $\alpha$ - $\text{Sr}_2\text{Cu}(\text{BO}_3)_2$ .

Atom	x	y	z	$B_{\text{eq}}^*$
Sr	0.3285(1)	0.1049(1)	0.6591(1)	0.66(1)
Cu	0	0	0	0.53(2)
B	0.805(1)	0.2521(6)	0.6597(8)	0.5(1)
O(1)	0.7950(7)	0.4068(4)	0.1813(6)	0.8(1)
O(2)	0.0375(7)	0.1863(4)	0.1850(6)	0.8(1)
O(3)	0.5909(9)	0.3388(4)	0.6146(6)	0.8(1)

Atom	$U_{11}$	$U_{22}$	$U_{33}$	$U_{12}$	$U_{13}$	$U_{23}$
Sr	0.0080(1)	0.0084(2)	0.0084(2)	-0.0004(1)	0.0036(1)	0.0008(1)
Cu	0.0077(3)	0.0065(3)	0.0062(3)	0.0005(3)	0.0033(2)	0.0002(2)
B	0.010(2)	0.009(2)	0.002(1)	0.001(2)	0.002(1)	0.001(1)
O(1)	0.012(2)	0.006(1)	0.010(1)	0.000(1)	0.003(1)	-0.001(1)
O(2)	0.011(1)	0.011(2)	0.011(1)	-0.002(1)	0.007(1)	-0.002(1)
O(3)	0.012(2)	0.011(2)	0.010(1)	0.004(1)	0.006(1)	0.002(1)

$$*B_{\text{eq}} = (8\pi^2/3)\sum_i\sum_j U_{ij}a_i^*a_j^*a_i\cdot a_j$$

as a distorted square antiprism. A similar coordination environment without the additional O atom exists in the compound  $\text{Sr}_2\text{ScLi}(\text{B}_2\text{O}_5)_2$  where the Sr atom occupies an irregular heptacoordinate site between two layers of O atoms (10). The Sr-O distances vary from 2.509(4) Å to 2.670(4) Å with an average value of 2.59(3) Å. This compares well

Table 2.3 Selected distances (Å) and angles (°) for  $\alpha$ -Sr<sub>2</sub>Cu(BO<sub>3</sub>)<sub>2</sub>.

Atoms	Distance		Angle
Sr-0(3)	2.509(4)	0(1)-Sr-0(1)	95.4(1)
Sr-0(2)	2.528(4)	0(2)-Sr-0(2)	76.4(1)
Sr-0(1)	2.536(3)	0(3)-Sr-0(3)	74.5(1)
Sr-0(1)	2.606(4)	0(3)-Sr-0(3)	82.7(1)
Sr-0(3)	2.629(4)	0(2)-Sr-0(3)	81.8(1)
Sr-0(3)	2.642(4)	0(2)-Sr-0(3)	125.3(1)
Sr-0(2)	2.670(4)		
Cu-0(1)	1.921(3) × 2	0(1)-Cu-0(2)	85.8(2)
Cu-0(2)	1.938(3) × 2	0(1)-Cu-0(1)	180
		0(2)-Cu-0(2)	180
B-0(1)	1.407(6)	0(1)-B-0(2)	117.2(4)
B-0(2)	1.378(6)	0(2)-B-0(3)	122.4(4)
B-0(3)	1.358(6)	0(3)-B-0(1)	120.4(4)

with the average Sr-O distances of 2.61 Å in SrCuO<sub>2</sub> (11), 2.59 Å in Sr<sub>2</sub>CuO<sub>3</sub> (12), and 2.69 Å in SrB<sub>4</sub>O<sub>7</sub> (13). The BO<sub>3</sub> groups are metrically quite regular. The average B-O distance, 1.38(2) Å, compares to similar interactions observed in a variety of other simple orthoborates discovered in this lab (10,14) and by others (1). All O atoms are bonded to four cations.

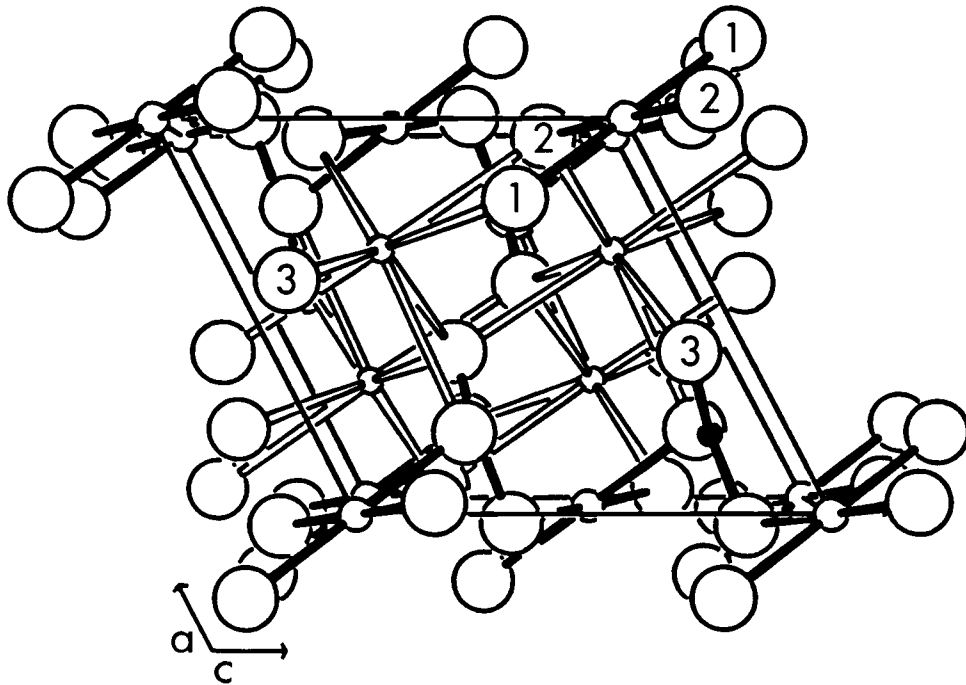
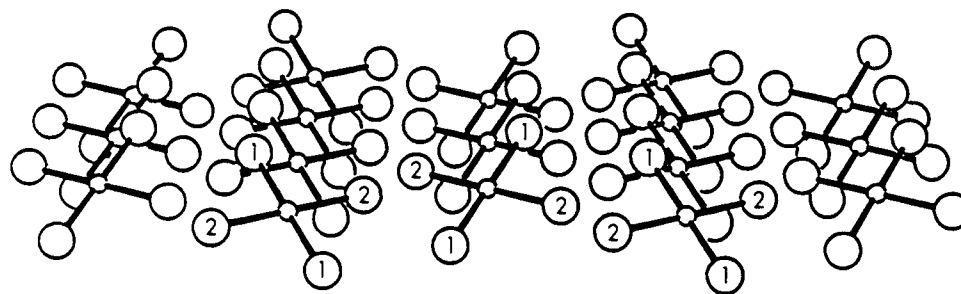


Figure 2.1 Sketch of the unit cell of the structure of  $\alpha\text{-Sr}_2\text{Cu}(\text{BO}_3)_2$  viewed down the  $\underline{b}$  axis.

The large open circles represent O atoms, the smallest open circles with unshaded bonds represent Sr atoms, the small open circles with shaded bonds represent Cu atoms, and the solid circles with shaded bonds represent B atoms.\*

\*The same schematic representations will be used throughout this work with K, Rb, Cs, and Ba substituting for Sr and Zn substituting for Cu.

(a)



(b)

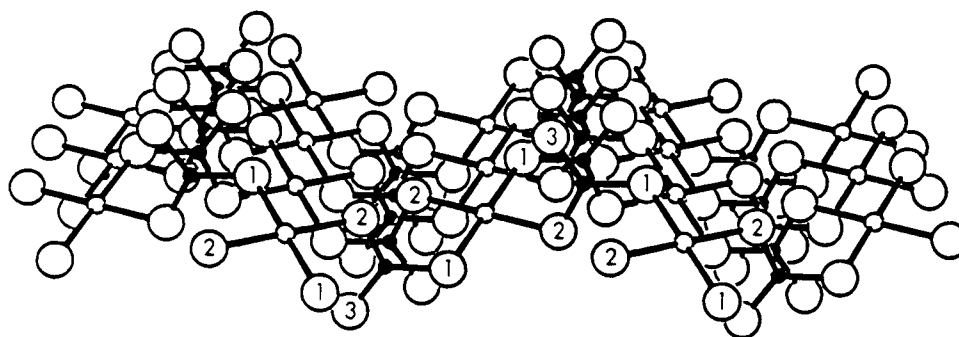


Figure 2.2 Sketches of the copper borate network in  $\alpha\text{-Sr}_2\text{Cu}(\text{BO}_3)_2$ .

(a) The herringbone pattern of  $\text{CuO}_4$  square planes viewed down the  $\underline{c}$  axis.

(b) The herringbone pattern with bridging  $\text{BO}_3$  groups.

### Structure of $\beta$ -phase

Final atomic coordinates and thermal factors are listed in Table 2.4 with selected interatomic distances and angles appearing in Table 2.5. A drawing of the contents of the unit cell is given in Figure 2.3.

Because of the presence of three crystallographically independent Sr atoms this structure appears to be more complicated than the  $\alpha$ -phase. Rather than an extended copper borate network, this structure is composed of isolated units of stoichiometry  $\text{Cu}_2(\text{BO}_3)_4$ , Figure 2.4a. Two highly distorted square planes occupied by the Cu atoms are bridged by two  $\text{BO}_3$  groups by sharing O vertices. The terminal edges are completed by the sharing of two cis O atoms of the square plane with planar  $\text{BO}_3$  groups. These edges are pinched by the  $\text{BO}_3$  groups to afford the angles  $72.7(2)^\circ$  and  $72.9(3)^\circ$  for the interactions O(3)-Cu(1)-O(3) and O(5)-Cu(2)-O(5), respectively. The planarity of the  $\text{CuO}_4$  groups is also perturbed as evidenced by the angles O(3)-Cu(1)-O(7),  $159.2(2)^\circ$ , and O(5)-Cu(2)-O(6),  $170.2(2)^\circ$ . As seen in Figure 2.4b, there is substantial deviation from planarity of the  $\text{Cu}_2(\text{BO}_3)_4$  unit with a bend at the atom O(6). The angle B(3)-O(6)-Cu(2),  $116.6(4)^\circ$ , contrasts to that observed for the angle B(3)-O(7)-Cu(1),  $138.2(4)^\circ$ . These angles are consistent with the chemically distinct nature of these atoms; atom O(6) is four-coordinate, binding to atoms B(3), Cu(2), and Sr(2,3), while atom O(7) is five-coordinate, binding to atoms B(3), Cu(1), and Sr(1-3). The Cu-O and B-O distances are similar to those observed in the  $\alpha$ -phase.

The copper borate units are bridged by Sr atoms occupying sites

Table 2.4 Final atomic coordinates and temperature factors for  $\beta$ - $\text{Sr}_2\text{Cu}(\text{BO}_3)_2$ .

Atom	x	y	z	$B_{\text{eq}}$
Sr(1)	0	0	0	1.05(3)
Sr(2)	0.3839(1)	1/4	0.95434(6)	0.75(3)
Sr(3)	0.16218(7)	0.02423(5)	0.71699(4)	0.74(2)
Cu(1)	0.3120(1)	1/4	0.57219(8)	0.81(4)
Cu(2)	0.0280(1)	1/4	0.29959(7)	0.84(4)
B(1)	0.066(1)	1/4	0.1276(7)	0.9(3)
B(2)	0.491(1)	1/4	0.7125(7)	0.7(3)
B(3)	0.1271(8)	0.4355(6)	0.4329(5)	0.8(2)
O(1)	0.0764(8)	1/4	0.6997(4)	0.9(2)
O(2)	0.0766(8)	1/4	0.0275(4)	1.1(2)
O(3)	0.4416(5)	0.1415(4)	0.6657(3)	0.8(1)
O(4)	0.3015(5)	0.4649(4)	0.8867(3)	1.1(2)
O(5)	0.0604(6)	0.1430(4)	0.1846(3)	1.3(2)
O(6)	0.4825(5)	0.1260(4)	0.1048(3)	0.8(1)
O(7)	0.1961(5)	0.1059(4)	0.5219(3)	1.0(1)

Atom	$U_{11}$	$U_{22}$	$U_{33}$	$U_{12}$	$U_{13}$	$U_{23}$
Sr(1)	0.0100(4)	0.0146(4)	0.0154(4)	0.0025(3)	0.0002(3)	0.0029(3)
Sr(2)	0.0105(3)	0.0102(3)	0.0079(3)	0	0.0005(3)	0
Sr(3)	0.0095(2)	0.0096(2)	0.0092(2)	-0.0005(2)	-0.0001(2)	-0.0003(2)
Cu(1)	0.0112(4)	0.0092(4)	0.0105(5)	0	-0.0035(4)	0
Cu(2)	0.0144(5)	0.0089(4)	0.0084(5)	0	0.0003(4)	0
B(1)	0.014(4)	0.008(4)	0.012(4)	0	-0.001(3)	0
B(2)	0.011(4)	0.006(4)	0.008(4)	0	0.000(3)	0
B(3)	0.011(3)	0.010(3)	0.010(3)	0.004(2)	0.004(2)	0.000(2)
O(1)	0.014(3)	0.018(3)	0.004(2)	0	0.002(2)	0
O(2)	0.014(3)	0.020(3)	0.010(3)	0	0.000(2)	0
O(3)	0.009(2)	0.012(2)	0.011(2)	0.000(1)	0.001(1)	0.001(2)
O(4)	0.016(2)	0.012(2)	0.014(2)	-0.001(2)	-0.005(2)	-0.001(2)
O(5)	0.028(2)	0.012(2)	0.011(2)	0.002(2)	0.002(2)	0.001(2)
O(6)	0.012(2)	0.009(2)	0.011(2)	0.000(1)	-0.003(1)	0.001(2)
O(7)	0.012(2)	0.013(2)	0.010(2)	-0.003(2)	-0.004(2)	-0.001(2)

Table 2.5 Selected distances (Å) and angles (°) for  $\beta$ -Sr<sub>2</sub>Cu(BO<sub>3</sub>)<sub>2</sub>.

Atoms	Distance		Angle
Sr(1)-O(7)	2.600(4) x 2	0(7)-Sr(1)-O(3)	61.1(1)
Sr(1)-O(3)	2.750(4) x 2	0(3)-Sr(1)-O(4)	67.0(1)
Sr(1)-O(4)	2.785(4) x 2	0(4)-Sr(1)-O(7)	52.4(1)
Sr(1)-O(2)	2.800(2) x 2	0(2)-Sr(1)-O(3)	66.4(1)
Sr(1)-O(5)	2.972(4) x 2	0(5)-Sr(1)-O(2)	49.5(1)
Sr(2)-O(2)	2.539(6)	0(2)-Sr(2)-O(1)	148.1(2)
Sr(2)-O(1)	2.544(6)	0(1)-Sr(2)-O(4)	81.4(1)
Sr(2)-O(6)	2.550(4) x 2	0(6)-Sr(2)-O(6)	63.7(2)
Sr(2)-O(4)	2.582(4) x 2	0(4)-Sr(2)-O(6)	82.9(1)
Sr(2)-O(7)	2.863(4) x 2	0(7)-Sr(2)-O(7)	66.2(2)
Sr(3)-O(6)	2.483(4)	0(6)-Sr(3)-O(5)	66.3(1)
Sr(3)-O(4)	2.527(4)	0(4)-Sr(3)-O(3)	72.5(1)
Sr(3)-O(1)	2.547(2)	0(1)-Sr(3)-O(7)	68.4(2)
Sr(3)-O(3)	2.574(4)	0(3)-Sr(3)-O(5)	70.0(1)
Sr(3)-O(3)	2.636(4)	0(3)-Sr(3)-O(3)	116.7(2)
Sr(3)-O(7)	2.792(4)	0(7)-Sr(3)-O(6)	71.0(1)
Sr(3)-O(5)	2.816(4)	0(5)-Sr(3)-O(6)	66.3(1)
Sr(3)-O(5)	2.819(5)	0(5)-Sr(3)-O(5)	96.3(1)
Cu(1)-O(3)	1.988(4) x 2	0(3)-Cu(1)-O(3)	72.7(2)
Cu(1)-O(7)	1.920(4) x 2	0(7)-Cu(1)-O(7)	109.1(2)
		0(3)-Cu(1)-O(7)	88.3(2)
Cu(2)-O(5)	1.955(4) x 2	0(5)-Cu(2)-O(5)	72.9(3)
Cu(2)-O(6)	1.897(4) x 2	0(6)-Cu(2)-O(6)	90.4(2)
		0(5)-Cu(2)-O(6)	98.2(2)
B(1)-O(2)	1.35(1)	0(2)-B(1)-O(5)	123.5(4)
B(1)-O(5)	1.394(7) x 2	0(5)-B(1)-O(5)	112.9(7)
B(2)-O(1)	1.35(1)	0(1)-B(2)-O(3)	121.9(3)
B(2)-O(3)	1.388(6) x 2	0(3)-B(2)-O(3)	116.1(7)
B(3)-O(4)	1.361(7)	0(4)-B(3)-O(6)	122.1(5)
B(3)-O(6)	1.385(7)	0(6)-B(3)-O(7)	117.6(5)
B(3)-O(7)	1.386(7)	0(7)-B(3)-O(4)	120.2(5)

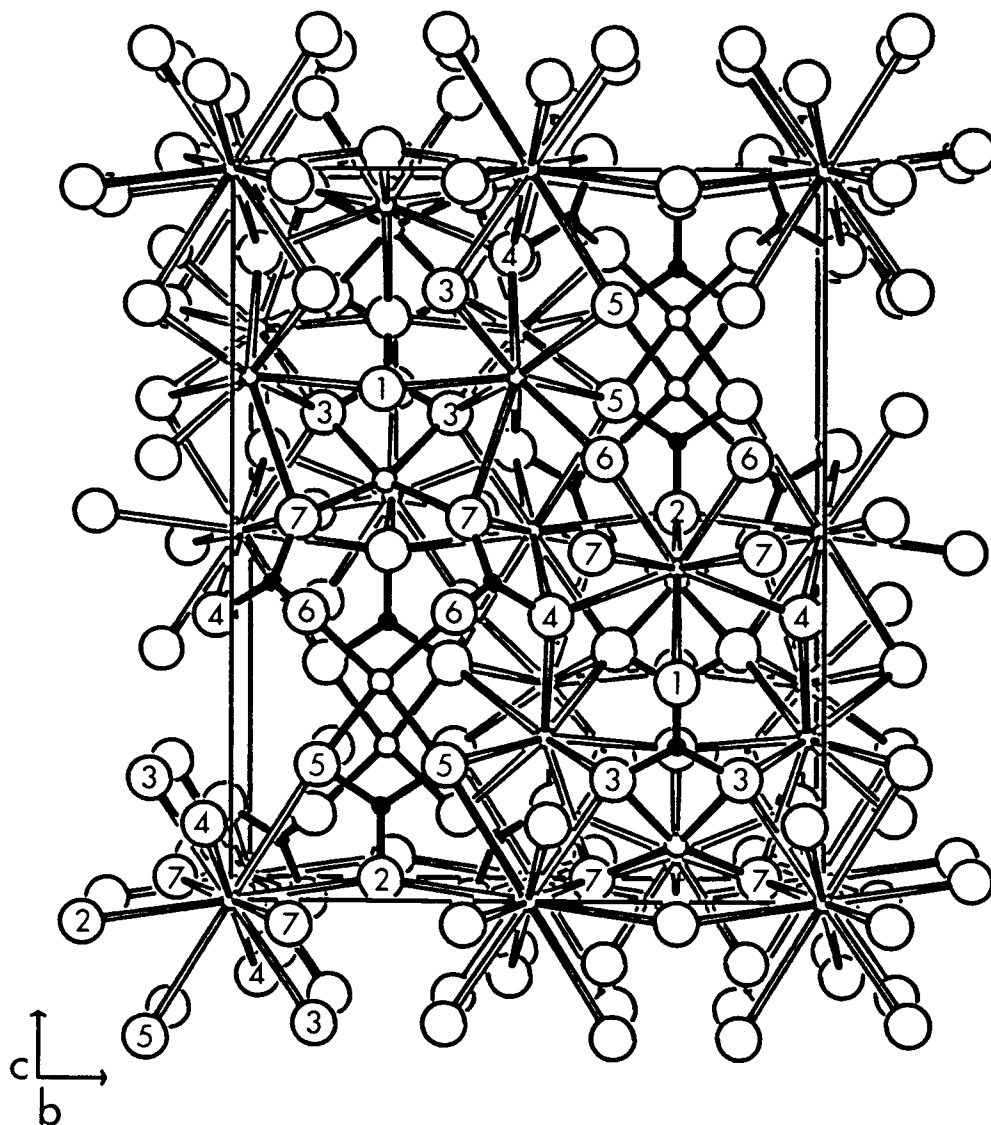


Figure 2.3 Sketch of the unit cell of  $\beta\text{-Sr}_2\text{Cu}(\text{BO}_3)_2$  viewed down the  $a$  axis.

of high coordination numbers. The atom Sr(1) occupies a site, Figure 2.5a, with ten O atoms that are located at distances ranging from 2.600(4) to 2.972(4) Å. Its environment may be described as a highly distorted bicapped cube. Atom Sr(2) occupies an irregular square antiprismatic site, Figure 2.5b, with the Sr depressed toward the plane formed by the atoms O(1), O(2), and O(4); representative angles include O(1)-Sr(2)-O(4), 81.4(1)°, and O(6)-Sr(2)-O(6), 63.7(2)°. The Sr(2)-O(7) distance, 2.863(4) Å, is considerably longer than the remaining Sr(2)-O distances (mean = 2.56(1) Å). Atom Sr(3) occupies an irregular eightfold dodecahedral site, Figure 2.5c, with distances ranging from 2.483(4) to 2.819(5) Å. From these descriptions for the environments of the cations, atoms O(1), O(2), O(4), and O(6) are each observed to bond to four cations and the atoms O(3), O(5), and O(7) each bond to five cations.

We note that we have prepared the Ba analog of the title compound and find it to crystallize only in the  $\beta$ -form, consistent with the larger crystal radius of the Ba atom relative to the Sr atom.

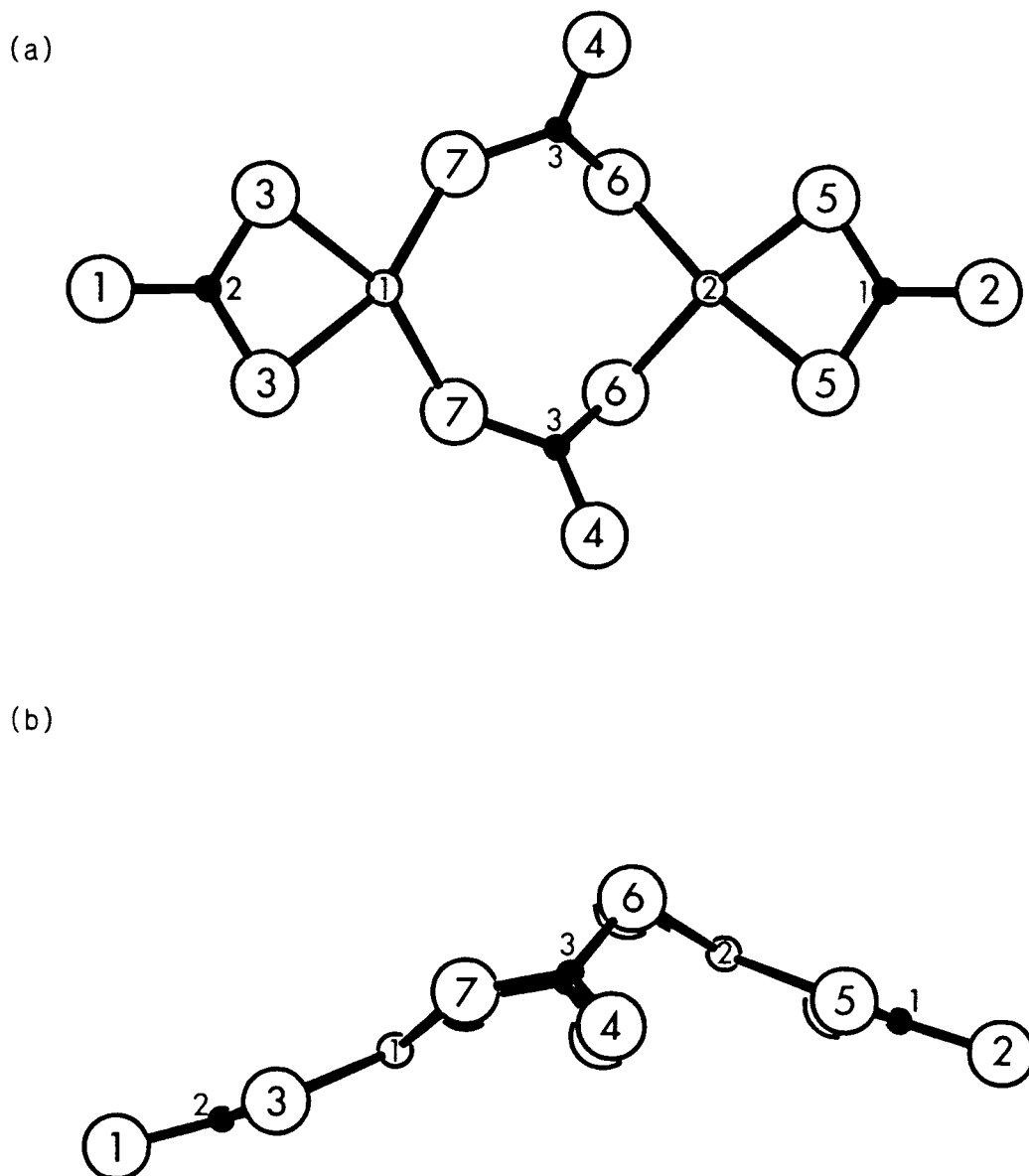


Figure 2.4 Sketches of the  $\text{Cu}_2(\text{BO}_3)_4$  unit in  $\beta\text{-Sr}_2\text{Cu}(\text{BO}_3)_2$ .

(a) View perpendicular to the  $\underline{b}$  axis.

(b) View parallel to the  $\underline{b}$  axis.

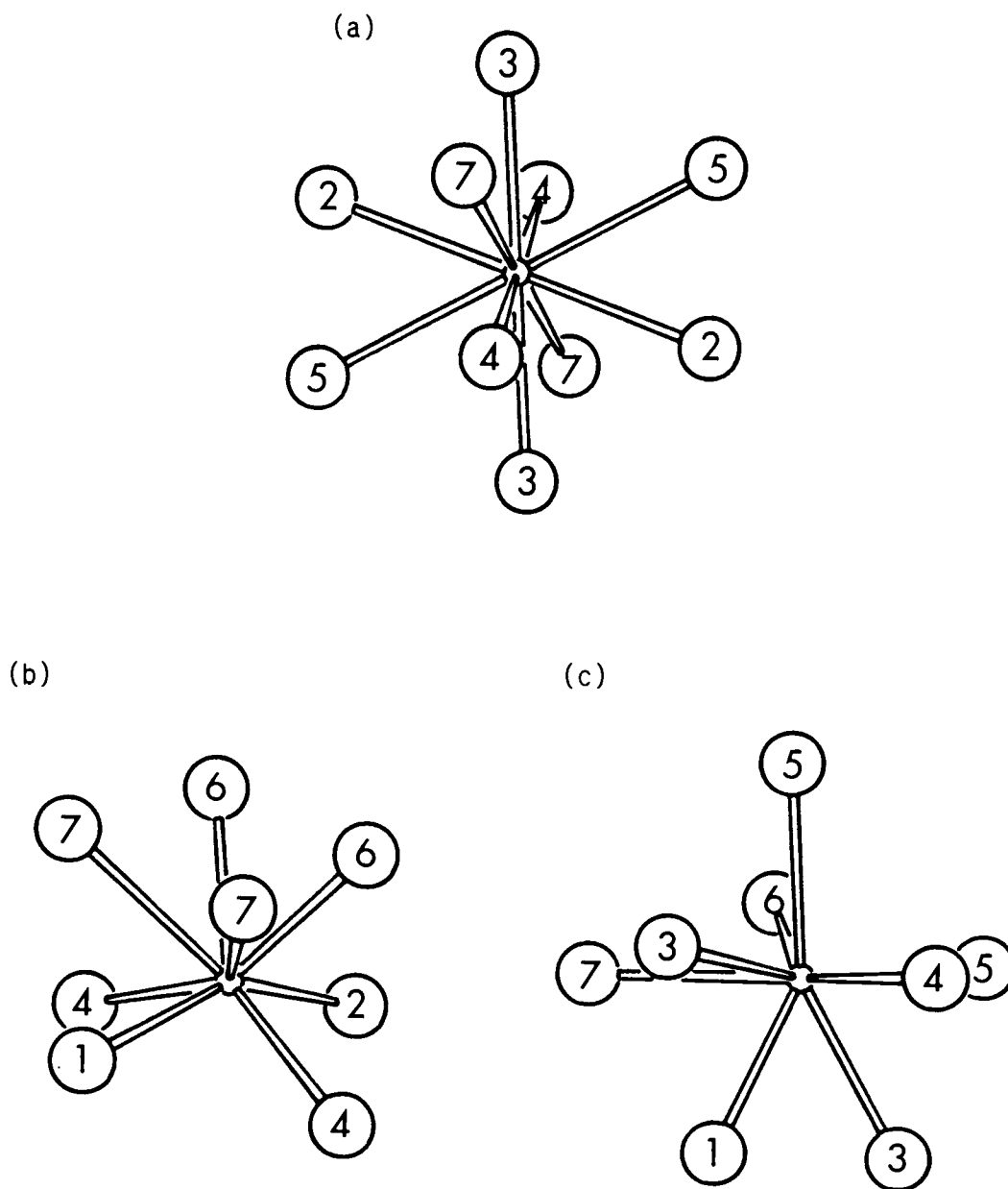


Figure 2.5 Sketches of the Sr environments for  $\beta$ - $\text{Sr}_2\text{Cu}(\text{BO}_3)_2$ .

(a) Sr(1) (b) Sr(2) (c) Sr(3)

## Discussion

The effective magnetic moments at 23°C of the  $\alpha$ - and  $\beta$ -forms are 1.70(2) and 1.72(2) BM, respectively. These values are consistent with the  $d^9$  electronic configuration for isolated Cu(II) ions and spin-only contributions to the magnetic moment. Values of  $\mu_{\text{eff}}$  for Cu(II) molecular complexes typically range from 1.7-1.9 BM (16) and average 1.63 BM for  $\text{ACuO}_2$  where A = Ca, Sr, or Ba (17).

Four other borates with a similar formula  $\text{A}_2^{2+}\text{B}^{2+}(\text{BO}_3)_2$  have been reported. The compound  $\text{Ba}_2\text{Mg}(\text{BO}_3)_2$  is isomorphous to the trigonal mineral buetschliite,  $\text{K}_2\text{Ca}(\text{CO}_3)_2$  (18), the compound  $\text{Ca}_2\text{Mg}(\text{BO}_3)_2$  is tetragonal, and the compounds  $\text{Ba}_2\text{Ca}(\text{BO}_3)_2$  and  $\text{Sr}_2\text{Mg}(\text{BO}_3)_2$  are related to buetschliite (19). These materials all appear to crystallize in structures that are similar to calcite and dolomite, containing discrete layers of trigonal borate or carbonate groups with the cations located between these layers. The title compound exists in structures of lower symmetry with structural motifs that are different from these reported borates.

Borates and carbonates are often isostructural, and the compounds  $\text{M}_2\text{Cu}(\text{CO}_3)_2$  with M = alkali metal could be expected to be isomorphous to the title compound. Three such carbonates have been reported; they are the potassium compound  $\text{K}_2\text{Cu}(\text{CO}_3)_2$  (20), the sodium compound  $\text{Na}_2\text{Cu}(\text{CO}_3)_2$  (21), and the mineral chalconatronite,  $\text{Na}_2\text{Cu}(\text{CO}_3)_2 \cdot 3\text{H}_2\text{O}$  (22). The compound  $\text{K}_2\text{Cu}(\text{CO}_3)_2$  is face-centered orthorhombic (Fdd2) with square-planar coordination of the Cu atom, chalconatronite is monoclinic (P2<sub>1</sub>/n) with square-pyramidal coor-

dination of the Cu atom, while the compound  $\text{Na}_2\text{Cu}(\text{CO}_3)_2$  is isomorphous to the  $\alpha$ -phase of the title compound. Structural differences between the two isomorphs are a substantial elongation of the unique axis,  $b$ , (8.19(2) Å in the carbonate versus 8.796(2) Å in the borate) and a six-coordinate Na atom (23) instead of the seven-coordination of the Sr atom. The larger coordination number results from displacement and distortion of the  $\text{CuO}_4$  square planes in the borate relative to those in the carbonate. Specifically, the Sr-O(2) interaction of 2.670(1) Å does not find a counterpart in the carbonate. As a Sr shares the edge  $\text{O}(1)\cdots\text{O}(2)$  of the square plane, a more acute angle,  $85.8(2)^\circ$ , occurs in comparison with that ( $88.7(5)^\circ$ ) observed in the carbonate. The atom O(2) is three-coordinate in the carbonate whereas it is four-coordinate in the borate.

The discrete unit  $\text{Cu}_2(\text{BO}_3)_4$  of the unique  $\beta$ -phase has not previously been observed. The large coordination numbers for the Sr atom, however, are common in borates. A coordination number of nine has been observed in the compounds  $\text{Sr}_3(\text{BO}_3)_2$  (24),  $\text{SrB}_4\text{O}_7$  (13),  $\text{Sr}_3\text{Sc}(\text{BO}_3)_3$  (25), and  $\text{SrNaBO}_3$  (26). Of course, such high coordination numbers should be anticipated since a substantial portion of the available bonding electron density is locked into the covalent  $\text{BO}_3$  units, forcing the Sr atom to bind to a greater number of O atoms to satisfy its bonding requirements.

The transition from the  $\alpha$ -phase to the  $\beta$ -phase occurs at  $800 \pm 10^\circ\text{C}$  as determined by differential thermal analysis. On heating a sample of the  $\alpha$ -phase a strong endothermic response is observed while on cooling no signal is observed. X-ray powder diffractograms of

samples of the  $\alpha$ -phase that have been heated and rapidly cooled through the transition temperature reveal the presence of  $\beta$ -phase only. Thus it is easy to quench the  $\beta$ -phase in place. The technique of cooling the solute/flux solution at  $6^\circ/\text{hour}$  through the transition temperature affords a solubility of the  $\alpha$ -phase that is great enough for the growth of single crystals at lower temperatures.

From consideration of the DTA data and the results of the structure determinations it is clear that the phase transition is first order. The structure of the  $\alpha$ -phase exhibits one crystallographically independent Sr atom with a coordination number of seven while the  $\beta$ -phase exhibits larger coordination numbers for the three crystallographically independent Sr atoms. Moreover, 50% of the O atoms exhibit a higher coordination number in the  $\beta$ -phase with a substantial reorganization of the copper borate substructure. The transformation from the  $\alpha$ -phase to the  $\beta$ -phase is thus characterized by the extensive bond scission and reformation of a first-order transition.

### Acknowledgements

Funds for this work were provided by the Murdock Charitable Trust of the Research Corporation. The X-ray diffraction system was purchased with funds provided by the US National Science Foundation (CHE-8604239) and by the donors of the Foursight! program at Oregon State University.

## References

1. G. Heller, Topics in Current Chemistry **131**, 39 (1986).
2. A. Zletz (Amoco Corp.), US Patent Application 709, 790, 11 March 1985.
3. K. Yvon, W. Jeitschko, and E. Parthe, J. Appl. Cryst. **10**, 73 (1977).
4. E. R. Howells, D. C. Phillips, and D. Rodgers, Acta Crystallogr. **3**, 210 (1950).
5. G. J. Gilmore, "MITHRIL: A Computer Program for the Automatic Solution of Crystal Structures from X-Ray Data," University of Glasgow, Scotland (1983).
6. N. Walker and D. Stuart, Acta Crystallogr., Sect. A **24**, 214 (1968).
7. L. N. Mulay and E. A. Boudreaux, "Theory and Applications of Molecular Diamagnetism," pp. 306-307, Wiley, New York (1976).
8. H. Behm, Acta Crystallogr., Sect. B **38**, 2781 (1982).
9. M. Martinez-Ripoll, S. Martinez-Carrera, and S. Garcia-Blanco, Acta Crystallogr., Sect. B **27**, 677 (1971).
10. P. D. Thompson and D. A. Keszler, Solid State Ionics **32/33**, 521 (1989).
11. C. L. Teske and H. Müller-Buschbaum, Z. Anorg. Allg. Chem. **379**, 234 (1970).
12. C. L. Teske and H. Müller-Buschbaum, Z. Anorg. Allg. Chem. **371**, 325 (1969).
13. A. Perloff and S. Block, Acta Crystallogr. **20**, 274 (1966).
14. D. A. Keszler and H. Sun, Acta Crystallogr., Sect. C **44**, 1505 (1988).
15. R. W. Smith and D. A. Keszler, Acta Crystallogr., Sect. C, in press.
16. E. A. Boudreaux and L. N. Mulay, "Theory and Applications of Molecular Paramagnetism," p. 54, Wiley, New York (1976).

17. M. Arjomand and D. J. Machin, J. Chem. Soc., Dalton Trans., 1061 (1975).
18. A. Pabst, Am. Mineral. **59**, 353 (1974).
19. J. M. P. J. Verstegen, J. Electrochem. Soc. **121**, 1631 (1974).
20. A. Farrand, A. K. Gregson, B. W. Skelton, and A. H. White, Aust. J. Chem. **33**, 431 (1980).
21. A. Mosset, J.-J. Bonnet, and J. Galy, Z. Krist. **148**, 165 (1978).
22. P. C. Healy and A. H. White, J. Chem. Soc., Dalton Trans., 1913 (1972).
23. From the positional parameters reported by Healy and White (ref. 22), we find that the Na atom occupies a sixfold coordination site with Na-O distances ranging from 2.35 to 2.55 Å rather than the fivefold site as originally reported.
24. L. Richter and F. Müller, Z. Anorg. Allg. Chem. **467**, 123 (1980).
25. P. D. Thompson and D. A. Keszler, results to be published.
26. H. Sun and D. A. Keszler, Inorg. Chem., submitted.

## CHAPTER 3

STRUCTURE OF  $\text{Ba}_2\text{Cu}(\text{BO}_3)_2$ 

Robert W. Smith and Douglas A. Keszler

Department of Chemistry and Center for Advanced Materials Research

Oregon State University

Gilbert Hall 153

Corvallis, Oregon 97331-4003, USA

Acta Crystallographica, Section C, in press

### Abstract

Dibarium copper orthoborate,  $M_r = 455.82$ , orthorhombic,  $Pnma$ ,  $\underline{a} = 8.023(1)$ ,  $\underline{b} = 11.290(1)$ ,  $\underline{c} = 13.889(1)$  Å,  $V = 1258.1(3)$  Å<sup>3</sup>,  $Z = 8$ ,  $D_x = 4.81$  g cm<sup>-3</sup>, Mo  $K\alpha$ ,  $\lambda = 0.71069$  Å,  $\mu = 157.21$  cm<sup>-1</sup>,  $F(000) = 1592$ ,  $T = 298$  K,  $R = 0.020$ , and  $R_w = 0.031$  for 2069 averaged reflections. The structure features discrete units of formula  $Cu_2(BO_3)_4$  that are interconnected by three crystallographically independent Ba atoms. The copper borate unit is composed of two highly distorted O square planes occupied by the Cu atoms that are bridged by two triangular  $BO_3$  groups. One edge of each  $CuO_4$  group is shared with an additional  $BO_3$  group, resulting in the acute O-Cu-O angles  $71.8(1)^\circ$  and  $72.3(2)^\circ$ .

## Introduction

As part of our program in the synthesis and characterization of new solid-state borates, we recently synthesized the polymorphic compound  $\text{Sr}_2\text{Cu}(\text{BO}_3)_2$  (1) which undergoes a first order phase transition from a low temperature form to a high temperature form at  $800^\circ\text{C}$ . The high temperature  $\beta$ -form exhibits larger coordination numbers for the Sr atoms and a substantial rearrangement of the copper borate network relative to that of the low temperature  $\alpha$ -form.

From an analysis of the phase system  $\text{BaO-CuO-B}_2\text{O}_3$  we have determined that the Ba analog  $\text{Ba}_2\text{Cu}(\text{BO}_3)_2$  crystallizes in one form only, isostructural to  $\beta\text{-Sr}_2\text{Cu}(\text{BO}_3)_2$ . Herein, we describe the crystal structure of this new compound.

## Experimental

Powder samples of the title compound were prepared by grinding stoichiometric ratios of  $\text{Ba}(\text{NO}_3)_2$  (reagent grade, Mallinckrodt),  $\text{Cu}(\text{NO}_3)_2 \cdot 2\frac{1}{2}\text{H}_2\text{O}$  (reagent grade, Mallinckrodt), and  $\text{B}_2\text{O}_3$  (99.99%, Morton Thiokol) under hexane followed by heating at  $900^\circ\text{C}$  for 18 hours; the heating was interrupted several times to grind the sample. Crystals were grown from a melt composed of 50 mol%  $\text{LiBO}_2$  and 50 mol%  $\text{Ba}_2\text{Cu}(\text{BO}_3)_2$ . A crystal with dimensions  $0.22 \times 0.08 \times 0.04$  mm was selected for data collection. Unit cell parameters were derived from a least-squares analysis of the angle settings of 25 reflections in the range  $30^\circ \leq 2\theta \leq 45^\circ$  that were automatically centered on a Rigaku AFC6R diffractometer. Intensity data were collected with the  $\omega$ - $2\theta$  scan technique; intensities of three standard reflections monitored throughout data collection exhibited an average fluctuation of 2.3%. From 4064 reflections measured to  $(\sin\theta_{\text{max}})/\lambda = 1.28 \text{ \AA}^{-1}$  in the index range  $-12 \leq h \leq 12$ ,  $0 \leq k \leq 17$ ,  $0 \leq l \leq 21$ , 2069 unique data with  $F_o^2 \geq 3\sigma(F_o^2)$  were obtained.

All calculations were performed on a microVax II computer with programs from the TEXRAY crystallographic software package (2). Because unit cell dimensions and systematic absences of reflections indicated that the compound was isostructural to  $\beta$ - $\text{Sr}_2\text{Cu}(\text{BO}_3)_2$ , the coordinates for this structure were used as a trial solution. Following refinement with isotropic thermal parameters, the data were corrected for absorption with the computer program DIFABS (3) and subsequently averaged ( $R_{\text{int}} = 0.024$ ). Final refinement on  $F_o$  for

those data having  $F_o^2 \geq 3\sigma(F_o^2)$  with 113 variables and 2069 observations resulted in  $R = 0.020$ ,  $R_w = 0.031$ , and  $\Delta/\sigma = 0.06$  where the weights are derived from counting statistics and a value of  $p = 0.05$ . The isotropic extinction parameter =  $4.5 \times 10^{-7}$  (4) and  $S = 0.92$ . A maximum peak of  $0.77 \text{ e } \text{\AA}^{-3}$  is observed in the final difference electron density map, corresponding to 0.40% of a Ba atom. Final atomic coordinates of the compound are given in Table 3.1.

Table 3.1 Final atomic coordinates for  $\text{Ba}_2\text{Cu}(\text{BO}_3)_2$ .

Atom	x	y	z	$B_{\text{eq}}$
Ba(1)	0	0	0	0.86(1)
Ba(2)	0.37931(4)	1/4	0.95179(2)	0.75(1)
Ba(3)	0.16013(2)	0.01993(2)	0.71717(1)	0.69(1)
Cu(1)	0.30766(8)	1/4	0.57279(5)	0.87(2)
Cu(2)	0.03874(8)	1/4	0.30007(4)	0.80(2)
B(1)	0.0634(7)	1/4	0.1290(4)	0.9(2)
B(2)	0.4896(6)	1/4	0.7078(4)	0.6(2)
B(3)	0.1337(5)	0.4281(3)	0.4365(3)	0.7(1)
O(1)	0.0762(5)	1/4	0.7093(3)	1.0(1)
O(2)	0.0676(5)	1/4	0.0336(3)	1.2(1)
O(3)	0.4386(3)	0.1461(2)	0.6615(2)	0.9(1)
O(4)	0.2993(3)	0.4740(2)	0.8936(2)	1.1(1)
O(5)	0.0603(4)	0.1472(2)	0.1864(2)	1.3(1)
O(6)	0.4981(3)	0.1304(2)	0.1055(2)	1.0(1)
O(7)	0.1932(3)	0.1125(2)	0.5235(2)	1.0(1)

The magnetic moment of the compound was measured at 22°C by the Gouy method. Measurements were made at a field strength of 5 kgauss, using an Alpha Model AL 7500 water-cooled magnet with 4 inch pole faces and a 1.5 inch air gap. The Gouy tube was calibrated with the standard  $\text{HgCo}(\text{SCN})_4$ . Diamagnetic corrections to molar susceptibilities were made from reported values (5).

### Discussion

A drawing of the contents of the unit cell is illustrated in Figure 3.1 and selected interatomic distances and angles are listed in Table 3.2. The compound is isostructural to the high temperature form of the orthoborate  $\text{Sr}_2\text{Cu}(\text{BO}_3)_2$ . The volume of the unit cell is

Table 3.2 Selected distances (Å) and angles (°) for  $\text{Ba}_2\text{Cu}(\text{BO}_3)_2$ .

Atoms	Distance		Angle
Cu(1)-O(3)	2.000(2) x 2	O(3)-Cu(1)-O(3)	71.8(1)
Cu(1)-O(7)	1.929(3) x 2	O(7)-Cu(1)-O(7)	107.2(2)
		O(3)-Cu(1)-O(7)	89.8(1)
Cu(2)-O(5)	1.967(3) x 2	O(5)-Cu(2)-O(5)	72.3(2)
Cu(2)-O(6)	1.911(3) x 2	O(6)-Cu(2)-O(6)	89.9(2)
		O(5)-Cu(2)-O(6)	98.6(1)
B(1)-O(2)	1.325(7)	O(2)-B(1)-O(5)	124.5(2)
B(1)-O(5)	1.409(4) x 2	O(5)-B(1)-O(5)	111.0(4)
B(2)-O(1)	1.345(6)	O(1)-B(2)-O(3)	123.0(2)
B(2)-O(3)	1.399(4) x 2	O(3)-B(2)-O(3)	114.0(4)
B(3)-O(4)	1.366(4)	O(4)-B(3)-O(6)	120.4(3)
B(3)-O(6)	1.400(4)	O(6)-B(3)-O(7)	118.5(3)
B(3)-O(7)	1.378(4)	O(7)-B(3)-O(4)	121.1(3)

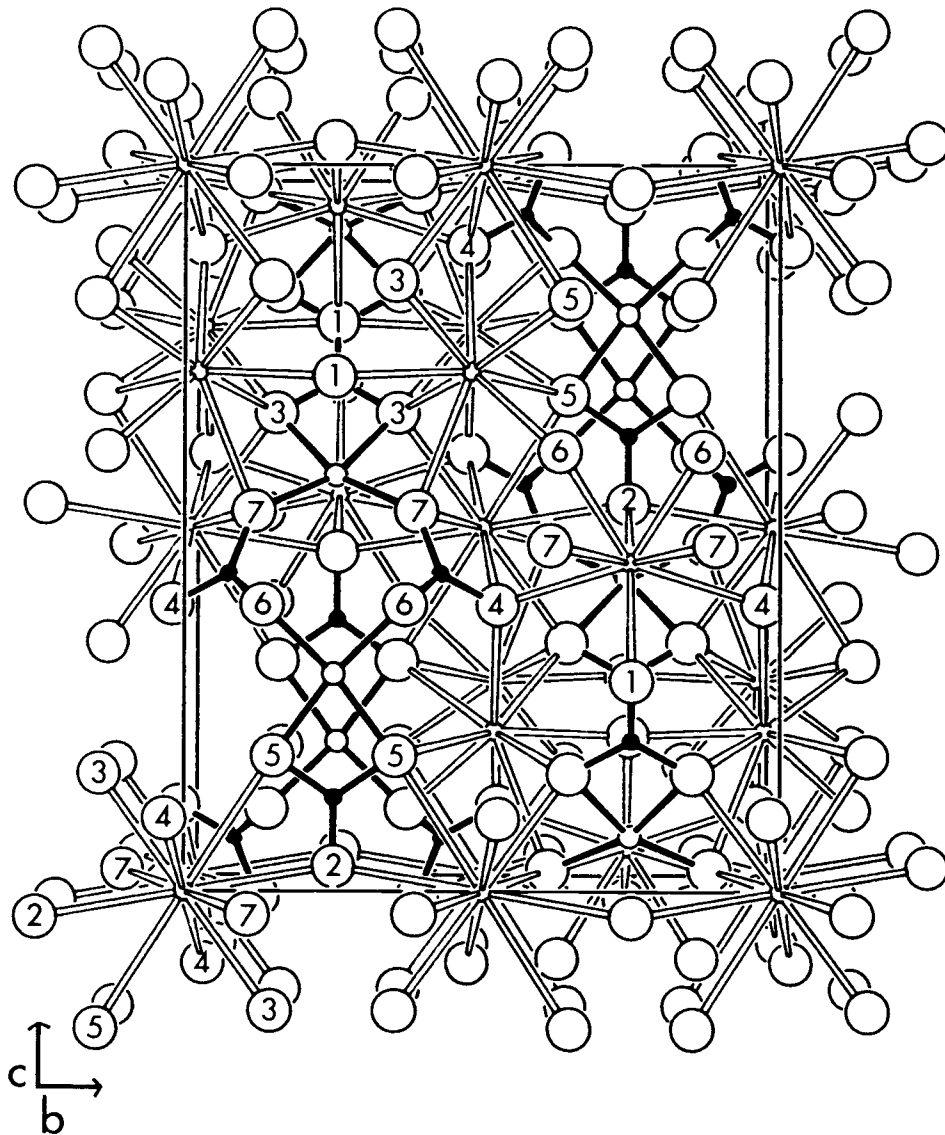


Figure 3.1 Labeled sketch of the unit cell for  $\text{Ba}_2\text{Cu}(\text{BO}_3)_2$ .

approximately 13% larger than that of the Sr analog, reflecting the larger crystal radius of the Ba atom.

The primary structural feature is the discrete unit  $\text{Cu}_2(\text{BO}_3)_4$  illustrated in Figure 3.2. It consists of two highly distorted O square planes that are occupied by Cu atoms. These planes are bridged by sharing O vertices with two  $\text{BO}_3$  triangles centered by atom B(3). At each end of the unit a  $\text{CuO}_4$  group shares an edge with a triangular  $\text{BO}_3$  group. Such an edge-shared  $\text{BO}_3$  group is somewhat unusual in the structural chemistry of borates; it forces, in the present material, the acute angles  $71.8(1)^\circ$  and  $72.3(2)^\circ$  for the interactions O(3)-Cu(1)-O(3) and O(5)-Cu(2)-O(5), respectively. The unit exhibits mirror symmetry with the atoms Cu(1), Cu(2), B(1), B(2), O(1), and O(2) occupying positions on the mirror plane at  $y = \frac{1}{4}$ . Also, as seen in Figure 3.2, when viewed along the direction [010] a substantial deviation from planarity is observed with a significant bend at atom O(6).

The average Cu(1)-O and Cu(2)-O distances,  $1.96(2) \text{ \AA}$  and  $1.94(2) \text{ \AA}$ , are comparable to that,  $1.95(1) \text{ \AA}$ , reported for the compound  $3\text{CuO} \cdot \text{B}_2\text{O}_3$  (6). Perturbations in the planarity of the  $\text{CuO}_4$  groups are evidenced by the angles O(3)-Cu(1)-O(7),  $160.2(1)^\circ$ , and O(5)-Cu(2)-O(6),  $169.5(1)^\circ$ . Dissimilar deviations from a square geometry are noted from the angles O(6)-Cu(2)-O(6),  $89.9(2)^\circ$ , and O(7)-Cu(1)-O(7),  $107.2(2)^\circ$ . These angles are consistent with the chemical inequivalence of the atoms O(6) and O(7); atom O(6) binds to four nearest cations while atom O(7) binds to five cations.

The mean B-O bond length,  $1.38(1) \text{ \AA}$ , agrees with the expected

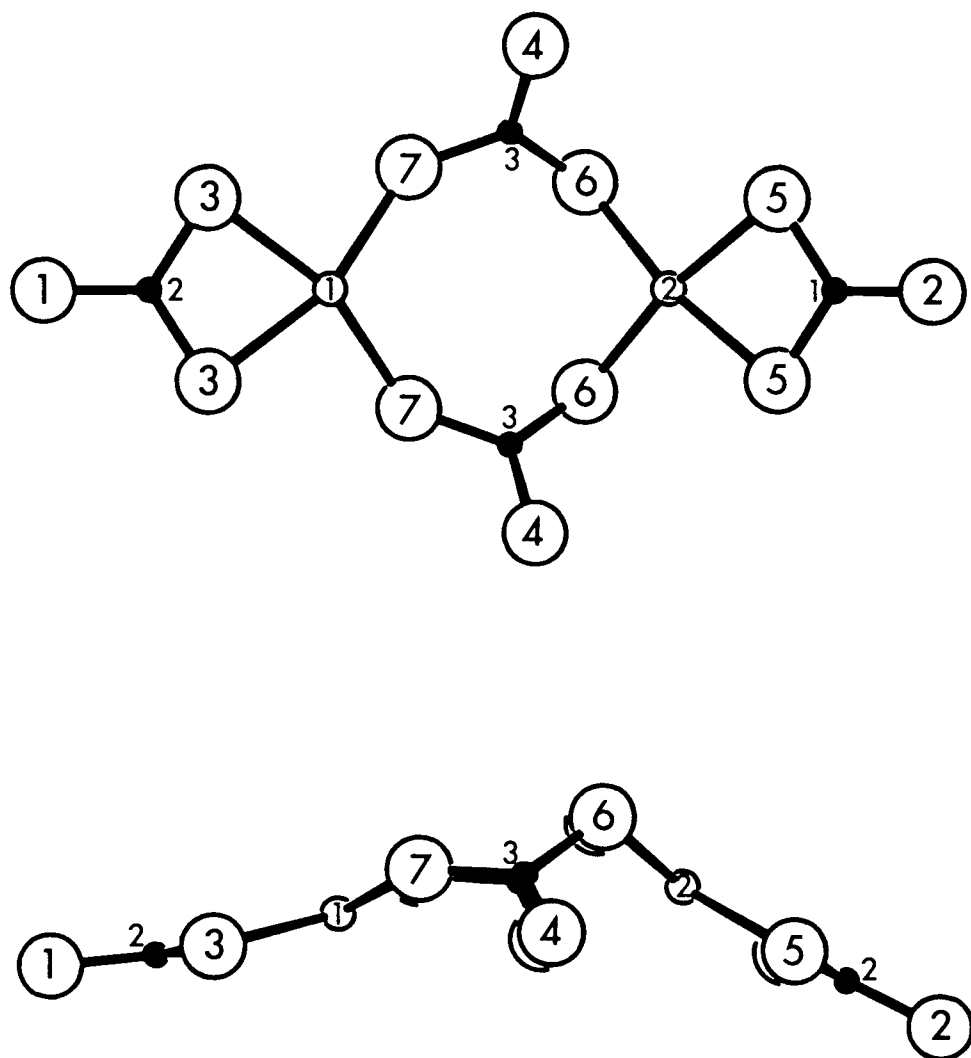


Figure 3.2 Sketches of the  $\text{Cu}_2(\text{BO}_3)_4$  unit.  
 (top) View along the direction orthogonal  
 to the mirror plane at  $y = \frac{1}{4}$ .  
 (bottom) View along  $[010]$ .

value, 1.375 Å (7). Substantial reductions below the ideal trigonal angle, 120°, are observed for the interactions O(5)-B(1)-O(5), 111.0(4)°, and O(3)-B(2)-O(3), 114.0(4)°, that are involved in edge-sharing with the CuO<sub>4</sub> group.

The environments of the three crystallographically inequivalent Ba atoms are depicted in Fig. 3.3. Atom Ba(1) binds to ten O atoms placed at the vertices of a distorted bicapped cube. Atoms Ba(2) and Ba(3) each coordinate to eight O atoms placed at the vertices of a distorted square antiprism and an irregular dodecahedron, respectively. The mean Ba-O distances are 2.90(4), 2.79(4), and 2.81(5) Å for the interactions Ba(1)-O, Ba(2)-O, and Ba(3)-O, respectively. These values compare well to the values 2.90 Å for a ten-coordinate Ba atom and 2.80 Å for an eight-coordinate Ba atom calculated from crystal radii (8).

The effective magnetic moment for the compound at 22°C is 1.74(2) BM. This is a typical value for a d<sup>9</sup>, Cu<sup>2+</sup> compound with primarily spin-only contributions to the magnetic moment.

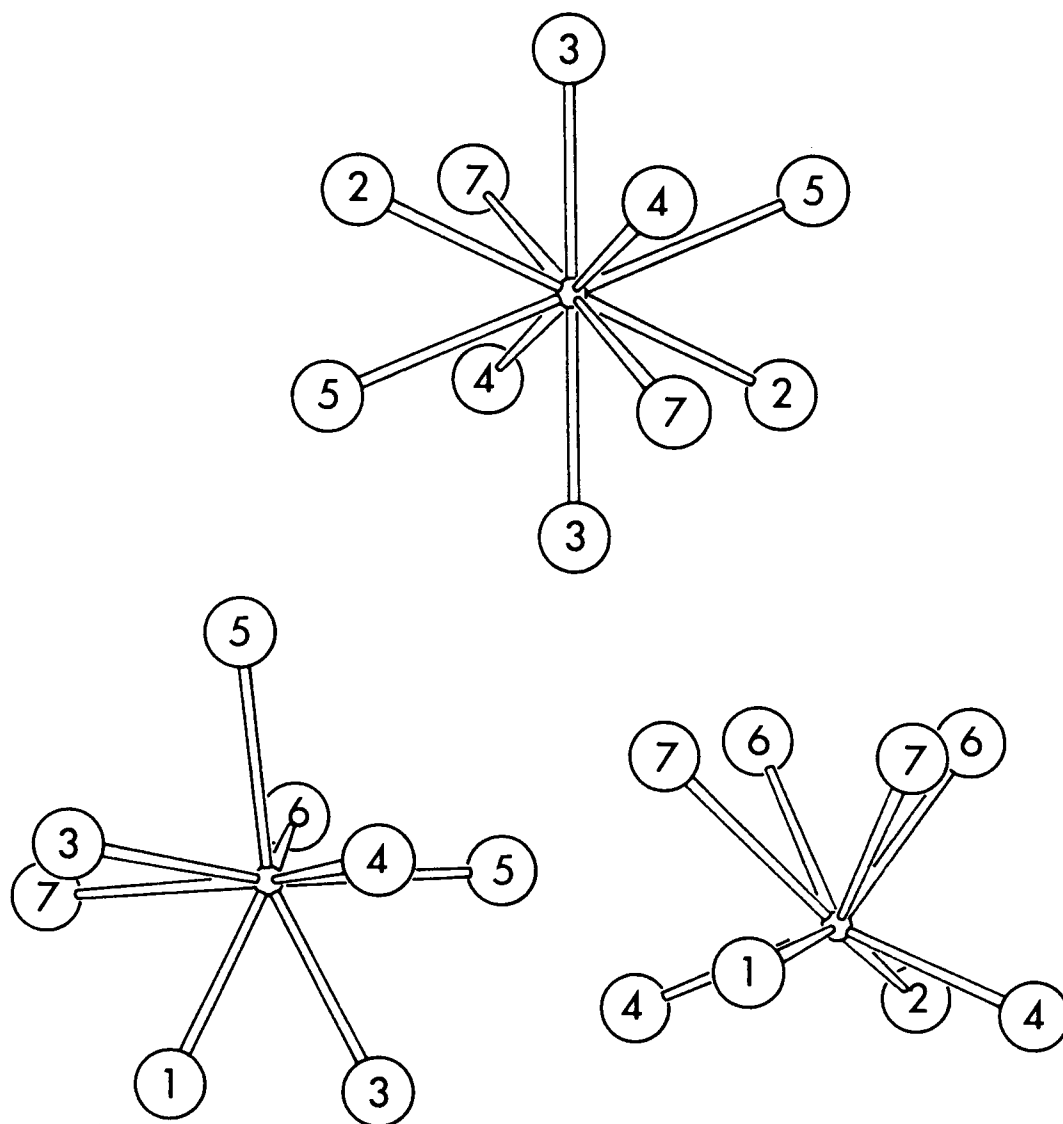


Figure 3.3 Sketches of Ba environments in  $\text{Ba}_2\text{Cu}(\text{BO}_3)_2$ .  
(clockwise from top: environments for Ba(1), Ba(2), and Ba(3)).

### Acknowledgements

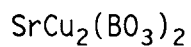
Funds for this work were provided by the Murdock Charitable Trust of the Research Corporation. DAK thanks the Alfred P. Sloan Foundation for a research fellowship (1989-1991).

## References

1. R. W. Smith and D. A. Keszler, J. Solid State Chem. **81**, 305 (1989).
2. Molecular Structure Corporation, "TEXRAY," MSC, 3200A Research Forest Drive, The Woodlands, TX 77381, USA (1985).
3. N. Walker and D. Stuart, Acta Crystallogr., Sect. A **39**, 158 (1983).
4. W. H. Zachariasen, Acta Crystallogr., Sect. A **24**, 214 (1968).
5. L. N. Mulay and E. A. Boudreaux, "Theory and Application of Molecular Diamagnetism," pp. 306-307, Wiley, New York (1976).
6. H. Behm, Acta Crystallogr., Sect. B **38**, 2781 (1982).
7. A. F. Wells, "Structural Inorganic Chemistry, 4th ed.," p. 862, Clarendon Press, Oxford (1975).
8. R. D. Shannon and C. T. Prewitt, Acta Crystallogr., Sect. B **25**, 925 (1969).

## CHAPTER 4

SYNTHESIS, STRUCTURE, AND PROPERTIES OF THE ORTHOBORATE



Robert W. Smith and Douglas A. Keszler

Department of Chemistry and Center for Advanced Materials Research

Oregon State University

Gilbert Hall 153

Corvallis, Oregon 97331-4003, USA

For Submission to Journal of Solid State Chemistry

### Abstract

The new orthoborate  $\text{SrCu}_2(\text{BO}_3)_2$  has been synthesized and its structure determined by single-crystal X-ray methods. It crystallizes in a tetragonal cell of dimensions  $a = 8.995(1)$  and  $c = 6.649(1)$  Å with  $Z = 4$ ; the space group is  $I\bar{4}2m$ . The structure was determined from 604 independent reflections and refined to the final residuals  $R = 0.040$  and  $R_w = 0.051$ . It is composed of  $\text{CuO}_4$  rectangles and  $\text{BO}_3$  triangles that are connected to form an infinite two-dimensional sheet; Sr atoms are interleaved between successive sheets. The compound decomposes at  $970(3)^\circ\text{C}$  to CuO and amorphous strontium borate; the CuO is reduced to finely divided Cu metal by heating at  $300^\circ\text{C}$  in a reducing atmosphere. The corrected molar susceptibility of the borate is  $2.16(3)$  BM at  $22^\circ\text{C}$ .

## Introduction

Copper occurs in a wide variety of catalysts used in the industrial production of chemicals. These include the production of methanol from synthesis gas (1) and the hydration of acrylonitrile to acrylamide (2). In each case the activity of the catalyst is directly proportional to the surface area of the copper catalyst. Consequently, catalyst efficacy may be enhanced from new materials that afford effective methods for producing finely divided particles.

As part of our program to synthesize incongruent phases that will afford, on decomposition, catalytic species impregnated on supports of varying acidities, we have discovered a new compound in the Sr-Cu-B-O system. This simple orthoborate,  $\text{SrCu}_2(\text{BO}_3)_2$ , decomposes above  $970^\circ\text{C}$  to finely divided  $\text{CuO}$  and amorphous strontium borate. Subsequent heating at  $300^\circ\text{C}$  in a reducing atmosphere reduces the  $\text{CuO}$  to  $\text{Cu}$  metal.

In this report we describe the preparation, crystal structure, magnetic moment, and phase decomposition of the new compound  $\text{SrCu}_2(\text{BO}_3)_2$  and the characteristics of the  $\text{CuO}$  and  $\text{Cu}$  metal that are produced by heat treatment.

## Experimental

### Synthesis

The title compound was prepared by grinding a stoichiometric ratio of  $\text{Sr}(\text{NO}_3)_2$  (reagent grade, Mallinckrodt),  $\text{Cu}(\text{NO}_3)_2 \cdot 2\frac{1}{2}\text{H}_2\text{O}$  (reagent grade, Mallinckrodt), and  $\text{B}_2\text{O}_3$  (99.99%, Morton Thiokol) under hexane to a fine powder and then calcining at  $600^\circ\text{C}$  for 30 minutes. The samples were then heated at  $850^\circ\text{C}$  for 18 hours with the heat treatment interrupted several times to grind the sample. Except for some weak lines attributable to  $\text{CuO}$ , the powder X-ray diffractograms were single phase as determined by analysis of data from a Philips powder diffractometer equipped with graphite-monochromated  $\text{Cu K}\alpha$  radiation.

Single crystals were grown with the compound  $\text{LiBO}_2$  as a flux. A mixture in the solute:flux ratio of 7:1 by mass was heated in a Pt crucible to  $850^\circ\text{C}$ , cooled at  $6^\circ\text{C}/\text{hour}$  to  $600^\circ\text{C}$ , then air-quenched. Blue single crystals were physically separated from the crucible for structure determination.

### X-ray Work

A crystal with dimensions  $0.20 \times 0.08 \times 0.03$  mm was chosen for structure analysis. Lattice parameters were refined from 20 reflections in the range  $30^\circ < 2\theta < 40^\circ$  that were automatically centered on a Rigaku AFC6R diffractometer equipped with monochromatic  $\text{Mo K}\alpha$  radiation. Intensity data in the range of indices  $-19 \leq h \leq 19$ ,  $0 \leq k \leq 19$ , and  $0 \leq l \leq 14$  were collected with the  $\omega$ - $2\theta$  scan technique at

a scan speed of  $16^\circ/\text{minute}$  in  $\omega$  and a scan width  $\Delta\omega = (1.25 + 0.3 \tan\theta)^\circ$ . From 2061 reflections measured to  $2\theta = 100^\circ$ , 604 unique data having  $F_0^2 \geq 3\sigma(F_0^2)$  were obtained. Three reflections monitored every 199 measurements showed no significant deviations throughout the data collection.

All calculations were performed on a microVax II computer with programs from the TEXRAY crystallographic software package (3). The Laue symmetry  $4/mmm$  and the systematic absence  $hkl, h+k+l = 2n+1$ , are consistent with the acentric groups  $I422$ ,  $I4mm$ ,  $I\bar{4}m2$ , and  $I\bar{4}2m$  and the centric group  $I4/mmm$ . The statistical distribution of intensities indicate that the structure is acentric (4). The Patterson vectors also indicate that the structure is layered with the heavy Sr atoms separated from sheets of Cu, B, and O atoms by  $z = \frac{1}{4}$ . A successful solution was found by drawing numerous layers of appropriate composition in the four acentric space groups that were consistent with the Patterson map and afforded reasonable interatomic distances. Successful solution and refinement were achieved with the space group  $I\bar{4}2m$ .

Following refinement with isotropic thermal parameters, the data were corrected for absorption with the computer program DIFABS (5) and subsequently averaged. Final least-squares refinement on  $F_0$  with data having  $F_0^2 \geq 3\sigma(F_0^2)$  and anisotropic temperature factors on each atom resulted in the residuals  $R = 0.040$  and  $R_w = 0.051$ . The largest peak in the final difference map has a height of 2.4% of an Sr atom. Additional crystal data and experimental conditions are summarized in Table 4.1.

Table 4.1 Crystal data and experimental conditions for  $\text{SrCu}_2(\text{BO}_3)_2$ .

Crystal data	Experimental conditions
Diffractometer	Rigaku AFC6R
Radiation	Graphite monochromated Mo $K\alpha$
Formula wt., amu	332.33
$a$ , Å	8.995(1)
$c$ , Å	6.649(1)
$V$ , Å <sup>3</sup>	537.9(1)
Space group	$I\bar{4}2m$
$D_{\text{calc}}$ , g cm <sup>-3</sup>	4.13
Crystal vol., mm <sup>3</sup>	0.0005
F(000)	616
Z	4
Linear abs. coeff., cm <sup>-1</sup>	175.33
$\mu$ factor	0.05
No. unique data with $F_0^2 > 3\sigma(F_0^2)$	604
$R_{\text{int}}$	0.076
$R(F)$	0.040
$R_w(F)$	0.051
Error in observation of unit wt., e <sup>2</sup>	1.34

Unit cell parameters were also determined from powder X-ray data by least-squares refinement of  $2\theta$  values. Powder samples were ground and sieved with a 100 mesh wire screen and then annealed at  $700^{\circ}\text{C}$  for 2 hours. Eight intense reflections in the range  $30^{\circ} < 2\theta < 60^{\circ}$  were collected on a Philips diffractometer using Si (NBS Standard Reference Material 640b) as the internal standard. The refined cell parameters  $a = 8.991(1) \text{ \AA}$  and  $c = 6.660(3) \text{ \AA}$  compare well to those from the single-crystal data.

### Measurements

A Harrop model DT-726 differential thermal analyzer interfaced to a PC via a Metrabyte DAS-8 A/D converter and Series M1000 signal conditioner was used to obtain DTA data. The sample and reference ( $\text{Al}_2\text{O}_3$ ) were enclosed in Pt cups and heated at  $10^{\circ}\text{C}/\text{minute}$ . A strong endothermic signal observed at  $970(3)^{\circ}\text{C}$  corresponds to decomposition of the phase.

The effective magnetic moment was obtained at  $22^{\circ}\text{C}$  by the Guoy method. The measurement was made at a field strength of 5 kG using an Alpha Model AL 7500 water-cooled magnet with 4 inch pole faces and a 1.5 inch air gap. The Guoy tube was calibrated with  $\text{HgCo}(\text{SCN})_4$ . Diamagnetic corrections to molar susceptibilities were made from reported values except for the  $\text{Sr}^{2+}$  ion whose correction was determined by interpolation (6).

## Results and Discussion

### Structure

Final atomic coordinates and thermal parameters are listed in Table 4.2 and selected bond distances and angles are given in Table 4.3. Views of the unit cell along the  $a$  and  $c$  axes are shown in Figures 4.1 and 4.2, respectively.

The structure is a simple, new type exhibiting layers of interconnected triangular, planar  $\text{BO}_3$  and rectangular, planar  $\text{CuO}_4$  groups. These infinite two-dimensional layers extend parallel to the plane (001) (Figure 4.2); a portion of the layer is depicted in Figure 4.3. Each  $\text{CuO}_4$  rectangle shares one edge with a  $\text{BO}_3$  triangle through the O(2) atoms and the opposite edge with another  $\text{CuO}_4$  group through the O(1) atoms, affording a layer of Cu-centered dimeric units bridged by  $\text{BO}_3$  groups. The connectivity affords hollows defined by four O(2) atoms. Successive stacking of the sheets with the application of the improper 4-fold axis of rotation generates distorted cubic pockets of O(2) atoms between the layers that are occupied by the Sr atoms. A similar two-dimensional layered structure is seen in the pyroborate  $\text{BaCuB}_2\text{O}_5$  in which the Ba atoms interleave successive sheets comprised of vertex-sharing  $\text{CuO}_4$  squares and  $\text{B}_2\text{O}_5$  groups (7).

The average Cu-O distance of 1.94(1) Å is similar to values determined in other complex copper(II) borates, e.g. 1.930(6) Å in  $\alpha\text{-Sr}_2\text{Cu}(\text{BO}_3)_2$ , 1.94(3) Å in  $\beta\text{-Sr}_2\text{Cu}(\text{BO}_3)_2$  (8), and 1.95(2) Å in  $\text{Ba}_2\text{Cu}(\text{BO}_3)_2$  (9). Bond angles reflect the distortion of the  $\text{CuO}_4$  groups that arises from sharing the O(2)···O(2) edge with a B atom

Table 4.2 Final atomic coordinates and temperature factors for  
 $\text{SrCu}_2(\text{BO}_3)_2$ .

Atom	Wyckoff Notation	x	y	z	$B_{\text{eq}}$
Sr	4(c)	0	1/2	0	0.71(2)
Cu	8(i)	0.11412(1)	0.11412	0.2783(2)	0.93(1)
B	8(i)	0.2953(4)	0.2953	0.243(1)	0.74(9)
O(1)	8(i)	0.4004(4)	0.4004	0.212(1)	1.5(1)
O(2)	16(j)	0.3276(3)	0.1456(3)	0.254(1)	0.9(1)

Atom	$U_{11}$	$U_{22}$	$U_{33}$	$U_{12}$	$U_{13}$	$U_{23}$
Sr	0.0108(3)	0.0107(3)	0.0054(2)	0	0	0
Cu	0.0081(2)	0.0081	0.0191(4)	-0.0001(2)	0.0004(2)	0.0004
B	0.008(1)	0.008	0.012(2)	-0.000(1)	-0.001(1)	-0.001
O(1)	0.009(1)	0.009	0.040(4)	0.000(1)	-0.007(1)	-0.007
O(2)	0.009(1)	0.008(1)	0.018(1)	0.001(1)	0.001(1)	0.002(1)

From symmetry constraints  $U_{12}$ ,  $U_{13}$ , and  $U_{23} = 0$  for Sr and  $U_{11} = U_{22}$  and  $U_{13} = U_{23}$  for Cu, B, and O(1).

Table 4.3 Selected distances (Å) and angles (°) for SrCu<sub>2</sub>(BO<sub>3</sub>)<sub>2</sub>.

Atoms	Distance		Angle
Sr-0(2)	2.608(4) × 4	0(2)-Sr-0(2)	79.12(8)
Sr-0(2)	2.640(4) × 4	0(2)-Sr-0(2)	66.34(4)
Cu-0(1)	1.929(3) × 2	0(1)-Cu-0(1)	82.2(2)
Cu-0(2)	1.947(3) × 2	0(2)-Cu-0(2)	72.9(2)
		0(1)-Cu-0(2)	102.4(1)
		0(1)-Cu-0(2)	174.7(2)
B-0(1)	1.353(7)	0(1)-B-0(2)	122.9(2)
B-0(2)	1.379(4) × 2	0(2)-B-0(2)	114.1(4)

and the 0(1)···0(1) edge with a Cu atom. The acute angle of 72.9(2)° for 0(2)-Cu-0(2) is similar to values observed in  $\beta$ -Sr<sub>2</sub>Cu(BO<sub>3</sub>)<sub>2</sub> and Ba<sub>2</sub>Cu(BO<sub>3</sub>)<sub>2</sub> where edges are shared between rectangular CuO<sub>4</sub> and triangular BO<sub>3</sub> polyhedra (8,9). The shared edge 0(1)···0(1) affords a smaller acute angle of 82.2(2)°. Planarity of the CuO<sub>4</sub> rectangle is only slightly distorted as evidenced by the angle 0(1)-Cu-0(2), 174.7(2)°. Inspection of the central portion of the unit cell sketched in Figure 4.1 reveals that 0(1) atoms occupy positions over the Cu atom along the *c* axis, affording the appearance of cubane-like fragments Cu<sub>4</sub>O<sub>4</sub>. These Cu-0(1) interactions that are approximately

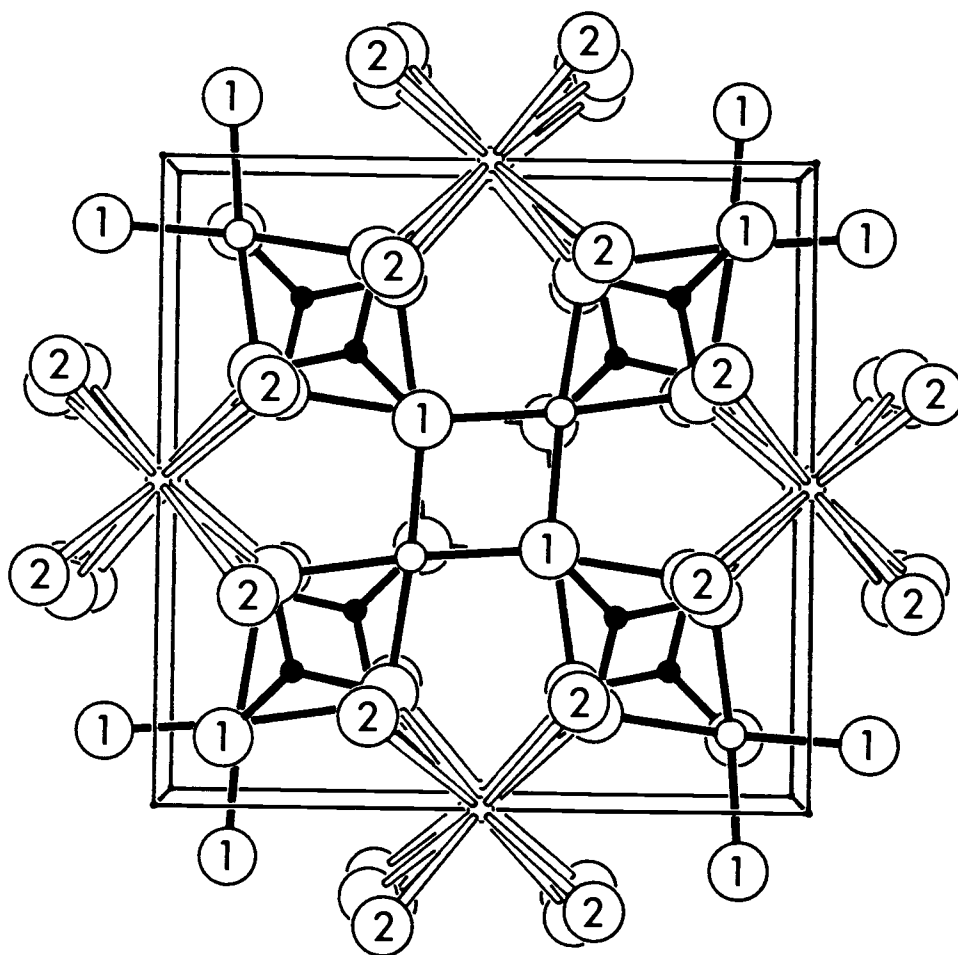


Figure 4.1 Sketch of the unit cell viewed down [001].

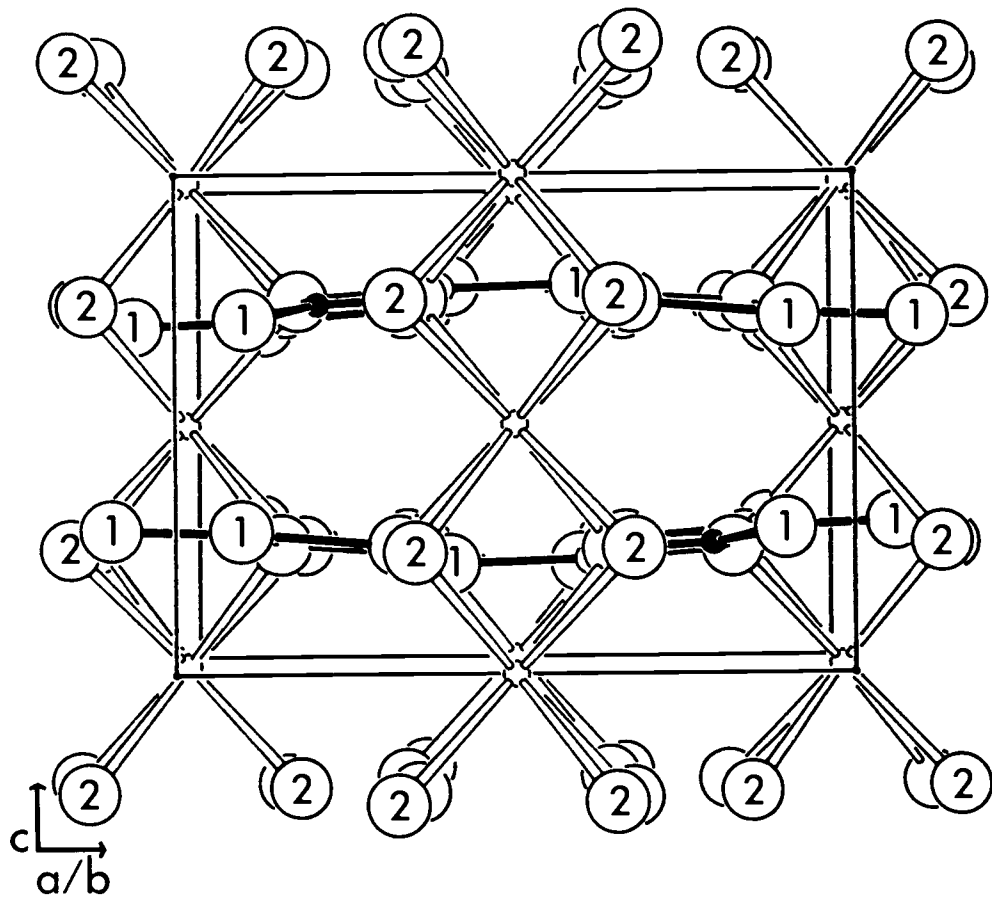


Figure 4.2 Sketch of the unit cell viewed down  $\langle 100 \rangle$ .

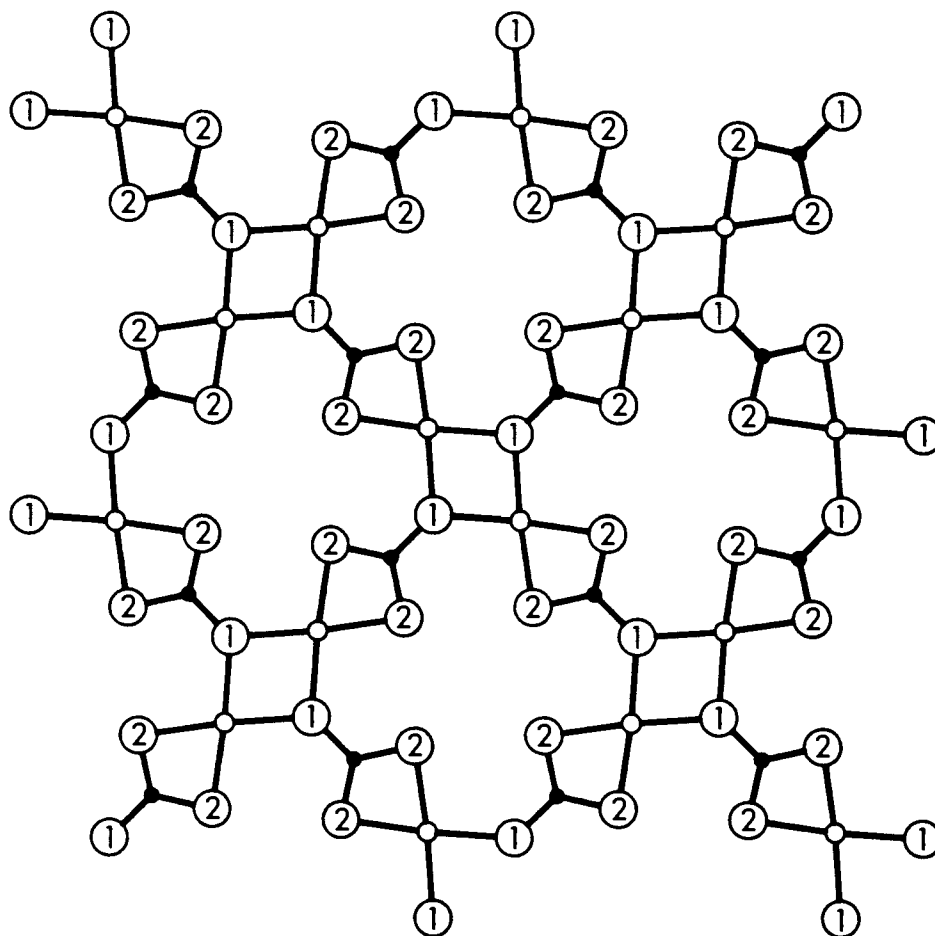


Figure 4.3 Sketch of a portion of the infinite Cu-B-O network parallel to the (001) plane.

parallel to the  $c$  axis are greater than 3.25 Å.

The orthoborate groups are somewhat irregular. The average B-O bond distance of 1.37(1) Å compares well to the expected distance of 1.365 Å for a three-coordinate B atom (10). Bond angles are only slightly distorted because of the shared edge O(2)···O(2) with the Cu atom. Thus, the O(2)-B-O(2) angle is reduced from the ideal 120° to 114.1(1)° and the O(1)-B-O(2) angles are increased to 122.9(2)°.

The Sr atom occupies an eight-coordinate, distorted cubic environment with the cube elongated along the improper fourfold axis as evidenced by the angles shown in Figure 4.4. The average Sr-O distance is 2.62(2) Å which is similar to the expected value of 2.63 Å that is calculated from the crystal radii of the eight-coordinate Sr<sup>2+</sup> ion and the four-coordinate O<sup>2-</sup> ion (11). Atom O(1) is three-coordinate, bonding to two Cu atoms and one B atom, and atom O(2) is four-coordinate, bonding to two Sr atoms, one Cu atom, and one B atom.

### Effective Magnetic Moment

The effective magnetic moment at 22°C of the title compound is 2.16(3) BM. This value is less than the expected spin-only value of 2.83 BM for a compound with two atoms with a d<sup>9</sup> electronic configuration. The moment likely results from antiferromagnetic coupling between the Cu atoms of the dimer by exchange coupling through the O(1) atoms.

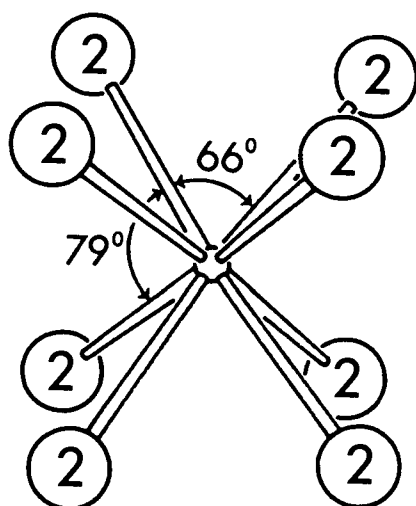


Figure 4.4 Sr environment in  $\text{SrCu}_2(\text{BO}_3)_2$ .

### Differential Thermal Analysis

Samples of  $\text{SrCu}_2(\text{BO}_3)_2$  were heated at  $10^\circ\text{C}/\text{minute}$  to  $1050^\circ\text{C}$  on the DTA. A strong signal was observed at  $970^\circ\text{C}$  which indicated decomposition of the sample. Inspection of the samples revealed that they had melted and changed color from blue to black. Analysis of powder X-ray diffractograms of the black samples revealed only peaks attributable to  $\text{CuO}$ , a result of incongruent melting. On reduction of the  $\text{CuO}$  to  $\text{Cu}$  metal, an X-ray pattern exhibits only peaks attributable to  $\text{Cu}$  metal. Thus, the strontium borate remains amorphous throughout the heat treatment.

### Particle Size Analysis

A primary concern in processing catalytic materials is maximizing the surface area of the active component. Results from previous studies have indicated that very active  $\text{Cu}$  catalysts can be produced from decomposition of a single-phase  $\text{Cu-Zn}$  mixed basic carbonate (12) which affords finely dispersed  $\text{CuO}$ .

The title compound also decomposes to finely divided  $\text{CuO}$  which can be reduced to  $\text{Cu}$  metal. We used Scherrer's equation [1]

$$L_{hkl} = 0.89\lambda/\beta_{hkl}\cos\theta \quad [1]$$

to determine the crystallite size of the products  $\text{CuO}$  and  $\text{Cu}$ ;  $L_{hkl}$  is the particle dimension,  $\lambda$  is the radiation wavelength, and  $\beta_{hkl}$  is the peak width (radians) at half height observed for the sample minus the peak width observed for the internal standard  $\text{NaCl}$  (13),

the standard having a crystallite dimension much greater than 2000 Å. It is assumed in Equation [1] that peak broadening arises only from crystallite size and not from lattice distortions or stresses.

Heating the title compound for 30 minutes at 1050°C afforded a sample of CuO with a mean crystallite dimension of 320 Å as measured by the widths of the  $(11\bar{1})$ -(002), (111)-(200), and  $(20\bar{2})$  reflections. Subsequent heating at 300°C in 5% H<sub>2</sub>/Ar for 3 hours resulted in Cu particles with an average dimension of 390 Å as determined from the widths of the (111), (200), and (220) reflections. Assuming that the Cu crystallite morphology is spherical, this size corresponds to a Cu surface area of 17 m<sup>2</sup>/g of Cu metal. This value compares with surface areas of 38-77 m<sup>2</sup>/g for mixed Cu/Zn oxides prepared from hydroxycarbonate precursors as determined by reaction of N<sub>2</sub>O with the reduced Cu metal (14). Although the quantitative results from the Scherrer method are usually unreliable, the results do indicate that small particles are produced since annealed samples of CuO and Cu metal afford little broadening of the measured X-ray diffraction peaks.

Attempts to synthesize the Ni and Pd analogs of the strontium copper diorthoborate were unsuccessful. Solid-state reactions, coprecipitation methods, and freeze-drying techniques resulted in the formation of SrB<sub>2</sub>O<sub>4</sub> and NiO or Pd metal.

### Acknowledgements

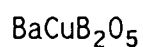
This work was supported by the National Science Foundation, Solid-State Chemistry Program. DAK thanks the Alfred P. Sloan Foundation for a research fellowship (1989-1991).

## References

1. G. C. Chinchin, P. J. Denny, D. G. Porter, G. D. Short, M. S. Spencer, K. C. Waugh, and D. A. Whan, Prepr. Pap.-Am. Chem. Soc., Div. Fuel Chem. **29**, 178 (1984).
2. E. Otsuka, T. Takahashi, N. Hashimoto, and F. Matsuda, Chem. Econ. Eng. Rev. **7** (4), 29 (1975).
3. Molecular Structure Corporation, "TEXRAY," 3200A Research Forest Drive, The Woodlands, TX 77381, USA (1985).
4. E. R. Howells, D. C. Phillips, and D. Rodgers, Acta Crystallogr. **3**, 210 (1950).
5. N. Walker and D. Stuart, Acta Crystallogr., Sect. A **24**, 214 (1968).
6. L. N. Mulay and E. A. Boudreaux, "Theory and Applications of Molecular Diamagnetism," pp. 306-307, Wiley, New York (1976).
7. R. W. Smith and D. A. Keszler, results to be published.
8. R. W. Smith and D. A. Keszler, J. Solid State Chem. **81**, 305 (1989).
9. R. W. Smith and D. A. Keszler, Acta Crystallogr., Sect. C, in press.
10. A. F. Wells, "Structural Inorganic Chemistry, 4th ed.," p. 862, Clarendon Press, Oxford (1975).
11. R. D. Shannon and C. T. Prewitt, Acta Crystallogr., Sect. B **25**, 925 (1969).
12. G. Petrini, A. Bossi, and F. Garbassi, Studies in Surface Science and Catalysis **16**, 735 (1983).
13. H. P. Klug and L. E. Alexander, "X-Ray Diffraction Procedures," p. 689, Wiley, New York (1974).
14. G. Moretti, G. Fierro, M. Lo Jacono, and P. Porta, Surface and Interface Analysis **14**, 325 (1989).

## CHAPTER 5

SYNTHESIS, STRUCTURE, AND PROPERTIES OF THE ACENTRIC PYROBORATE



Robert W. Smith and Douglas A. Keszler

Department of Chemistry and Center for Advanced Materials Research

Oregon State University

Gilbert Hall 153

Corvallis, Oregon 97331-4003, USA

For Submission to Chemistry of Materials

### Abstract

The new acentric pyroborate  $\text{BaCuB}_2\text{O}_5$  has been synthesized and its structure determined by single-crystal X-ray methods. It crystallizes in the monoclinic space group  $C2$  with a cell of dimensions  $a = 6.4848(6)$ ,  $b = 9.1652(9)$ ,  $c = 3.9713(5)$  Å, and  $\beta = 96.14(1)^\circ$ . The structure was determined from 1281 independent reflections and refined to the final residuals  $R = 0.039$  and  $R_w = 0.049$ . It is composed of tetrahedrally distorted  $\text{CuO}_4$  squares and double-triangular  $\text{B}_2\text{O}_5$  groups that are connected to form an infinite two-dimensional layer; Ba atoms interleave parallel layers. The magnetic moment at  $22^\circ\text{C}$  is  $1.69(3)$  BM. Parallel orientation of the pyroborate groups is conducive to enhanced efficiency for optical frequency conversion.

## Introduction

Solid-state borates exhibit a variety of physical and chemical properties, ranging from the nonlinear optical features of the compound  $\text{LiB}_3\text{O}_5$  (1) to the catalytic properties of the copper borate  $\text{Cu}_2\text{Al}_6\text{B}_4\text{O}_{17}$  (2). As part of our effort in the exploratory synthesis of new borates we have investigated the phase diagram  $\text{BaO-CuO-B}_2\text{O}_3$ . In this report we describe the synthesis, structure, and properties of the new acentric pyroborate  $\text{BaCuB}_2\text{O}_5$  which has resulted from this investigation.

## Experimental

### Synthesis and Crystal Growth

The title compound was prepared by grinding a stoichiometric ratio of  $\text{Ba}(\text{NO}_3)_2$  (reagent grade, Mallinckrodt),  $\text{Cu}(\text{NO}_3)_2 \cdot 2\frac{1}{2}\text{H}_2\text{O}$  (reagent grade, Mallinckrodt), and  $\text{B}_2\text{O}_3$  (99.99%, Morton Thiokol) under hexane to a fine powder and calcining at  $600^\circ\text{C}$  for 30 minutes. The samples were then heated at  $800^\circ\text{C}$  for 18 hours with several grindings. Samples were single phase as determined by analysis of X-ray patterns obtained from an automated Philips powder diffractometer equipped with graphite-monochromated  $\text{Cu K}\alpha$  radiation.

Single crystals were grown from a  $\text{PbO}$  flux. A mixture in the solute:flux ratio of 4:1 by mass was heated in a Pt crucible to  $930^\circ\text{C}$ , cooled at  $6^\circ/\text{hour}$  to  $600^\circ\text{C}$ , then air-quenched. Green single crystals were physically separated from the crucible for structure analysis.

### X-ray Work

A crystal with dimensions  $0.24 \times 0.14 \times 0.08$  mm was chosen for structure analysis. Lattice parameters were refined from 15 reflections in the range  $35^\circ < 2\theta < 43^\circ$  that were automatically centered on a Rigaku AFC6R diffractometer equipped with monochromatic  $\text{Mo K}\alpha$  radiation. Intensity data in the range  $0 \leq h \leq 14$ ,  $0 \leq k \leq 20$ , and  $-9 \leq l \leq 9$  were collected with the  $\omega$ - $2\theta$  scan technique at a scan speed of  $16^\circ/\text{minute}$  in  $\omega$  and a scan width  $\Delta\omega = (1.55 + 0.3 \tan\theta)^\circ$ . From 1349 reflections measured to  $2\theta = 100^\circ$ , 1281 unique data having

$F_0^2 \geq 3\sigma(F_0^2)$  were obtained.

Unit cell parameters were also determined from powder X-ray data by least-squares refinement of  $2\theta$  values. Powder samples were ground and sieved with a 100 mesh wire screen and then annealed at 700°C for 2 hours. The  $2\theta$  values of fourteen intense reflections in the range  $26^\circ < 2\theta < 56^\circ$  were determined and corrected using Si (NBS Standard Reference Material 640b) as the internal standard. The cell parameters obtained are  $a = 6.485(2)$ ,  $b = 9.170(3)$ ,  $c = 3.974(1)$  Å, and  $\beta = 96.11(3)^\circ$  which compare well to the single-crystal data.

#### Structure Solution and Refinement

All calculations were performed on a microVax II computer with programs from the TEXRAY crystallographic software package (3). Three space groups are consistent with the systematic absences  $hk1$  ( $h+k = 2n+1$ ),  $h01$  ( $h = 2n+1$ ), and  $0k0$  ( $k = 2n+1$ ), acentric  $C2$  or  $Cm$  and centric  $C2/m$ . Results from SHG experiments (vide infra) and the statistical distribution of intensities (4) indicate that the structure is acentric. We favor the space group  $C2$  on the basis of the successful refinement in this group.

The positional parameters for the Ba and Cu atoms were found by using the computer program MITHRIL (5) and the remaining atomic coordinates were determined from subsequent difference electron density maps. Following refinement with isotropic thermal parameters the data were corrected for absorption with the computer program DIFABS (6). Final least-squares refinement on  $F_0$  with data having  $F_0^2 \geq 3\sigma(F_0^2)$  and anisotropic temperature factors resulted in the residuals

Table 5.1 Crystal data and experimental conditions for BaCuB<sub>2</sub>O<sub>5</sub>.

Diffractometer	Rigaku AFC6R
Radiation	Graphite monochromated Mo K $\alpha$ ( $\lambda = 0.70926 \text{ \AA}$ )
Formula wt., amu	302.49
$a$ , $\text{\AA}$	6.4848(6)
$b$ , $\text{\AA}$	9.1652(9)
$c$ , $\text{\AA}$	3.9713(5)
$\beta$ , deg.	96.14(1)
$V$ , $\text{\AA}^3$	234.68(8)
Space group	C2
$D_{\text{calc}}$ , $\text{g cm}^{-3}$	4.28
Crystal vol., $\text{mm}^3$	0.0027
$F(000)$	270
$Z$	2
Linear abs. coeff., $\text{cm}^{-1}$	128.10
$p$ factor	0.05
No. unique data with $F_0^2 > 3\sigma(F_0^2)$	1281
$R(F_0)$	0.039
$R_w(F_0)$	0.049
Error in observation of unit wt., $e^2$	2.40

$R = 0.039$  and  $R_w = 0.049$ . The largest peak in the final difference map has a height of .91% of a Ba atom. Additional crystal data and experimental conditions are summarized in Table 5.1.

### Magnetic Moment

The effective magnetic moment was obtained at 22°C by the Guoy method. Measurements were made at a field strength of 5 kG using an Alpha Model AL 7500 water-cooled magnet with 4 inch pole faces and a 1.5 inch air gap. The Guoy tube was calibrated with  $\text{HgCo}(\text{SCN})_4$ . Diamagnetic corrections the molar susceptibility were made from reported values (7).

### Second Harmonic Generation

A measurement of the efficiency of second harmonic generation by  $\text{BaCuB}_2\text{O}_5$  crystals was obtained with the apparatus schematically diagrammed in Figure 5.1. A  $\text{Nd}^{3+}$ :YAG laser was used to produce the incident IR radiation at a wavelength of 1060 nm. Visible light was filtered out with a Corning 1-75 filter having a transmittance of 87% at 1060 nm and 0% at 530 nm. Several dozen large crystals were placed on a glass quartz plate inside the cell. The intensity of the second harmonic was monitored with a photomultiplier attached to an oscilloscope. IR radiation was filtered from the output with a Corning 7-57 filter having a transmittance of 88% at 530 nm and 1% at 1060 nm. SHG measurements of  $\text{KH}_2\text{PO}_4$  (KDP) crystals served as a standard for the measurement; they were obtained before and after data acquisition from the sample of  $\text{BaCuB}_2\text{O}_5$  crystals.

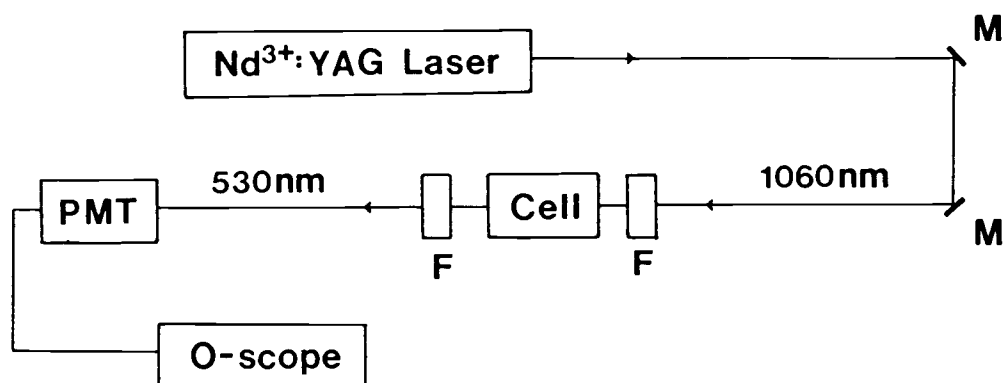


Figure 5.1 Schematic diagram of the apparatus used for SHG measurements.

## Results

### Structure

Final atomic coordinates and anisotropic thermal parameters are given in Table 5.2, selected bond distances and angles are listed in Table 5.3, and a drawing of the the unit cell is shown in Figure 5.2.

The structure is a new type that is best described as containing infinite two-dimensional sheets of fused  $B_2O_5$  double-triangles and  $CuO_4$  squares that extend parallel to the (001) plane; Ba atoms interleave successive sheets. A portion of the infinite, two-dimensional copper pyroborate layer is shown in Figure 5.3. The layer includes tetrahedrally distorted  $CuO_4$  squares, each connected to three pyroborate groups. One pyroborate group shares an edge with the  $CuO_4$  group through two cis O(2) atoms while the other two pyroborate groups share vertices through one O(3) atom each. Hollows bordered by O atoms are present in each layer. The Ba atoms occupy sites above and below these hollows that result from successive stacking of the sheets along the  $c$  axis.

The  $2[CuB_2O_5]$  layer exhibits considerable deviations from planarity. The  $CuO_4$  squares (Figure 5.4a) are tetrahedrally distorted; each pair of trans O vertices is pulled either above or below the plane of the square. This is illustrated by the trans O(2)-Cu-O(3) angle of  $144.0(2)^\circ$ . The four cis O-Cu-O angles also exhibit the tetrahedral distortion with values ranging from  $92.7(2)^\circ$  to  $99.8(3)^\circ$ . Cu-O bond lengths average  $1.93(5)$  Å and are comparable to bond distances seen in other copper borates discovered in this lab,

Table 5.2 Final atomic coordinates and temperature factors for  
BaCuB<sub>2</sub>O<sub>5</sub>.

Atom	Wyckoff Notation	x	y	z	B <sub>eq</sub>	
Ba	2(a)	0	0.0048	0	0.641(7)	
Cu	2(b)	0	0.5946(1)	1/2	0.79(2)	
B	4(c)	0.1792(7)	0.3135(5)	0.401(1)	0.6(1)	
O(1)	2(b)	0	0.2428(6)	1/2	1.0(1)	
O(2)	4(c)	0.2137(5)	0.4577(4)	0.465(1)	0.8(1)	
O(3)	4(c)	0.3123(6)	0.2327(4)	0.243(1)	1.0(1)	

Atom	U <sub>11</sub>	U <sub>22</sub>	U <sub>33</sub>	U <sub>12</sub>	U <sub>13</sub>	U <sub>23</sub>
Ba	0.0086(1)	0.0088(1)	0.0070(1)	0	0.0008(1)	0
Cu	0.0067(2)	0.0050(2)	0.0182(3)	0	0.0013(2)	0
B	0.007(1)	0.004(1)	0.011(1)	0.001(1)	0.001(1)	0.000(1)
O(1)	0.010(1)	0.006(1)	0.022(2)	0	0.005(1)	0
O(2)	0.007(1)	0.006(1)	0.019(1)	-0.001(1)	0.003(1)	-0.001(1)
O(3)	0.013(1)	0.009(1)	0.017(1)	0.004(1)	0.006(1)	0.002(1)

From symmetry constraints  $U_{12} = U_{23} = 0$  for Ba, Cu, and O(1).

Table 5.3 Selected bond distances (Å) and angles (°) for BaCuB<sub>2</sub>O<sub>5</sub>.

Atoms	Distance		Angle
Ba-O(2)	2.703(4) × 2	O(2)-Ba-O(2)	161.6(1)
Ba-O(2)	2.788(4) × 2	O(2)-Ba-O(2)	162.2(1)
Ba-O(1)	2.950(4) × 2	O(1)-Ba-O(1)	84.6(1)
Ba-O(3)	2.980(4) × 2	O(3)-Ba-O(3)	66.4(1)
Ba-O(3)	2.996(4) × 2	O(3)-Ba-O(3)	91.6(1)
		O(1)-Ba-O(3)	46.9(1)
		O(1)-Ba-O(3)	69.6(1)
		O(1)-Ba-O(2)	68.8(1)
		O(1)-Ba-O(2)	67.7(1)
		O(2)-Ba-O(3)	81.4(1)
		O(2)-Ba-O(3)	48.1(1)
		O(2)-Ba-O(3)	58.3(1)
		O(2)-Ba-O(3)	81.1(1)
Cu-O(2)	1.885(3) × 2	O(2)-Cu-O(2)	96.6(2)
Cu-O(3)	1.965(4) × 2	O(3)-Cu-O(3)	99.8(3)
		O(2)-Cu-O(3)	92.7(2)
		O(2)-Cu-O(3)	144.0(2)
B-O(3)	1.345(6)	O(3)-B-O(2)	121.4(4)
B-O(2)	1.359(5)	O(2)-B-O(1)	121.0(4)
B-O(1)	1.422(5)	O(1)-B-O(3)	117.6(4)

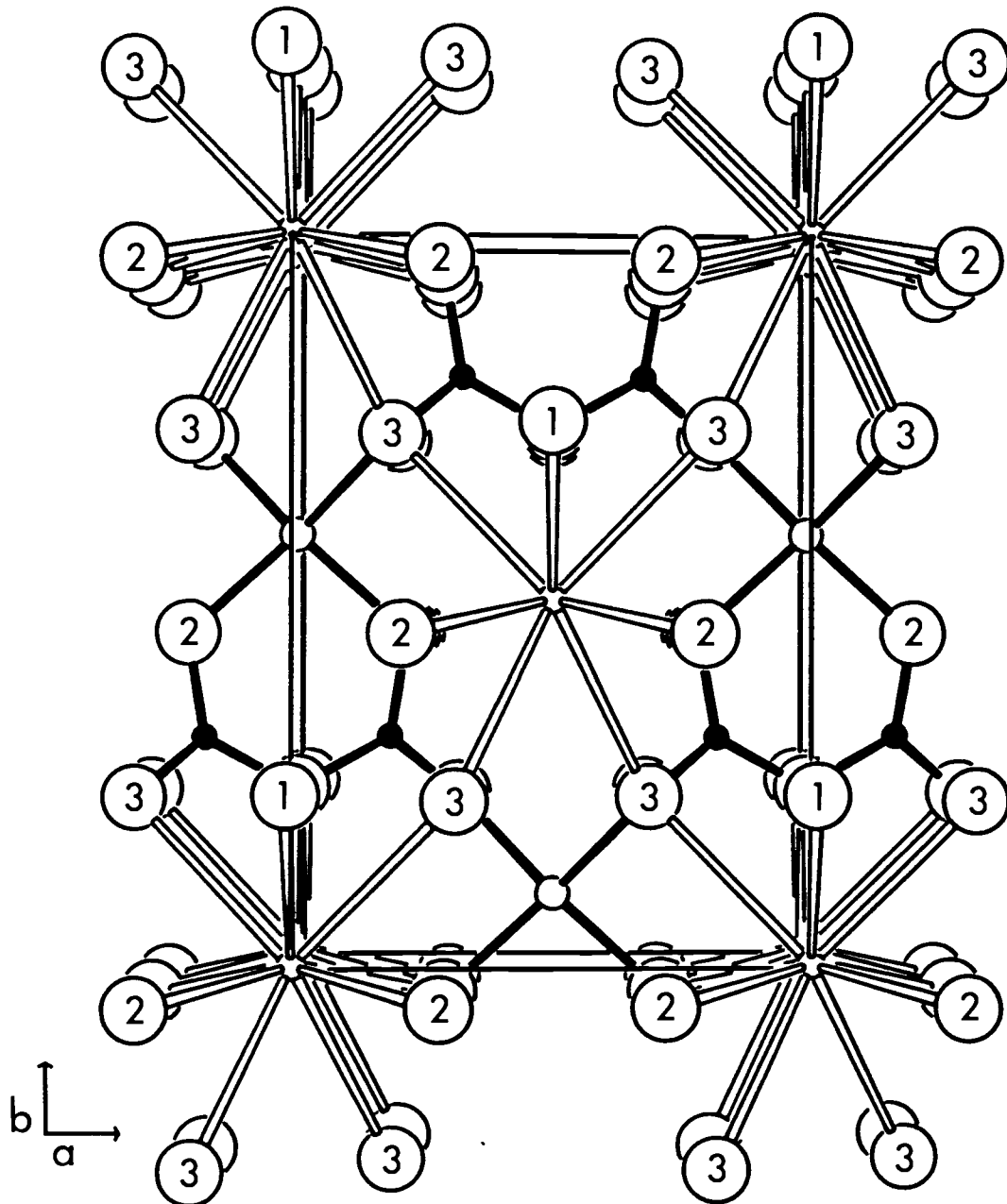


Figure 5.2 Labeled sketch of the unit cell viewed along the  $c$  axis.

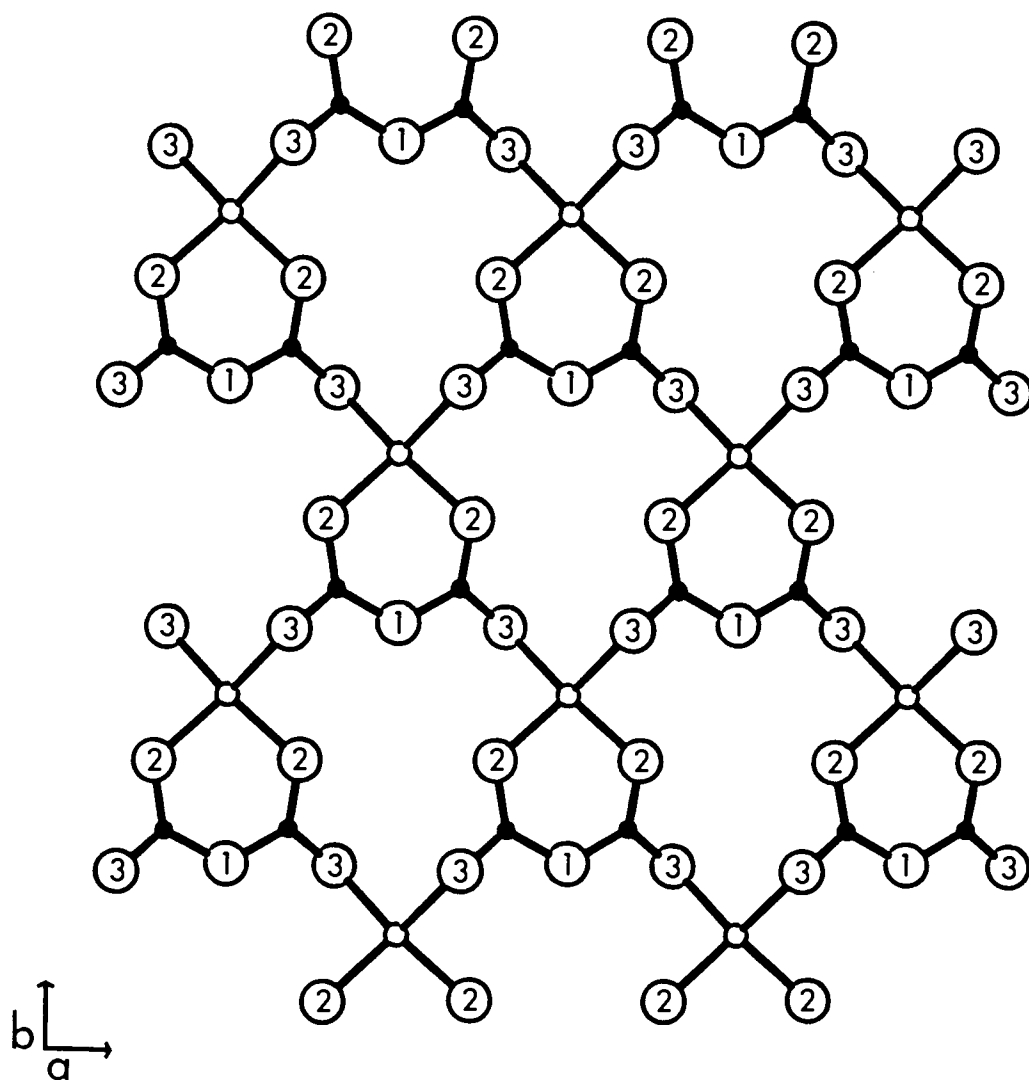


Figure 5.3 Sketch of a portion of the Cu-B-O network viewed along the  $c$  axis.

e.g. 1.94(1) Å for  $\text{SrCu}_2(\text{BO}_3)_2$  (8), 1.930(6) Å for  $\alpha\text{-Sr}_2\text{Cu}(\text{BO}_3)_2$ , 1.94(4) Å for  $\beta\text{-Sr}_2\text{Cu}(\text{BO}_3)_2$  (9), and 1.95(4) Å for  $\text{Ba}_2\text{Cu}(\text{BO}_3)_2$  (10).

Typical structural characteristics are displayed by the pyroborate anion (Figure 5.4b). The B-O(1)-B angle is  $125.8(5)^\circ$  and the two triangles exhibit a twist in opposite directions of about  $8^\circ$  from planarity. These values compare to the values  $140^\circ$  and  $14^\circ$  observed in  $\text{Co}_2\text{B}_2\text{O}_5$  (11) and the values  $135^\circ$  and  $16^\circ$  in  $\text{Mg}_2\text{B}_2\text{O}_5$  (12). The B-O(1) bond is also significantly longer than the other two B-O bonds (1.422(5) Å vice 1.35(1) Å). The central atom O(1) binds to two B atoms whereas the terminal atoms O(2) and O(3) bind to only one B atom. The greater  $\sigma$  electron density that atom O(1) must share with the B atoms weakens the B-O(1) bonds and increases their length.

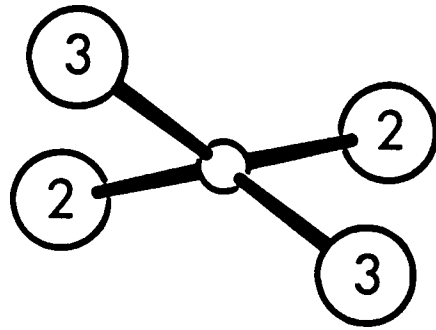
The Ba environment (Figure 5.5) may be described as a bicapped, square antiprism with the Ba atom resting near one of the square faces. Ten O atoms form bonds to Ba, five from each  $\frac{2}{3}[\text{CuB}_2\text{O}_5]$  sheet that are interleaved by the Ba atom. The average Ba-O distance is 2.88(9) Å which compares well to the expected value of 2.90 Å calculated from crystal radii for a ten-coordinate  $\text{Ba}^{2+}$  ion and a four-coordinate  $\text{O}^{2-}$  ion (13).

All O atoms are four-coordinate, forming distorted tetrahedra.

### Magnetic Moment

The effective magnetic moment at  $22^\circ\text{C}$  is 1.69(3) BM. This value is consistent with the  $d^9$  electronic configuration of the  $\text{Cu}^{2+}$  ion and spin-only contributions to the magnetic moment. Values typically range from 1.7-1.9 BM for copper(II) complexes (14) and

a)



b)

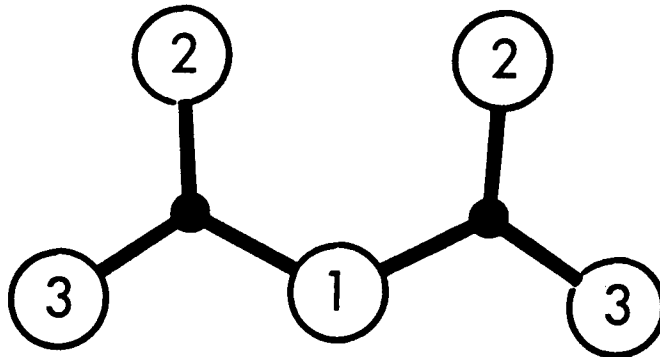


Figure 5.4 Sketches of the a)  $\text{CuO}_4$  and b)  $\text{B}_2\text{O}_5$  groups.

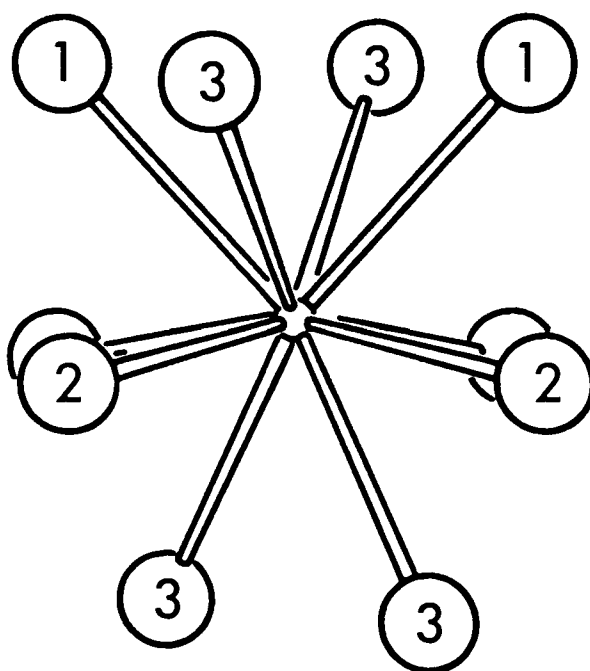


Figure 5.5 Coordination environment of Ba.

average 1.63 BM for  $ACuO_2$  for  $A = Ca, Sr, \text{ or } Ba$  (15).

## Discussion

The intensity of light produced by SHG in  $\text{BaCuB}_2\text{O}_5$  is 14% of that produced in KDP. The SHG signal provides further evidence that the compound crystallizes in an acentric group rather than the centric group  $C2/m$ . The observed signal is weaker than would be anticipated from the alignment of the  $\text{B}_2\text{O}_5$  chromophores. Absorption bands associated with the  $\text{Cu}^{2+}$  ion as well as the anticipated large birefringence of the material and resulting angular sensitivity to phase matching probably contribute to the small observed signal.

SHG or optical frequency conversion is one application in materials science resulting from the nonlinear interaction of light with matter; the subject has been recently reviewed (16). Recent advances in producing new materials with applications in nonlinear optics (NLO) have resulted from "molecular engineering". These advances have been made possible in part by computational studies that assist in explaining NLO effects in terms of the electronic and crystal structures of materials. Many new compounds have been developed in this manner, including borates. Among these compounds are  $\beta\text{-BaB}_2\text{O}_4$  (BBO) (17),  $\text{LiB}_3\text{O}_5$  (LBO) (1),  $\text{KB}_5\text{O}_8 \cdot 4\text{H}_2\text{O}$  (18),  $\text{CdLiBO}_3$  (19), and  $\text{YAl}_3(\text{BO}_3)_4$  (20). BBO exhibits a wide transparency region and a high birefringence that allow the production of the fifth harmonic of the  $\text{Nd}^{3+}$ :YAG laser (21) and LBO exhibits a threshold for 50% power conversion that is nearly two orders of magnitude lower than that of the popular frequency converter KDP (22).

One theory that has proved particularly useful for anticipating

the SHG properties of new materials is the Anionic Group Theory developed by Chen (23). Chen proposed that NLO susceptibility in inorganic crystals is localized in certain clusters of orbitals that are associated with an anionic group or chromophore. The associated cations have little effect on nonlinearities. Furthermore, the nonlinearity of a material can be evaluated as a superposition of all the microscopic SHG coefficients of the appropriate anionic groups. For a material to display efficient SHG, the individual anions must have large second-order SHG coefficients or susceptibilities and these coefficients must sum constructively over the entire structural unit with the anions occupying a large portion of the volume of the unit cell.

No pyroborate with SHG capabilities has been previously reported. However, the geometry of the  $B_2O_5$  group can be compared to the geometry of the  $B_3O_7$  group in the frequency converter LBO (24). The geometries of these two anions are similar. The  $B_3O_7$  group may be viewed as a  $B_2O_5$  group with an additional tetrahedrally coordinated B atom binding to two of the peripheral O atoms. Because of their comparative geometries, we expect some similarities in the magnitudes of the microscopic SHG coefficients for the two compounds.

What is the approximate magnitude of the nonlinearity that we should expect for the arrangement of pyroborate groups in the title compound? We can address this question by idealizing the structure with the assumption that all the pyroborate groups are planar and are perfectly aligned. If we then model each pyroborate group as two fused, simple orthoborate groups, a maximum SHG coefficient of

approximately  $8 \times 10^{-9}$  esu is anticipated. This value is greater than any known simple orthoborate and probably represents a lower limit for the pyroborate groups. The lack of a center of symmetry and the presence of the delocalized  $\pi$  system in the  $B_2O_5$  group should significantly enhance its transition moments thereby increasing the microscopic susceptibility of the group relative to orthoborate. Also the anticipated smaller energy gap of the  $B_2O_5$  group would contribute to a larger observed macroscopic nonlinearity. These effects should all sum to a nonlinearity that is similar in magnitude to that observed from BBO.

Of course the presence of the  $d^9$ ,  $Cu^{2+}$  ions in the compound has a significant effect on the SHG properties. The unpaired d electron can undergo electronic transitions that result in absorption bands in the frequency range of the second harmonic of the  $Nd^{3+}$ :YAG laser. These absorption effects could be overcome and used to advantage by identifying "windows" of small absorption cross section in the absorption spectrum with frequencies that match those of the fundamental and second harmonic of a different laser, *i.e.*  $Ti^{3+}$ : $Al_2O_3$ . In such an instance, the transition moments associated with the  $Cu^{2+}$  ions would likely contribute to a very much higher nonlinearity. Additional optical studies are ongoing in an attempt to identify an appropriate "window."

Attempts have been made to eliminate the absorption bands associated with the  $Cu^{2+}$  ion by substituting it with the  $Zn^{2+}$  ion. The attempted syntheses, however, afforded a new compound, the acentric orthoborate  $BaZn_2(BO_3)_2$  (25).

### Acknowledgements

We thank Dr. Joseph Nibler for his assistance in the SHG measurements. Funds for this research were provided by the National Science Foundation, Solid-State Chemistry Program. DAK thanks the Alfred P. Sloan Foundation for a research fellowship (1989-1991).

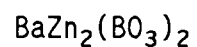
## References

1. C. Chen, B. Wu, A. Jiang, Y. Wu, R. Li et al., Nonlinear Opt. Mat. Symp., Boston (1985).
2. A. Zletz (Amoco Corp.), US Patent Application 709, 790, 11 Mar 1985.
3. Molecular Structure Corporation, "TEXRAY," 3200A Research Forest Drive, The Woodlands, TX 77381, USA (1985).
4. E. R. Howells, D. C. Phillips, and D. Rodgers, Acta Crystallogr. 3, 210 (1950).
5. G. J. Gilmore, "MITHRIL: A Computer Program for the Automatic Solution of Crystal Structures from X-ray Data," University of Glasgow, Scotland (1983).
6. N. Walker and D. Stuart, Acta Crystallogr., Sect. A 24, 214 (1968).
7. L. N. Mulay and E. A. Boudreaux, "Theory and Applications of Molecular Diamagnetism," pp. 306-307, Wiley, New York (1976).
8. R. W. Smith and D. A. Keszler, results to be published.
9. R. W. Smith and D. A. Keszler, J. Solid State Chem. 81, 305 (1989).
10. R. W. Smith and D. A. Keszler, Acta Crystallogr., Sect. C, in press.
11. S. V. Berger, Acta Chem. Scand. 4, 1054 (1950).
12. S. Block, G. Burley, A. Perloff, and R. D. Mason Jr., J. Res. Nat. Bur. Stand. 62, 95 (1959).
13. R. D. Shannon and C. T. Prewitt, Acta Crystallogr., Sect. B 25, 925 (1969).
14. E. A. Boudreaux and L. N. Mulay, "Theory and Applications of Molecular Paramagnetism," p. 54, Wiley, New York (1976).
15. M. Arjomand and D. J. Machin, J. Chem. Soc., Dalton Trans., 1061 (1975).
16. D. J. Williams, Angew. Chem. Int. Ed. Eng. 23, 690 (1984).

17. C. Chen, B. Wu, A. Jiang, and G. You, Sci. Sin. B 28, 235 (1985).
18. C. F. Dewey Jr., Appl. Phys. Lett. 26, 714 (1975).
19. X. Yin, Q. Huang, S. Ye, S. Lei, and C. Chen, Huaxue Xuebao 43 (9), 822 (1985).
20. N. I. Leonyuk and A. A. Filimonov, Krist. Tech. 9, 63 (1974).
21. C. Chen, Y. Fan, R. C. Eckardt, and R. L. Byer, SPIE Laser and Nonlinear Optical Materials 681, 12 (1986).
22. S. P. Velsko, Lawrence Livermore National Laboratory, private communication.
23. C. Chen and G. Liu, Ann. Rev. Mater. Sci. 16, 203 (1986).
24. V. H. König and R. Hoppe, Z. Anorg. Allg. Chem. 439, 71 (1978).
25. R. W. Smith and D. A. Keszler, results to be published.

## CHAPTER 6

SYNTHESIS, STRUCTURE, AND PROPERTIES OF THE ACENTRIC ORTHOBORATE



Robert W. Smith and Douglas A. Keszler

Department of Chemistry and Center for Advanced Materials Research

Oregon State University

Gilbert Hall 153

Corvallis, Oregon 97331-4003, USA

For Submission to Chemistry of Materials

### Abstract

The new orthoborate  $\text{BaZn}_2(\text{BO}_3)_2$  has been synthesized and its structure determined by single-crystal X-ray methods. It crystallizes in an orthorhombic cell with dimensions  $\underline{a} = 9.305(3)$ ,  $\underline{b} = 12.128(1)$ , and  $\underline{c} = 4.9255(8)$  Å; the space group is  $P2_12_12_1$ . The structure was determined from 876 independent reflections and refined to the final residuals  $R = 0.024$  and  $R_w = 0.034$ . It is composed of chains of vertex-sharing  $\text{ZnO}_4$  tetrahedra and  $\text{BO}_3$  triangles; the chains extend parallel to the  $\underline{c}$  axis. Ba atoms occupy holes that are afforded by interconnecting the chains along the  $\underline{a}$  and  $\underline{b}$  axes. Calculated nonlinearity coefficients indicate that the  $\text{BO}_3$  groups in the compound should afford a second harmonic signal that is approximately 10% of that of  $\text{YAl}_3(\text{BO}_3)_4$ .

## Introduction

Certain acentric borates are known to exhibit exceptional nonlinear optical properties. The material  $\beta$ -BaB<sub>2</sub>O<sub>4</sub> (1) is the only solid useful for the production of the fifth harmonic of the Nd<sup>3+</sup>:YAG laser. The compound LiB<sub>3</sub>O<sub>5</sub> exhibits a threshold for 50% power conversion that is two orders of magnitude lower than potassium dihydrogen phosphate (KDP) and the highest optical damage threshold reported for a nonlinear optical material (2).

In this report, we describe the synthesis, structure, and optical properties of a new acentric borate, the compound BaZn<sub>2</sub>(BO<sub>3</sub>)<sub>2</sub>. This material has resulted from our continuing studies of borates of formula XY<sub>2</sub>(BO<sub>3</sub>)<sub>2</sub> where X and Y are different cations with a formal charge of +2 (3a-d).

## Experimental

### Synthesis and Crystal Growth

The title compound was prepared by grinding a stoichiometric ratio of  $\text{Ba}(\text{NO}_3)_2$  (99.999%, Johnson Matthey),  $\text{Zn}(\text{NO}_3)_2 \cdot 6\text{H}_2\text{O}$  (99.999%, Johnson Matthey), and  $\text{B}_2\text{O}_3$  (99.99%, Morton Thiokol) under hexane to a fine powder followed by heating at  $600^\circ\text{C}$  for 30 minutes to decompose the nitrates. The samples were then heated at  $800^\circ\text{C}$  for 18 hours with several intermittent grindings. Samples were single phase as determined from analysis of X-ray powder diffractograms obtained with an automated Philips powder diffractometer equipped with graphite-monochromated  $\text{Cu K}\alpha$  radiation.

Single crystals were grown from the melt. A powder sample was heated to  $980^\circ\text{C}$ , cooled to  $860^\circ\text{C}$  at  $1.5^\circ\text{C}/\text{hour}$ , then air-quenched. Clear, colorless crystals were physically separated from the crucible for structure determination.

### X-ray Work

A rod-shaped crystal with dimensions  $0.25 \times 0.12 \times 0.10$  mm was chosen for structure analysis. Lattice parameters were refined from 10 reflections in the range  $26^\circ < 2\theta < 31^\circ$  that were automatically centered on a Rigaku AFC6R diffractometer equipped with  $\text{Mo K}\alpha$  radiation. Intensity data in the range of indices  $0 \leq h \leq 13$ ,  $0 \leq k \leq 17$ , and  $-6 \leq l \leq 6$  were collected with the  $\omega$ - $2\theta$  scan technique at a scan speed of  $16^\circ/\text{minute}$  in  $\omega$  and a scan width  $\Delta\omega = (1.50 + 0.30 \tan\theta)^\circ$ . From 1756 reflections measured to  $2\theta = 60^\circ$ , 876 unique data

having  $F_0^2 \geq 3\sigma(F_0^2)$  were obtained.

Unit cell parameters were also refined from powder X-ray data. A powder sample was ground under hexane, sieved with a 200 mesh wire screen, and annealed at 700°C for 2 hours. Eleven intense reflections in the range  $19^\circ < 2\theta < 45^\circ$  were measured and their Bragg angles corrected with Si (NBS Standard Reference Material 640b) as the internal standard. Least-squares refinement of the  $2\theta$  values afforded the dimensions  $\underline{a} = 9.332(3)$ ,  $\underline{b} = 12.121(5)$ , and  $\underline{c} = 4.922(2)$  Å; these compare well to the single-crystal data.

### Structure Solution and Refinement

All calculations were performed on a microVax II computer with programs from the TEXRAY crystallographic software package (4). The systematic absences  $h00$  ( $h = 2n + 1$ ),  $0k0$  ( $k = 2n + 1$ ), and  $00l$  ( $l = 2n + 1$ ) unambiguously define the acentric space group  $P2_12_12_1$ . Results from second-harmonic experiments (vide infra) and the statistical distribution of intensities (5) also indicate that the structure is acentric. Ba and Zn positional parameters were determined with the computer program SHELXS (6) and the B and O positions were found from subsequent difference electron density syntheses.

Following refinement with isotropic thermal parameters the data were corrected for absorption with the computer program DIFABS (7). The data were then averaged. Final least-squares refinement on  $F_0$  with data having  $F_0^2 \geq 3\sigma(F_0^2)$  and anisotropic temperature factors resulted in the residuals  $R = 0.024$  and  $R_w = 0.034$ . The largest peak in the final difference map has a height of 0.40% of a Ba atom.

Table 6.1 Crystal data and experimental conditions for  $\text{BaZn}_2(\text{BO}_3)_2$ .

Diffractometer	Rigaku AFC6R
Radiation	Graphite-monochromated Mo $K\alpha$ ( $\lambda = 0.70926 \text{ \AA}$ )
Formula wt., amu	385.71
$a$ , $\text{\AA}$	9.305(3)
$b$ , $\text{\AA}$	12.128(1)
$c$ , $\text{\AA}$	4.926(1)
$V$ , $\text{\AA}^3$	555.9(2)
Space group	$P2_12_12_1$
$D_{\text{calc}}$ , $\text{g cm}^{-3}$	4.61
Crystal vol., $\text{mm}^3$	0.0030
$F(000)$	696
$Z$	4
Linear abs. coeff., $\text{cm}^{-1}$	157.58
$p$ factor	0.05
No. unique data with $F_0^2 > 3\sigma(F_0^2)$	876
$R_{\text{int}}$	0.033
$R(F_0)$	0.024
$R_w(F_0)$	0.034
Error in observation of unit wt., $e^2$	1.03

Additional crystal data and experimental conditions are given in Table 6.1.

### Frequency Conversion Measurements

A measurement of the efficiency of second harmonic generation by a powdered sample of  $\text{BaZn}_2(\text{BO}_3)_2$  was obtained with the apparatus schematically diagrammed in Figure 6.1. A  $\text{Nd}^{3+}$ :YAG laser was used to produce the incident IR radiation at a wavelength of 1060 nm. Visible light was filtered out with a Corning 1-75 filter having a transmittance of 87% at 1060 nm and 0% at 530 nm. The powder was placed on a glass quartz plate inside the cell. The intensity of the second harmonic was monitored with a photomultiplier attached to an oscilloscope. IR radiation was filtered from the output with a Corning 7-57 filter having a transmittance of 88% at 530 nm and 1% at 1060 nm. SHG measurements of KDP powder served as a standard for the measurement; they were obtained before and after data acquisition from the sample of  $\text{BaZn}_2(\text{BO}_3)_2$ .

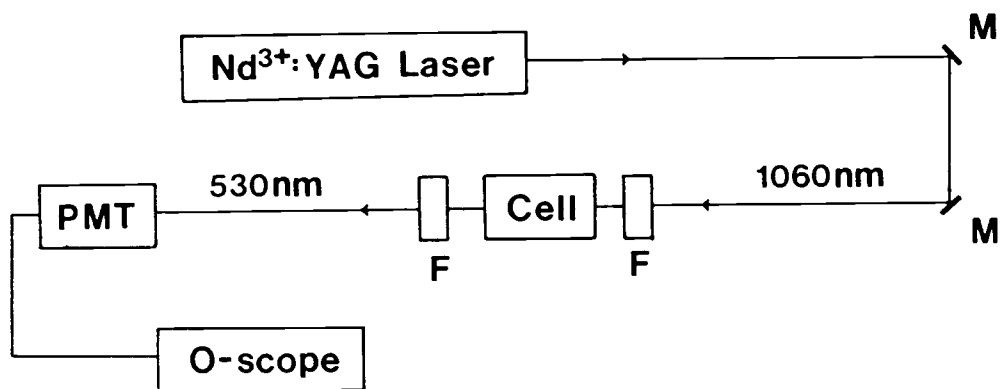


Figure 6.1 Schematic diagram of the apparatus used for SHG measurements.

## Results

### Structure

Final atomic coordinates and anisotropic temperature factors are listed in Table 6.2, selected interatomic distances and angles are listed in Table 6.3, and the contents of the unit cell are illustrated in Figure 6.2.

The structure is a new type exhibiting a framework of  $\text{ZnO}_4$  tetrahedra and  $\text{BO}_3$  triangles that share vertices. A portion of the framework is depicted in Figure 6.3. A zig-zag string of distorted  $\text{ZnO}_4$  tetrahedra sharing vertices O(3) extends in the  $\underline{c}$  direction. These tetrahedra are further bridged by atom B(2). The tetrahedra centered by atom Zn(1) do not share vertices but are bridged one to the other by atom B(1) with an additional connection to the Zn(2)-centered tetrahedra through atom B(2). Application of the  $2_1$  screw axis along  $\underline{b}$  to the fragment of Figure 6.3 completes the framework; vertex O(4) is shared by atoms Zn(1) and Zn(2) to afford the one-dimensional zinc oxide sublattice illustrated in Figure 6.4.

The framework may alternately be described as a condensation of the six- and eight-membered rings illustrated in Figure 6.5. The six-membered ring (Figure 6.5a) is composed of two Zn(2) atoms, one B(2) atom, two O(3) atoms, and one O(6) atom. The rings are fused through vertices O(3) and O(6) to form a chain that extends in the  $\underline{c}$  direction (Figure 6.3). The eight-membered ring (Figure 6.5b) is composed of two Zn(1) atoms, two B(1) atoms, two O(2) atoms, one O(4) atom, and one O(5) atom. The rings are fused by sharing terminal

Table 6.2 Final atomic coordinates and temperature factors for  
BaZn<sub>2</sub>(BO<sub>3</sub>)<sub>2</sub>.

Atom	x	y	z	B <sub>eq</sub>
Ba	0.39607(5)	0.22892(3)	0.0310(1)	1.04(2)
Zn(1)	0.36945(8)	0.89488(6)	0.0452(2)	0.89(3)
Zn(2)	0.6588(1)	0.03145(7)	0.9474(2)	0.99(3)
B(1)	0.4098(8)	0.0059(6)	0.558(2)	0.7(2)
B(2)	0.6663(8)	0.1669(6)	0.464(2)	0.9(3)
O(1)	0.5931(6)	0.2475(4)	0.595(1)	1.3(2)
O(2)	0.3335(5)	0.0932(4)	0.460(1)	1.3(2)
O(3)	0.2513(6)	0.4061(5)	0.380(1)	1.1(2)
O(4)	0.4602(6)	0.0113(5)	0.827(1)	1.2(2)
O(5)	0.5653(7)	0.4128(5)	0.086(1)	1.9(2)
O(6)	0.6683(6)	0.1569(5)	0.192(1)	1.1(2)

Atom	U <sub>11</sub>	U <sub>22</sub>	U <sub>33</sub>	U <sub>12</sub>	U <sub>13</sub>	U <sub>23</sub>
Ba	0.0130(2)	0.0127(2)	0.0137(2)	0.0018(1)	-0.0002(2)	0.0017(2)
Zn(1)	0.0120(4)	0.0114(4)	0.0103(4)	-0.0008(3)	0.0003(3)	0.0004(3)
Zn(2)	0.0120(4)	0.0137(4)	0.0119(4)	0.0005(3)	-0.0013(3)	0.0004(3)
B(1)	0.007(3)	0.010(3)	0.010(3)	0.001(2)	-0.004(3)	-0.001(3)
B(2)	0.008(3)	0.017(3)	0.009(3)	-0.002(3)	0.001(3)	0.003(3)
O(1)	0.025(3)	0.009(2)	0.016(2)	0.004(2)	0.012(2)	0.001(2)
O(2)	0.012(2)	0.016(2)	0.023(3)	0.001(2)	0.003(3)	0.012(2)
O(3)	0.016(2)	0.013(2)	0.011(2)	-0.001(2)	-0.004(2)	-0.001(2)
O(4)	0.014(2)	0.018(3)	0.012(3)	-0.004(2)	-0.002(2)	0.001(2)
O(5)	0.038(3)	0.021(3)	0.012(3)	-0.009(3)	-0.009(3)	0.003(2)
O(6)	0.014(2)	0.012(2)	0.013(3)	-0.004(2)	0.001(2)	-0.003(2)

Table 6.3 Selected bond distances ( $\text{\AA}$ ) and angles ( $^\circ$ ) in  $\text{BaZn}_2(\text{BO}_3)_2$ .

Atoms	Distance		Angle
Ba-0(1)	2.831(5)	0(1)-Ba-0(4)	71.0(1)
Ba-0(2)	2.740(5)	0(1)-Ba-0(5)	68.8(2)
Ba-0(3)	3.063(6)	0(1)-Ba-0(6)	69.7(2)
Ba-0(4)	2.887(6)	0(1)-Ba-0(6)	99.0(2)
Ba-0(5)	2.744(6)	0(3)-Ba-0(2)	84.0(2)
Ba-0(6)	2.759(6)	0(3)-Ba-0(5)	68.1(2)
Ba-0(6)	2.794(6)	0(3)-Ba-0(6)	62.2(2)
		0(3)-Ba-0(6)	117.3(2)
		0(5)-Ba-0(6)	94.1(2)
		0(5)-Ba-0(6)	72.9(2)
		0(2)-Ba-0(4)	76.3(2)
Zn(1)-0(1)	1.949(5)	0(1)-Zn(1)-0(2)	99.5(2)
Zn(1)-0(2)	1.940(5)	0(1)-Zn(1)-0(4)	112.8(2)
Zn(1)-0(4)	1.966(6)	0(1)-Zn(1)-0(5)	112.5(3)
Zn(1)-0(5)	1.926(6)	0(2)-Zn(1)-0(4)	104.2(2)
		0(2)-Zn(1)-0(5)	120.2(3)
		0(4)-Zn(1)-0(5)	107.4(3)
Zn(2)-0(3)	1.977(6)	0(3)-Zn(2)-0(3)	118.1(2)
Zn(2)-0(3)	1.933(6)	0(3)-Zn(2)-0(4)	102.3(2)
Zn(2)-0(4)	1.956(5)	0(3)-Zn(2)-0(6)	100.7(2)
Zn(2)-0(6)	1.942(5)	0(3)-Zn(2)-0(4)	116.4(2)
		0(3)-Zn(2)-0(6)	108.8(2)
		0(4)-Zn(2)-0(6)	109.2(2)
B(1)-0(2)	1.36(1)	0(2)-B(1)-0(4)	118.2(7)
B(1)-0(4)	1.41(1)	0(4)-B(1)-0(5)	118.4(6)
B(1)-0(5)	1.35(1)	0(5)-B(1)-0(2)	123.3(7)
B(2)-0(1)	1.35(1)	0(1)-B(2)-0(3)	118.3(8)
B(2)-0(3)	1.41(1)	0(3)-B(2)-0(6)	118.4(7)
B(2)-0(6)	1.35(1)	0(6)-B(2)-0(1)	123.1(7)

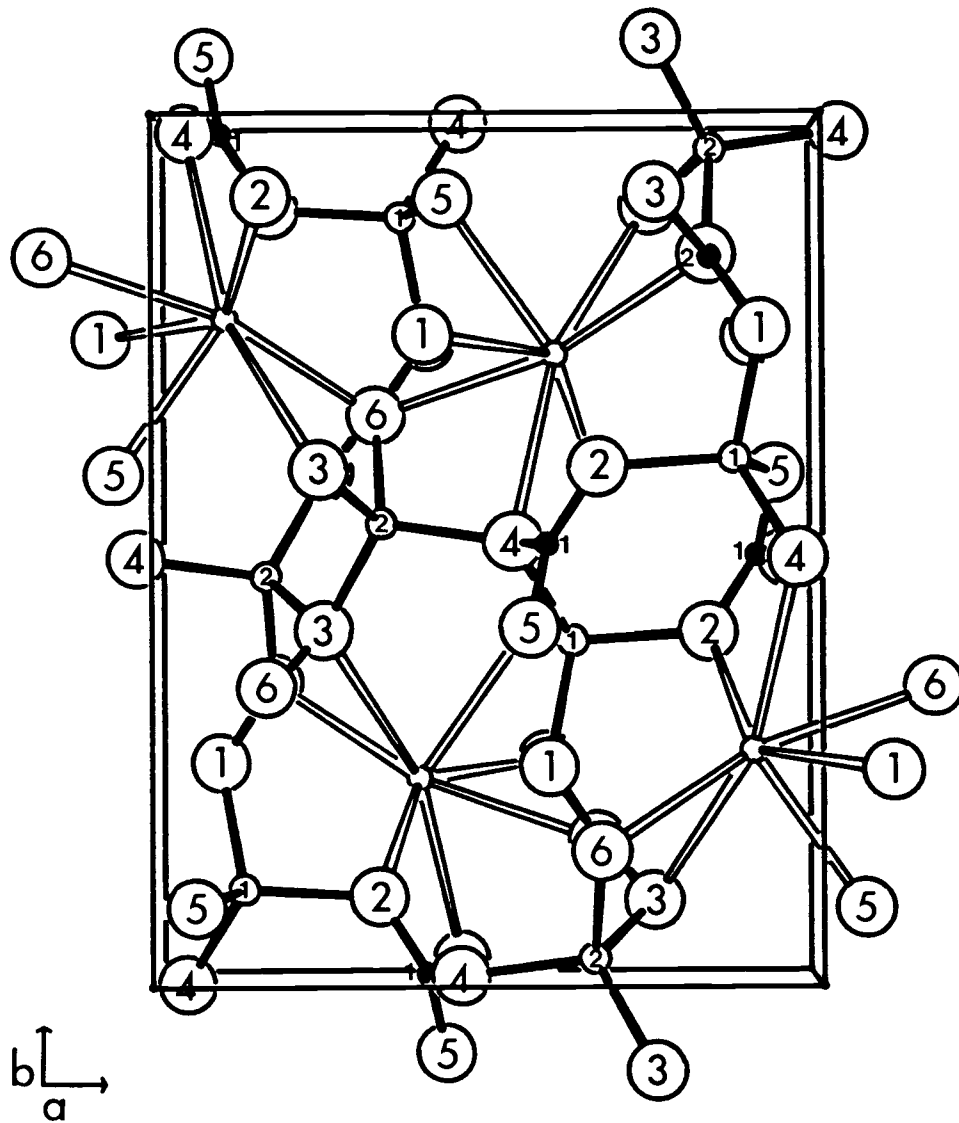


Figure 6.2 Labeled sketch of the unit cell  
viewed along the  $c$  axis.

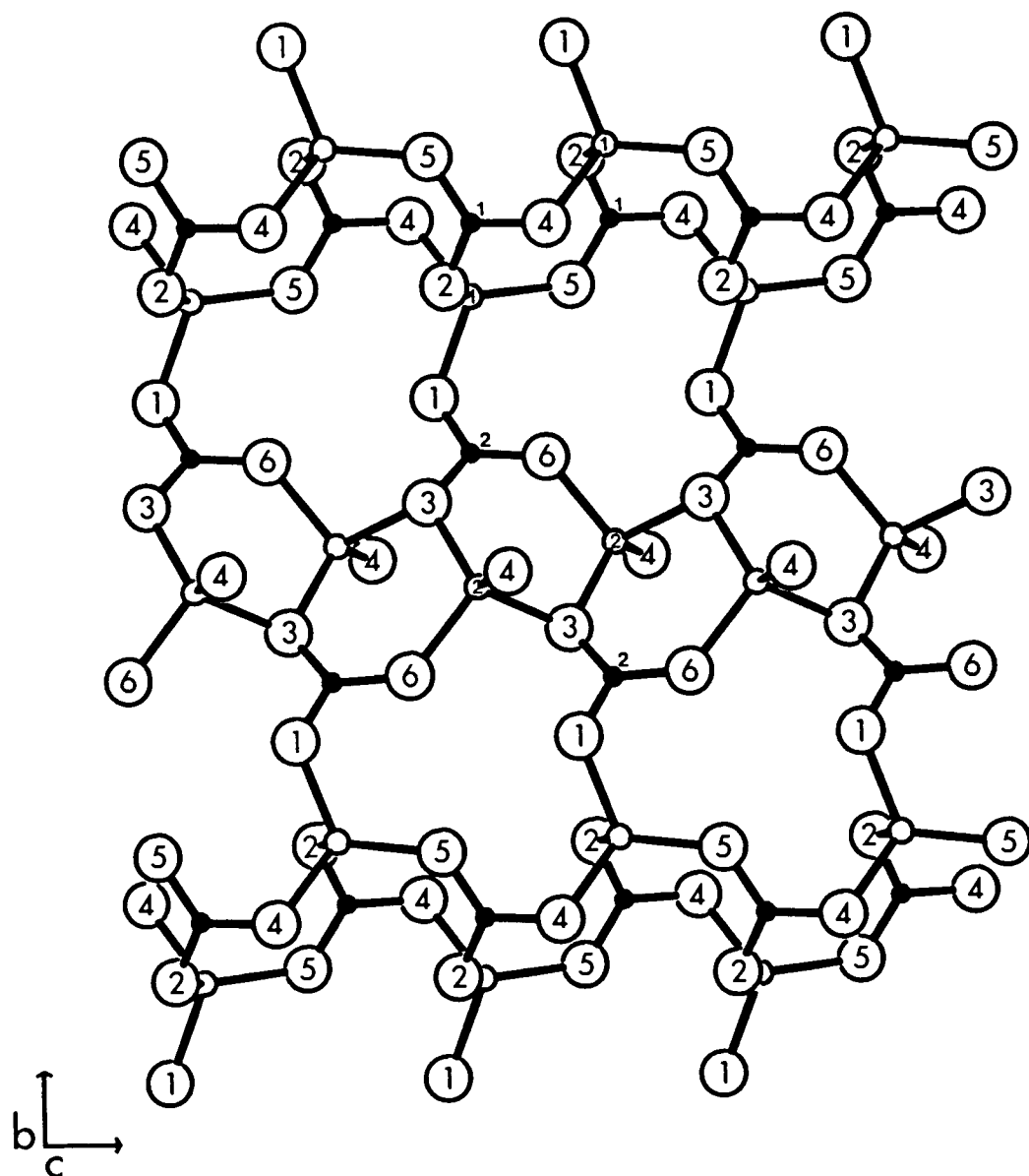


Figure 6.3 Sketch of a portion of the zinc borate network viewed along the  $a$  axis.

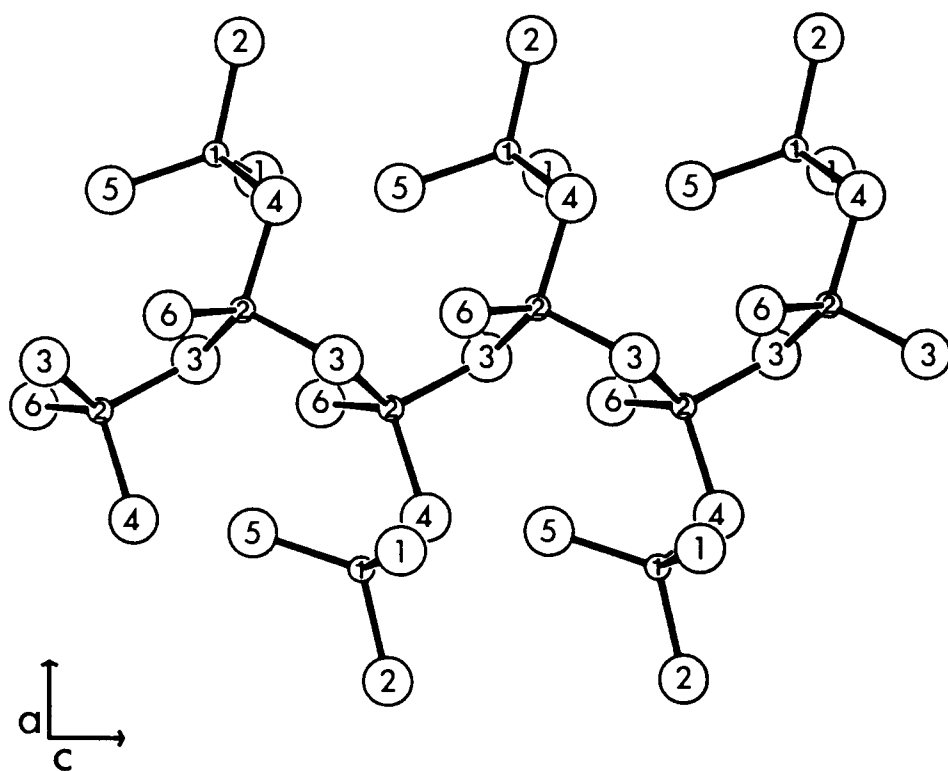


Figure 6.4 One-dimensional zinc oxide sublattice viewed along the  $b$  axis.

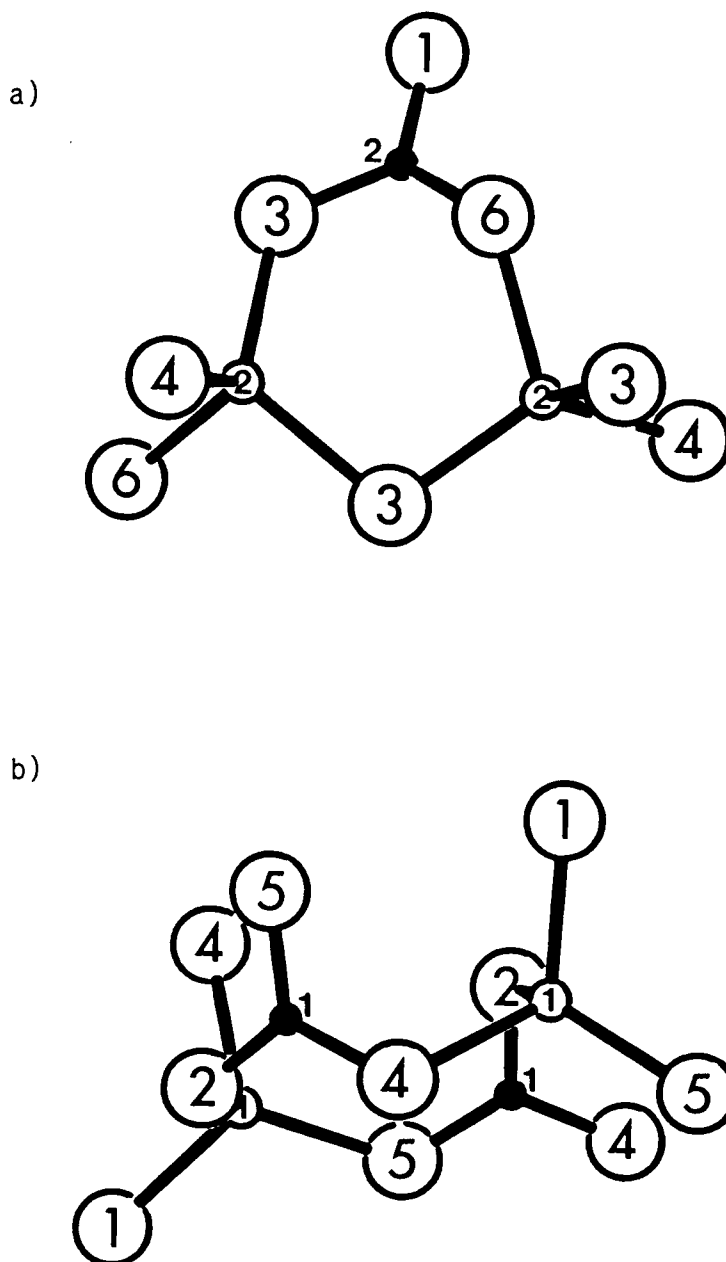


Figure 6.5 Sketches of a) six-membered  $Zn_2B_2O_8$  ring and b) eight-membered  $Zn_2B_2O_9$  ring.

vertices O(4) and O(5) to again form a chain that extends in the  $\underline{c}$  direction. The full three-dimensional network is realized by connecting the chains through vertices O(4).

The framework affords large open channels extending along the  $\underline{c}$  axis that are occupied by Ba atoms. The Ba atom (Figure 6.6) displays a seven-coordinate environment that may be described as a distorted trigonal-base, tetragonal-base. The average Ba-O distance is 2.8(1) Å which is comparable to the expected value of 2.77 Å calculated from the crystal radii of Ba<sup>2+</sup> and O<sup>2-</sup> ions (8). Seven-coordination of the Ba atom has also been observed in the borate Ba<sub>2</sub>Sc<sub>2</sub>B<sub>4</sub>O<sub>11</sub> (9).

Average distances for Zn-O and B-O bonds are normal. The average Zn-O bond distance is 1.95(2) Å which compares well to the value seen in Zn<sub>3</sub>(BO<sub>3</sub>)<sub>2</sub>, (1.97 Å) (10), and KZn<sub>4</sub>(BO<sub>3</sub>)<sub>3</sub> (1.95 Å) (11). The average B-O bond distance of 1.37(3) for the trigonal B atoms is similar to the expected value of 1.365 Å (12). Atoms O(1), O(2), and O(5) are three-coordinate and atoms O(3), O(4), and O(6) are four-coordinate.

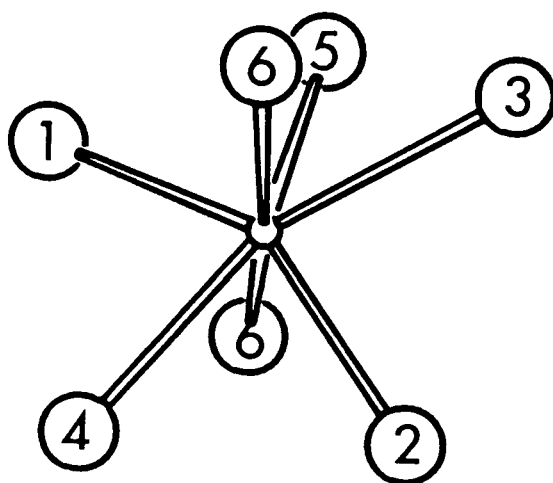


Figure 6.6 Coordination environment of the Ba atom.

## Discussion

The intensity of light produced by SHG of the 1060 nm line of a Nd<sup>3+</sup>:YAG laser from a powder of BaZn<sub>2</sub>(BO<sub>3</sub>)<sub>2</sub> was found to be equivalent to that produced from a powder of KDP. The result of the SHG experiment provides further evidence that the space group of BaZn<sub>2</sub>(BO<sub>3</sub>)<sub>2</sub> is acentric. Results from the determination of the SHG efficiency from powder data, however, is limited because of the scattering of radiation from the granules, a variety of factors affecting the phase-matching characteristics of the sample, and the possibility that the material fluoresces. Hence, the magnitude of the SHG signal from BaZn<sub>2</sub>(BO<sub>3</sub>)<sub>2</sub> powder should be viewed with some reservation.

Prompted by the observed magnitude of the SHG signal, we have computed the nonlinearity of the material by application of the Anionic Group Theory (13) with CNDO methods (14) for calculation of molecular orbital coefficients. In this computation, we assumed that the BO<sub>3</sub> groups are the principal chromophores contributing to the SHG signal. The extended zinc oxide submatrix, which could contribute to the nonlinearity, has not been included in the present model.

In a consideration of the nonlinearity of a simple orthoborate, the components of the hyperpolarizability tensor of an individual BO<sub>3</sub> group and their summation from the orientation of each group in the crystal structure must be determined. The density of the groups will also be important in determining the magnitude of the SHG signal. For a BO<sub>3</sub> group with D<sub>3h</sub> symmetry (Figure 6.7), the only nonzero components in the hyperpolarizability tensor are given by  $\beta_{xxx} = -\beta_{xyy} =$

$-\beta_{yxy} = -\beta_{yyx}$ . We find from computations that  $\beta_{xxx} = 0.475 \times 10^{-30}$  esu. To appreciate the effects of the relative orientations of the  $\text{BO}_3$  groups in  $\text{BaZn}_2(\text{BO}_3)_2$  we can consider the magnitude of the maximum nonlinearity that could be observed for a collection of  $\text{BO}_3$  groups having a density equal to that in  $\text{BaZn}_2(\text{BO}_3)_2$ . That is, consider a set of eight  $\text{BO}_3$  groups all aligned according to Figure 6.7. The maximum nonlinear coefficient,  $d_{11}$ , that could be observed for such a collection of groups would be proportional to  $8 \times \beta_{xxx} \times (\text{unit cell volume})^{-1} = 6.8 \times 10^{-9}$  esu. In the actual structure of  $\text{BaZn}_2(\text{BO}_3)_2$ , the only nonzero nonlinear coefficients resulting from the symmetry  $D_{2h}$  are  $d_{14} = d_{25} = d_{26}$ . We compute for  $d_{14}$  the value  $0.59 \times 10^{-9}$  esu.

The magnitude of the coefficient  $d_{14}$  is determined by the relative orientation of the  $\text{BO}_3$  groups. The two crystallographically distinct  $\text{BO}_3$  groups are displayed in Figure 6.8; each unit cell contains four  $\text{BO}_3$  groups of each set. In each set, the  $\text{BO}_3$  groups are related one to the other by the three  $2_1$  screw axes along the three crystallographic axes. The  $2_1$  screw axes afford pairs within each set that are oriented approximately antiparallel to each other, affording partial cancellation of the components of the hyperpolarizability tensor.

The magnitude of the calculated value is approximately 10% of that observed and calculated for the compound  $\text{YAl}_3(\text{BO}_3)_4$  (13), a compound that exhibits an SHG signal approximately 2.5 times greater than that of KDP. Consideration of the observed signal and the calculated nonlinearity suggest that single crystals of  $\text{BaZn}_2(\text{BO}_3)_2$

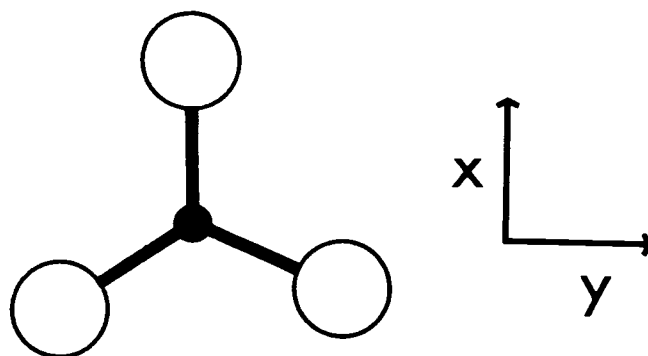


Figure 6.7 A single  $\text{BO}_3$  group in a cartesian coordinate system.

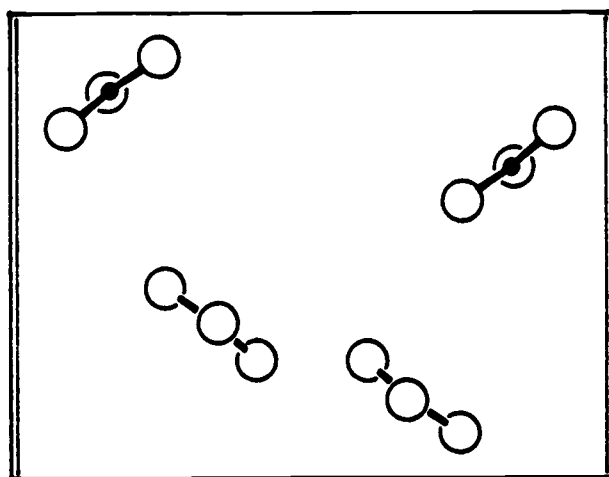
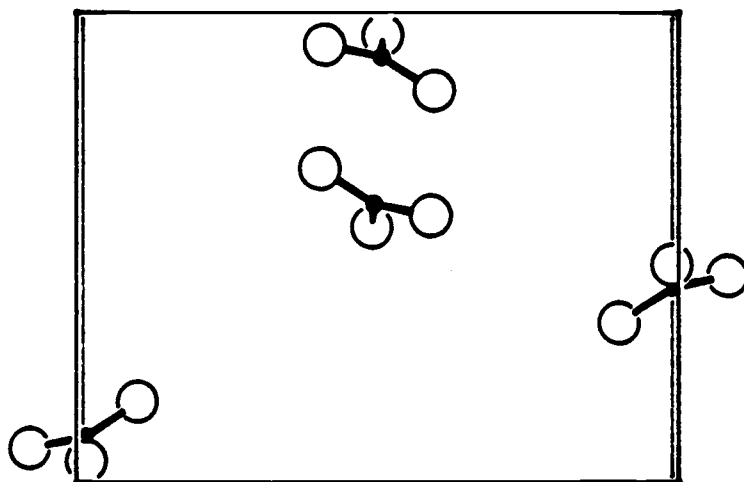


Figure 6.8 Two sets of BO<sub>3</sub> groups in the compound BaZn<sub>2</sub>(BO<sub>3</sub>)<sub>2</sub>.

should be analyzed and that the contribution of the  $\text{ZnO}_4$  groups to the nonlinearity should be determined.

### Acknowledgements

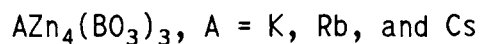
We thank Dr. Joseph Nibler for his assistance in the SHG measurements and Mr. Jinfan Huang for calculating the nonlinearities. Funds for this research were provided by the National Science Foundation, Solid-State Chemistry Program. DAK thanks the Alfred P. Sloan Foundation for a research fellowship (1989-1991).

## References

1. C. Chen, B. Wu, A. Jiang, and G. You, Sci. Sin. B **28**, 235 (1985).
2. S. P. Velsko, Lawrence Livermore National Laboratory, private communication.
3. e.g. (a)  $\text{Sr}_2\text{Cu}(\text{BO}_3)_2$ : R. W. Smith and D. A. Keszler, J. Solid State Chem. **81**, 305 (1989), (b)  $\text{Ba}_2\text{Cu}(\text{BO}_3)_2$ : R. W. Smith and D. A. Keszler, Acta Crystallogr., Sect. C, in press, (c)  $\text{SrCu}_2(\text{BO}_3)_2$ : R. W. Smith and D. A. Keszler, results to be published, (d)  $\text{SrBe}_2(\text{BO}_3)_2$ : K. I. Schaffers and D. A. Keszler, J. Solid State Chem., submitted.
4. Molecular Structure Corporation, "TEXRAY," 3200A Research Forest Drive, The Woodlands, TX 77381, USA (1985).
5. E. R. Howells, D. C. Phillips, and D. Rodgers, Acta Crystallogr. **3**, 210 (1950).
6. G. M. Sheldrick, "Crystallographic Computing 3," Eds. G. M. Sheldrick, C. Krüger, and R. Goddard, pp.175-189, Oxford University Press, Oxford (1985).
7. N. Walker and D. Stuart, Acta Crystallogr., Sect. A **24**, 214 (1968).
8. R. D. Shannon and C. T. Prewitt, Acta Crystallogr., Sect. B **25**, 925 (1969).
9. P. D. Thompson, J. Huang, R. W. Smith, and D. A. Keszler, results to be published.
10. W. H. Baur and E. Tillmanns, Z. Krist. **131**, 213 (1970).
11. R. W. Smith, J. L. Luce, and D. A. Keszler, results to be published.
12. A. F. Wells, "Structural Inorganic Chemistry, 4th ed.," p.862, Clarendon Press, Oxford (1975).
13. C. Chen and G. Liu, Ann. Rev. Mater. Sci. **16**, 203 (1986).
14. J. Huang and D. A. Keszler, results to be published.
15. N. I. Leonyuk and A. A. Filimonov, Krist. Tech. **9**, 63 (1974).

## CHAPTER 7

## THE FRAMEWORK ALKALI ZINC ORTHOBORATES



Robert W. Smith, Jeanne L. Luce, and Douglas A. Keszler

Department of Chemistry and Center for Advanced Materials Research

Oregon State University

Gilbert Hall 153

Corvallis, Oregon 97331-4003, USA

For Submission to Inorganic Chemistry

### Abstract

A new family of alkali zinc orthoborates  $AZn_4(BO_3)_3$  where  $A = K, Rb,$  and  $Cs$  has been synthesized and studied. The structures of the  $K$  and  $Rb$  analogs have been determined by single-crystal X-ray methods. The  $K$  analog crystallizes in a monoclinic cell of dimensions  $\underline{a} = 6.876(2), \underline{b} = 4.990(1), \underline{c} = 12.574(1) \text{ \AA}$ , and  $\beta = 92.92(1)^\circ$ ; the space group is  $P2/c$ . The  $Rb$  analog crystallizes in the same space group in a cell of dimensions  $\underline{a} = 6.849(2), \underline{b} = 5.000(2), \underline{c} = 12.718(2) \text{ \AA}$ , and  $\beta = 92.53(2)^\circ$ . For the  $Cs$  analog, a cell of dimensions  $\underline{a} = 6.871(2), \underline{b} = 5.019(2), \underline{c} = 12.961(3) \text{ \AA}$ , and  $\beta = 92.50(3)^\circ$  has been obtained from refinement of powder X-ray data. The structure is a new type composed of tetrahedral  $ZnO_4$  and triangular  $BO_3$  groups arranged in a three-dimensional framework by sharing 0 vertices. The framework affords channels with rectangular cross sections having dimensions  $2.6 \times 5.7 \text{ \AA}$  that extend in the  $[010]$  direction; the alkali atoms occupy sites inside these channels. Results of ion-exchange reactions designed for the exchange of the  $K^+$  cation are described.

## Introduction

While attempting to grow crystals of the new, acentric material  $\text{BaZn}_2(\text{BO}_3)_2$  (1) with the flux  $\text{LiBO}_2$ , we discovered a new compound that we found to be  $\text{BaLiZn}_3(\text{BO}_3)_3$ . Structure determination of the phase revealed a unique framework with Ba atoms occupying one-dimensional channels. We determined that Li and Zn atoms were disordered on the tetrahedral sites in the framework. To remove the disorder, we replaced the Ba atom with a K atom and the Li atom with a Zn atom and found an identical structure of stoichiometry  $\text{KZn}_4(\text{BO}_3)_3$ . Subsequent syntheses revealed that the Rb and Cs analogs also exist.

In this report we describe the syntheses and properties of the isomorphous compounds  $\text{AZn}_4(\text{BO}_3)_3$ ,  $A = \text{K}, \text{Rb}, \text{and Cs}$ , and the crystal structures of the K and Rb analogs. Because the channels that extend through the framework accommodate a variety of cations, we attempted several ion-exchange reactions with the K analog. The results of these studies are reported here.

## Experimental

### Syntheses

Each compound was prepared by grinding a stoichiometric ratio of  $\text{KNO}_3$  (Spectrum, reagent grade),  $\text{Rb}_2\text{CO}_3$  (Morton Thiokol, 99.9%), or  $\text{Cs}_2\text{CO}_3$  (Johnson Matthey, 99%) with  $\text{Zn}(\text{NO}_3)_2 \cdot 4.36\text{H}_2\text{O}$  (Morton Thiokol, reagent grade) and  $\text{B}_2\text{O}_3$  (Johnson Matthey, 99.99%) under hexane to a fine powder followed by heating at  $600^\circ\text{C}$  for one hour to decompose the nitrates. These samples were then reground and calcined at  $750^\circ\text{C}$  overnight. All samples were single phase as determined by X-ray powder diffraction using an automated Philips powder diffractometer equipped with a diffracted-beam monochromator set for  $\text{Cu K}\alpha$  radiation.

Single crystals of the K and Rb analogs were grown with the compound  $\text{PbO}$  as a flux. A mixture of solute:flux of 4:1 by weight was heated in a Pt crucible to  $930^\circ\text{C}$ , cooled at  $6^\circ\text{C}/\text{hour}$  to  $600^\circ\text{C}$ , then air-quenched. Clear, colorless crystals were physically removed from the crucible for structure determination.

### X-ray Work

A crystal of the K analog with dimensions  $0.20 \times 0.08 \times 0.04$  mm was selected for analysis. Unit cell parameters were determined from a least-squares analysis of 15 reflections in the range  $30^\circ < 2\theta < 39^\circ$  that were automatically centered on a Rigaku AFC6R diffractometer equipped with monochromatic  $\text{Mo K}\alpha$  radiation. Intensity data in the range of indices  $-9 \leq h \leq 9$ ,  $0 \leq k \leq 7$ , and  $0 \leq l \leq 17$  were collected

with the  $\omega$ - $2\theta$  scan technique at a scan speed of  $16^\circ/\text{minute}$  and a scan width of  $\Delta\omega = (1.50 + 0.3 \tan\theta)^\circ$ . From 1041 reflections measured to  $2\theta = 60^\circ$ , 994 unique data having  $F_0^2 \geq 3\sigma(F_0^2)$  were obtained.

Similarly, a crystal of the Rb analog with dimensions  $0.16 \times 0.10 \times 0.05$  mm was chosen. Lattice parameters were refined from 17 reflections in the range  $30^\circ < 2\theta < 43^\circ$ ; intensity data were collected with the same scan speed and width in the range of indices  $-8 \leq h \leq 8$ ,  $0 \leq k \leq 6$ , and  $0 \leq l \leq 16$ . From 791 reflections measured to  $2\theta = 55^\circ$ , 752 unique data were obtained.

Unit cell parameters were also obtained from the powders by least-squares analysis of  $2\theta$  values for 16-18 intense reflections in the range  $19^\circ < 2\theta < 55^\circ$ . Powdered Si (NBS Standard Reference Material 640b) was used as the internal standard.

### Structure Solution and Refinement

All calculations were performed on a microVax II computer with programs from the TEXRAY crystallographic software package (2). The systematic absence  $h0l, l = 2n + 1$ , is consistent with the acentric space group  $Pc$  and the centric space group  $P2/c$ . We favor the centric group  $P2/c$  because of the distribution of intensities (3) and the successful solution and refinement of the structure in this group. For the K analog, positional parameters for the K and Zn atoms were determined from the computer program MITHRIL (4) with the remaining atomic positions determined from analyses of subsequent difference electron density syntheses. The positional parameters of the atoms in the K analog were used as the trial solution for the Rb

compound.

Following refinement with isotropic thermal parameters, each set of data was corrected for absorption with the computer program DIFABS (5). Final least-squares refinement on  $F_o$  with those data having  $F_o^2 \geq 3\sigma(F_o^2)$  and anisotropic thermal parameters on each atom resulted in the residuals  $R = 0.029$  and  $R_w = 0.043$  for the compound  $KZn_4(BO_3)_3$  and  $R = 0.028$  and  $R_w = 0.039$  for the compound  $RbZn_4(BO_3)_3$ . The final difference maps contain no features greater than 0.6% of a Zn or Rb atom in the K and Rb derivatives, respectively.

## Results and Discussion

### Structure of $\text{KZn}_4(\text{BO}_3)_3$

Crystal data and atomic parameters for the compound  $\text{KZn}_4(\text{BO}_3)_3$  are listed in Table 7.1. Selected interatomic distances and angles are listed in Table 7.2. A labeled sketch of the unit cell is shown in Figure 7.1.

The structure is a new type, exhibiting a three-dimensional framework of distorted  $\text{ZnO}_4$  tetrahedra and  $\text{BO}_3$  triangles. The Zn-centered tetrahedra share vertices to form bands that extend parallel to the (100) plane (Figure 7.2). Atom B(1) shares 0 vertices with atom Zn(1) within a band while atom B(2) shares vertices with atom Zn(2) to bridge the bands. This connectivity affords large rectangular channels of approximate dimensions  $2.6 \times 5.7 \text{ \AA}$  that extend in the [010] direction (Figure 7.3). K atoms occupy these channels, binding to atoms O(4) and O(5).

The tetrahedral  $\text{ZnO}_4$  and triangular  $\text{BO}_3$  groups are metrically regular. The Zn-O bond distances average  $1.95(2) \text{ \AA}$ , a value that is similar to the value  $1.97 \text{ \AA}$  in the compound  $\text{Zn}_3(\text{BO}_3)_2$  (6) and the expected value of  $1.96 \text{ \AA}$  determined from crystal radii (7). The average B-O bond distance,  $1.38(2) \text{ \AA}$ , is typical for orthoborates discovered in this lab (8,9,10).

The K atom has been refined in the special position  $0, y, \frac{1}{4}$ ; refinement in this position affords a large thermal parameter and an irregular coordination environment. It binds to four O(5) atoms and two O(4) atoms with distances ranging from  $2.892(4) \text{ \AA}$  to  $3.221(4) \text{ \AA}$

Table 7.1 Crystal data for  $\text{KZn}_4(\text{BO}_3)_3$ .

Atom	x	y	z	$B_{\text{eq}}$		
space group P2/c, Z = 2, formula wt. 477.04 amu, $\mu = 118.01 \text{ cm}^{-1}$						
$\underline{a} = 6.876(2)$ , $\underline{b} = 4.990(1)$ , $\underline{c} = 12.574(1)$ , $\beta = 92.92(1)^\circ$						
994 unique reflections, 80 variables, R = 0.029, $R_w = 0.043$						
Atom	x	y	z	$B_{\text{eq}}$		
K	0	0.7047(4)	1/4	2.73(7)		
Zn(1)	0.48956(7)	0.6532(1)	0.12396(4)	0.87(2)		
Zn(2)	0.20828(7)	0.1649(1)	0.06022(4)	0.92(2)		
B(1)	1/2	0.160(1)	1/4	0.8(2)		
B(2)	0.1881(7)	0.346(1)	0.4507(4)	0.9(2)		
O(1)	1/2	0.8831(9)	1/4	1.2(2)		
O(2)	0.2764(5)	0.7955(7)	0.0352(3)	1.4(1)		
O(3)	0.4069(5)	0.2965(6)	0.1679(2)	1.2(1)		
O(4)	0.2591(5)	0.6068(6)	0.4351(2)	1.0(1)		
O(5)	0.0412(5)	0.2451(7)	0.3894(2)	1.4(1)		
Atom	$U_{11}$	$U_{22}$	$U_{33}$	$U_{12}$	$U_{13}$	$U_{23}$
K	0.035(1)	0.046(1)	0.0225(8)	0	-0.0049(7)	0
Zn(1)	0.0120(3)	0.0110(3)	0.0102(3)	0.0011(2)	0.0010(2)	-0.0006(2)
Zn(2)	0.0113(3)	0.0107(3)	0.0128(3)	0.0010(2)	0.0000(2)	0.0002(2)
B(1)	0.010(3)	0.006(3)	0.014(3)	0	0.003(2)	0
B(2)	0.010(2)	0.015(2)	0.012(2)	-0.003(2)	0.004(2)	0.000(2)
O(1)	0.028(2)	0.008(2)	0.009(2)	0	-0.002(2)	0
O(2)	0.020(2)	0.012(1)	0.021(2)	0.004(1)	-0.008(1)	-0.004(1)
O(3)	0.019(1)	0.009(1)	0.016(1)	-0.005(1)	-0.006(1)	0.003(1)
O(4)	0.012(1)	0.013(1)	0.012(1)	-0.003(1)	0.004(1)	0.000(1)
O(5)	0.012(1)	0.027(2)	0.013(1)	-0.006(1)	0.000(1)	-0.001(1)

From symmetry constraints  $U_{12} = U_{23} = 0$  for K, B(1), and O(1).

Table 7.2 Selected distances (Å) and angles (°) for  $\text{KZn}_4(\text{BO}_3)_3$ .

Atoms	Distance		Angle
K-0(5)	2.892(4) × 2		
K-0(4)	2.900(3) × 2		
K-0(5)	3.221(4) × 2		
Zn(1)-0(1)	1.955(3)	0(1)-Zn(1)-0(2)	104.4(1)
Zn(1)-0(2)	1.932(3)	0(1)-Zn(1)-0(3)	107.7(1)
Zn(1)-0(3)	1.957(3)	0(1)-Zn(1)-0(4)	112.7(1)
Zn(1)-0(4)	1.929(3)	0(2)-Zn(1)-0(3)	106.0(1)
		0(2)-Zn(1)-0(4)	119.3(1)
		0(3)-Zn(1)-0(4)	106.2(1)
Zn(2)-0(2)	1.932(3)	0(2)-Zn(2)-0(3)	105.2(1)
Zn(2)-0(3)	1.985(3)	0(2)-Zn(2)-0(4)	111.4(1)
Zn(2)-0(4)	1.988(3)	0(2)-Zn(2)-0(5)	119.0(2)
Zn(2)-0(5)	1.929(3)	0(3)-Zn(2)-0(4)	102.0(1)
		0(3)-Zn(2)-0(5)	107.7(1)
		0(4)-Zn(2)-0(5)	110.0(1)
B(1)-0(1)	1.380(7)	0(1)-B(1)-0(3)	119.9(3)
B(1)-0(3)	1.369(4) × 2	0(3)-B(1)-0(3)	120.1(5)
B(2)-0(2)	1.390(6)	0(2)-B(2)-0(4)	115.8(4)
B(2)-0(4)	1.408(5)	0(4)-B(2)-0(5)	121.7(4)
B(2)-0(5)	1.337(6)	0(5)-B(2)-0(2)	122.5(4)

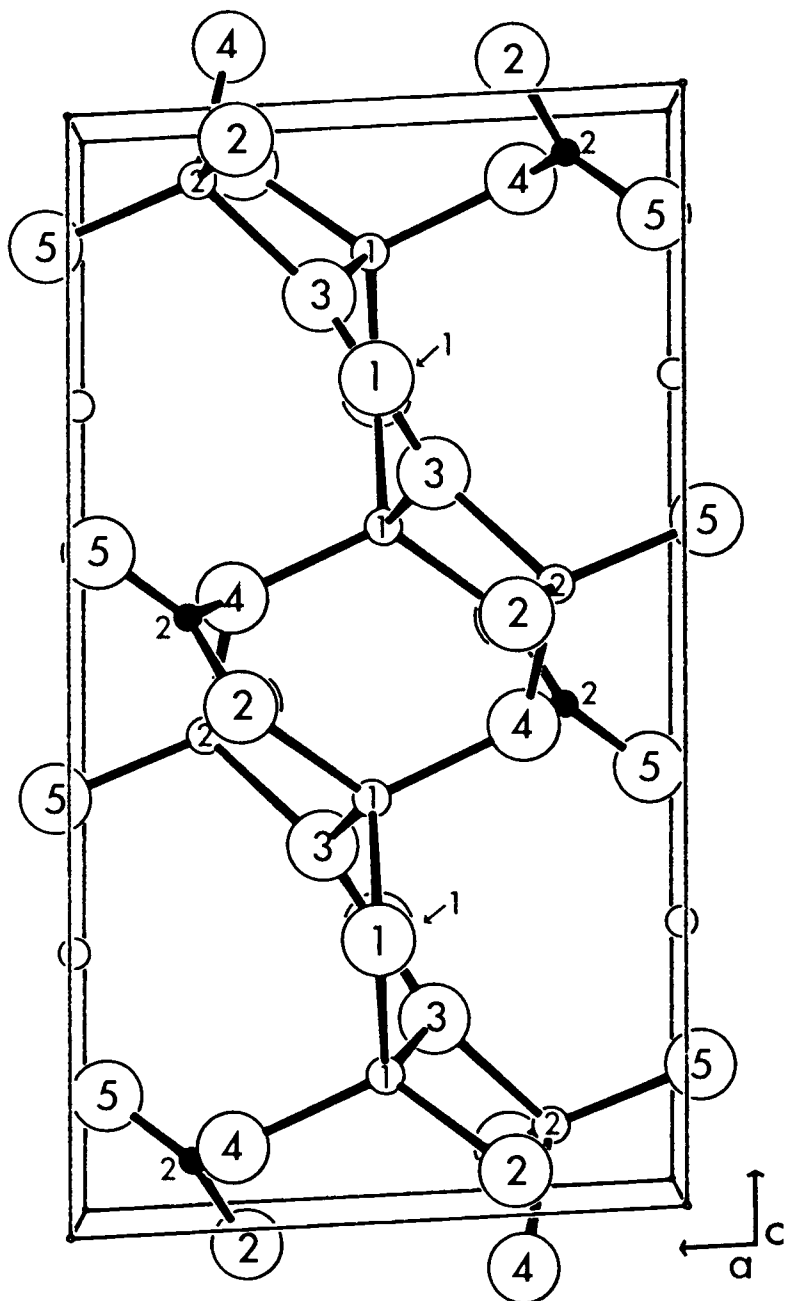


Figure 7.1 Labeled sketch of the unit cell of  $\text{KZn}_4(\text{BO}_3)_3$  viewed along the  $b$  axis.

The K atoms are drawn without bonds.

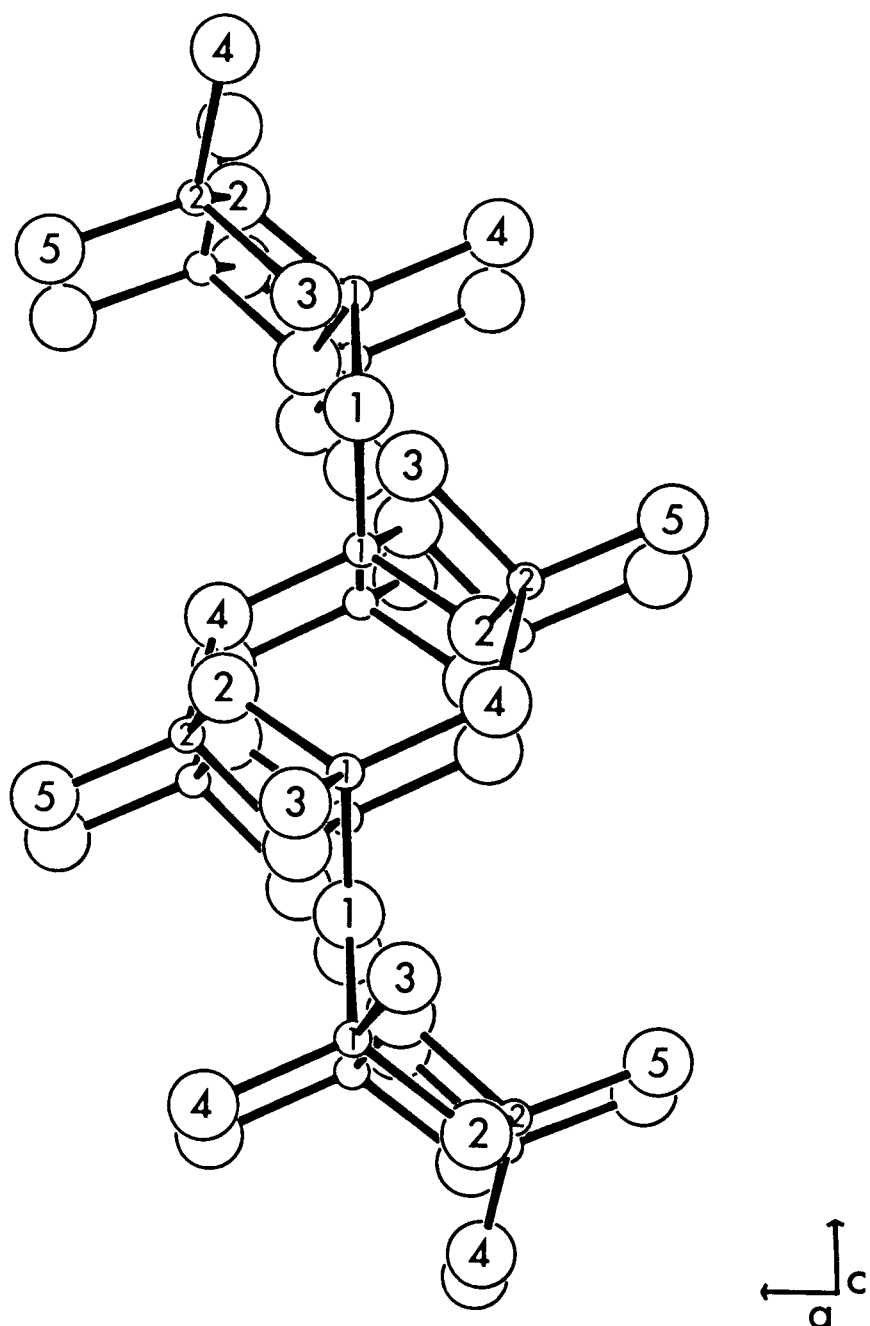


Figure 7.2 Sketch of the vertex-sharing ZnO<sub>4</sub> band extending in the b-c plane.

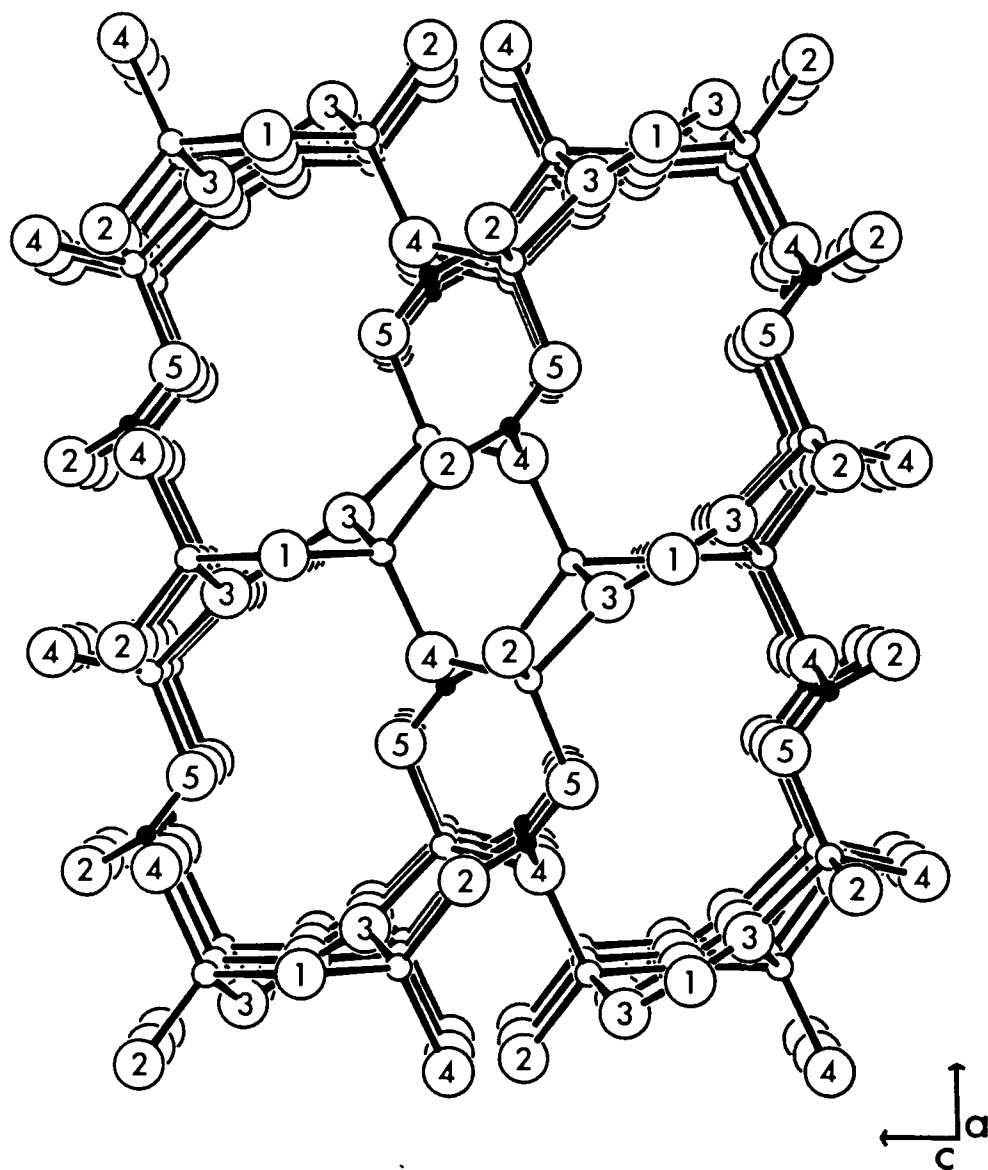


Figure 7.3 Sketch of the zinc borate network viewed along the  $b$  axis.

(Figure 7.4). From a cursory examination of the framework and consideration of the large thermal parameter, we attempted to refine the position of the K atom off the special position; all of these refinements afforded larger residuals. Additional evidence that the K atom occupies the special position may be obtained from consideration of the geometries about the O atoms.

Values of oxygen-centered angles are listed in Table 7.3. Atoms O(1), O(2), and O(3), at the periphery of the channels, are

Table 7.3 Oxygen centered angles ( $^{\circ}$ ) in  $\text{KZn}_4(\text{BO}_3)_3$ .

Atoms	Angle	Atoms	Angle
Zn(1)-O(1)-Zn(1)	108.1(2)	K-O(4)-Zn(1)	101.3(1)
Zn(1)-O(1)-B(1)	125.9(1)	K-O(4)-Zn(2)	114.4(1)
B(1)-O(1)-Zn(1)	125.9(1)	K-O(4)-B(2)	95.7(3)
		Zn(1)-O(4)-Zn(2)	115.7(2)
Zn(1)-O(2)-Zn(2)	116.1(2)	Zn(1)-O(4)-B(2)	119.2(3)
Zn(2)-O(2)-B(2)	120.6(3)	Zn(2)-O(4)-B(2)	110.1(3)
B(2)-O(2)-Zn(1)	123.0(3)		
		K-O(5)-K	109.3(1)
Zn(1)-O(3)-Zn(2)	107.9(1)	K-O(5)-Zn(2)	107.9(1)
Zn(2)-O(3)-B(1)	128.9(3)	K-O(5)-B(2)	95.7(3)
B(1)-O(3)-Zn(1)	122.4(3)	K-O(5)-Zn(2)	87.1(1)
		K-O(5)-B(2)	132.2(3)
		Zn(2)-O(5)-B(2)	123.7(3)

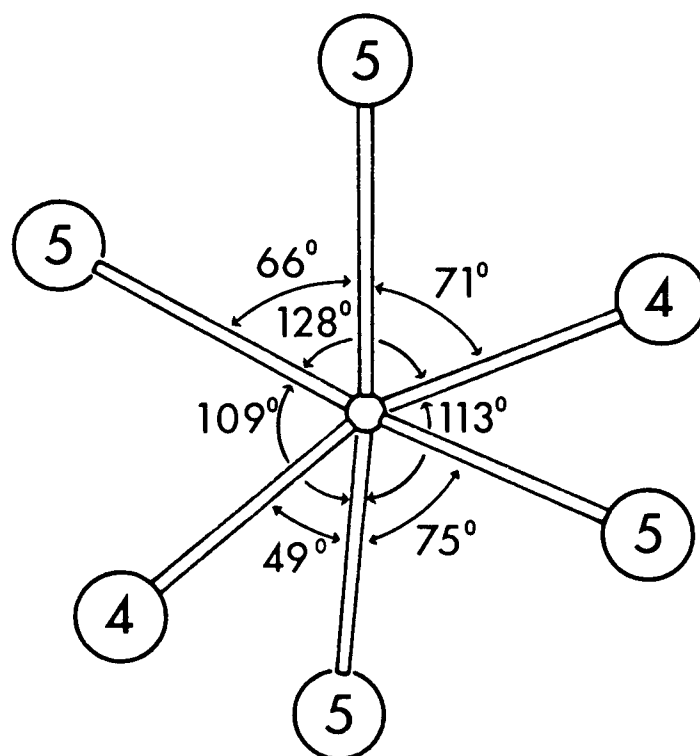


Figure 7.4 Coordination environment of K.

three-coordinate, binding only to Zn and B atoms of the framework. Each exhibits the expected trigonal bond angle of approximately  $120^\circ$ , suggesting there is no additional interaction with a K atom. Atom O(4) exhibits typical tetrahedral bond angles with bonds to the framework atoms Zn(1), Zn(2), and B(2) and the K atom. Atom O(5) bonds to only two atoms in the framework and exhibits more distorted angles that range from  $87.1(1)^\circ$  to  $132.2(3)^\circ$ . The bonding requirements of atom O(5) are satisfied by placing the K atom in the center of the channel. The framework bonds of atoms O(5) are affected by the two K-O(5) bonds; the shortest Zn-O and B-O bonds are the interactions Zn(2)-O(5) and B(2)-O(5). Because the K-O bond is highly ionic, considerable electron density is donated to the O(5) atom from the K atom. Hence, the covalent Zn(2)-O(5) and B(2)-O(5) bonds are strengthened by the availability of greater electron density.

#### Structures of $\text{RbZn}_4(\text{BO}_3)_3$ and $\text{CsZn}_4(\text{BO}_3)_3$

Crystal data for  $\text{RbZn}_4(\text{BO}_3)_3$  are listed in Table 7.4; selected bond distances and angles are listed in Table 7.5.

The Rb analog exhibits little difference from the K compound. Rb-O distances are more uniform than the K-O counterparts; values range from  $2.998(4)$  Å to  $3.159(5)$  Å in the former compared with  $2.892(4)$  Å to  $3.221(4)$  Å in the latter. The Zn-O and B-O distances and angles are statistically the same as those observed for the K analog.

Single crystals of the Cs derivative suitable for X-ray analysis could not be grown with the fluxes  $\text{PbO}$ ,  $\text{LiBO}_2$ , and  $\text{NaCl}$ . Analysis of powder X-ray diffraction patterns indicates that the Cs

Table 7.4 Crystal data for  $\text{RbZn}_4(\text{BO}_3)_3$ .

space group P2/c, Z = 2, formula wt. 523.41 amu, $\mu = 166.19 \text{ cm}^{-1}$ $\underline{a} = 6.849(2)$ , $\underline{b} = 5.000(2)$ , $\underline{c} = 12.718(2) \text{ \AA}$ , $\beta = 92.53(2)^\circ$ 752 unique reflections, 80 variables, R = 0.028, $R_w = 0.039$						
Atom	x	y	z	$B_{\text{eq}}$		
Rb	0	0.7253(2)	1/4	1.93(4)		
Zn(1)	0.4879(1)	0.6513(1)	0.12507(6)	0.89(3)		
Zn(2)	0.2089(1)	0.1666(1)	0.06101(6)	0.94(3)		
B(1)	1/2	0.156(2)	1/4	0.9(4)		
B(2)	0.192(1)	0.346(1)	0.4539(6)	1.0(3)		
O(1)	1/2	0.878(1)	1/4	1.2(2)		
O(2)	0.2758(7)	0.7977(9)	0.0383(4)	1.4(2)		
O(3)	0.4060(7)	0.2945(9)	0.1694(4)	1.2(2)		
O(4)	0.2627(6)	0.6027(8)	0.4387(3)	1.0(2)		
O(5)	0.0466(7)	0.242(1)	0.3920(4)	1.3(2)		
Atom	$U_{11}$	$U_{22}$	$U_{33}$	$U_{12}$	$U_{13}$	$U_{23}$
Rb	0.0252(5)	0.0288(6)	0.0191(5)	0	-0.0014(4)	0
Zn(1)	0.0116(4)	0.0105(4)	0.0117(4)	0.0010(3)	0.0016(3)	-0.0002(3)
Zn(2)	0.0111(4)	0.0103(4)	0.0143(4)	0.0006(3)	0.0001(3)	0.0003(3)
B(1)	0.011(5)	0.014(4)	0.009(5)	0	-0.000(4)	0
B(2)	0.013(3)	0.011(3)	0.013(3)	-0.001(3)	0.008(3)	-0.001(3)
O(1)	0.025(4)	0.008(3)	0.014(3)	0	0.004(3)	0
O(2)	0.019(2)	0.013(2)	0.018(2)	0.002(2)	-0.007(2)	-0.000(2)
O(3)	0.016(2)	0.015(2)	0.015(2)	-0.003(2)	-0.003(2)	0.003(2)
O(4)	0.013(2)	0.011(2)	0.015(2)	-0.001(2)	0.005(2)	0.001(2)
O(5)	0.008(2)	0.022(2)	0.019(2)	-0.006(2)	0.002(2)	0.001(2)

From symmetry constraints  $U_{12} = U_{23} = 0$  for Rb, B(1), and O(1).

Table 7.5 Selected distances (Å) and angles (°) for  $\text{RbZn}_4(\text{BO}_3)_3$ .

Atoms	Distance		Angle
Rb-0(5)	3.026(5) x 2		
Rb-0(4)	2.998(4) x 2		
Rb-0(5)	3.159(5) x 2		
Zn(1)-0(1)	1.950(4)	0(1)-Zn(1)-0(2)	104.5(2)
Zn(1)-0(2)	1.929(5)	0(1)-Zn(1)-0(3)	107.2(2)
Zn(1)-0(3)	1.960(5)	0(1)-Zn(1)-0(4)	114.0(1)
Zn(1)-0(4)	1.938(5)	0(2)-Zn(1)-0(3)	107.0(2)
		0(2)-Zn(1)-0(4)	117.6(2)
		0(3)-Zn(1)-0(4)	106.0(2)
Zn(2)-0(2)	1.926(5)	0(2)-Zn(2)-0(3)	104.6(2)
Zn(2)-0(3)	1.992(4)	0(2)-Zn(2)-0(4)	112.7(2)
Zn(2)-0(4)	1.985(4)	0(2)-Zn(2)-0(5)	117.6(2)
Zn(2)-0(5)	1.912(5)	0(3)-Zn(2)-0(4)	102.3(2)
		0(3)-Zn(2)-0(5)	108.8(2)
		0(4)-Zn(2)-0(5)	109.6(2)
B(1)-0(1)	1.39(1)	0(1)-B(1)-0(3)	120.2(4)
B(1)-0(3)	1.372(7) x 2	0(3)-B(1)-0(3)	119.6(8)
B(2)-0(2)	1.394(8)	0(2)-B(2)-0(4)	116.6(6)
B(2)-0(4)	1.390(8)	0(4)-B(2)-0(5)	122.0(6)
B(2)-0(5)	1.345(9)	0(5)-B(2)-0(2)	121.4(6)

derivative is isostructural to the K and Rb analogs. The powder diffractogram was indexed with a similar monoclinic cell and the parameters refined. No extraneous peaks were observed from a visual comparison of the experimental pattern with a pattern simulated from the atomic coordinates of the Rb analog (11). The ability to accommodate both the  $K^+$  and the  $Cs^+$  cations reveals the adaptability of the channels in the framework. We note, however, that we could not form the Na analog. Samples prepared using  $NaNO_3$  as a reactant and processed as described above contained  $Zn_3(BO_3)_2$  and  $ZnO$  as determined by X-ray powder analysis. The  $Na^+$  ion is apparently too small to occupy the large channels afforded by the zinc borate network, at least under the high-temperature preparative conditions.

### Unit Cell Parameters

Unit cell parameters refined from the powder data are listed in Table 7.6. Comparison of cell volumes reveals the expected expansion as the crystal radius of the alkali metal increases. The larger difference between the Cs and Rb analogs as compared with that between the Rb and K analogs reflects the greater difference in crystal radius for Rb vs. Cs as compared with K vs. Rb. Expansion of the unit cell occurs primarily from a lengthening of the c axis; in fact, the a axes of the Rb and Cs analogs are smaller than that of the K compound.

### Hydrate Formation and Ion Exchange

Ion exchange at low temperatures has long been a means to

Table 7.6 Cell parameters refined from powder data.

compound	$\underline{a}$ , Å	$\underline{b}$ , Å	$\underline{c}$ , Å	$\beta$ , °	$V$ , Å <sup>3</sup>
KZn <sub>4</sub> (BO <sub>3</sub> ) <sub>3</sub>	6.878(1)	4.989(1)	12.576(4)	92.93(2)	431.0(2)
RbZn <sub>4</sub> (BO <sub>3</sub> ) <sub>3</sub>	6.849(2)	4.999(2)	12.741(5)	92.56(3)	435.8(4)
CsZn <sub>4</sub> (BO <sub>3</sub> ) <sub>3</sub>	6.871(2)	5.019(2)	12.961(3)	92.50(3)	446.5(4)

prepare new compounds that cannot otherwise be obtained. In this manner, new oxides, oxide hydroxides, and hydrous oxides have been obtained through exchange of one cation for another, a proton, or a proton accompanied by a water molecule, respectively. For example, Li<sub>1-x</sub>H<sub>x</sub>AlO<sub>2</sub> has been reported to form when  $\alpha$ -LiAlO<sub>2</sub> is heated in benzoic acid (12). Ion exchange is common in channel or layered materials where the ions have a path for facile diffusion. To investigate the ion-exchange properties of AZn<sub>4</sub>(BO<sub>3</sub>)<sub>3</sub>, we chose to heat the K derivative in various solutions and melts of salts. Analysis of the resultant powders by X-ray diffraction provided evidence of new phases.

We first heated 2 g of KZn<sub>4</sub>(BO<sub>3</sub>)<sub>3</sub> in 150 g of benzoic acid at 140° to 170°C for 44 hours. The liquid acid was decanted and the resultant powder washed thrice with 100 mL of methanol and once with 100 mL of hot water; the powder was then dried in an oven at 135°C.

The only crystalline product was ZnO. Heating  $\text{KZn}_4(\text{BO}_3)_3$  in molten ammonium nitrate in a similar manner also afforded only ZnO.

We next attempted ion exchange in a concentrated aqueous solution by heating a 3:1 molar ratio of  $\text{NH}_4\text{NO}_3$  and  $\text{KZn}_4(\text{BO}_3)_3$  with several drops of water in a digestion bomb at  $135^\circ\text{C}$  for one day. A white powder was obtained by washing and drying the product. The product could not be identified from X-ray data of any reported anhydrous zinc borate or hydrous zinc borate. Heating this material at  $750^\circ\text{C}$  for one hour produced only  $\text{Zn}_3(\text{BO}_3)_2$  with a weight loss that was equivalent to one water molecule per formula unit of the anhydrous orthoborate. A mixture of the unknown material and ZnO was obtained by using  $\text{NaNO}_3$  instead of  $\text{NH}_4\text{NO}_3$ . Finally, heating either  $\text{KZn}_4(\text{BO}_3)_3$  or  $\text{Zn}_3(\text{BO}_3)_2$  with several drops of water in a digestion bomb at  $80^\circ\text{C}$  produces a mixture of the unknown material and ZnO, the latter being the major phase in each case. Therefore, we believe the unknown phase to be a new hydrated zinc borate. Of course, decomposition of  $\text{KZn}_4(\text{BO}_3)_3$  precludes ion-exchange reactions from occurring in heated aqueous solutions.

### Acknowledgements

This research was supported by the National Science Foundation, Solid-State Chemistry Program. DAK thanks the Alfred P. Sloan Foundation for a research fellowship (1989-1991).

### References

1. R. W. Smith and D. A. Keszler, results to be published.
2. Molecular Structure Corporation, "TEXRAY," 3200A Research Forest Drive, The Woodlands, TX 77381, USA (1985).
3. E. R. Howells, D. C. Phillips, and D. Rodgers, Acta Crystallogr. **3**, 210 (1950).
4. G. J. Gilmore, "MITHRIL: A Computer Program for the Automatic Solution of Crystal Structures from X-ray Data," University of Glasgow, Scotland (1983).
5. N. Walker and D. Stuart, Acta Crystallogr., Sect. A **24**, 214 (1968).
6. W. H. Baur and E. Tillmanns, Z. Krist. **131**, 213 (1970).
7. R. D. Shannon and C. T. Prewitt, Acta Crystallogr., Sect. B **25**, 925 (1969).
8. R. W. Smith and D. A. Keszler, J. Solid State Chem. **81**, 305 (1989).
9. R. W. Smith and D. A. Keszler, Acta Crystallogr., Sect. C, in press.
10. H. Sun and D. A. Keszler, Inorg. Chem., submitted.
11. K. Yvon, W. Jeitschko, and E. Parthe, J. Appl. Cryst. **10**, 73 (1977).
12. K. R. Poeppelmeier and D. O. Kipp, Inorg. Chem. **27**, 766 (1988).

## CHAPTER 8

THE PENTABORATE  $\text{Ba}_2\text{LiB}_5\text{O}_{10}$ 

Robert W. Smith and Douglas A. Keszler

Department of Chemistry and Center for Advanced Materials Research

Oregon State University

Gilbert Hall 153

Corvallis, Oregon 97331-4003, USA

Materials Research Bulletin 24, 725 (1989)

### Abstract

The structure of the compound  $\text{Ba}_2\text{LiB}_5\text{O}_{10}$  has been established by single-crystal X-ray methods. It crystallizes in the monoclinic space group  $P2_1/m$  in a cell of dimensions  $a = 4.414(1)$ ,  $b = 14.576(2)$ ,  $c = 6.697(2)$  Å, and  $\beta = 104.26(2)^\circ$  with  $Z = 2$ . Refinement from 2373 independent reflections affords the final residuals  $R = 0.021$  and  $R_w = 0.042$ . The structure exhibits a unique one-dimensional polyborate anion built from two crystallographically independent  $\text{BO}_3$  groups and a distinct  $\text{BO}_4$  group that share vertices. The polyanions are bridged by a Li atom occupying a distorted tetrahedral site and a Ba atom occupying an irregular eightfold coordinate site.

Materials Index: barium, lithium, borate

## Introduction

The pentaborate  $\text{Ba}_2\text{LiB}_5\text{O}_{10}$  has recently been synthesized during experiments to assess the efficacy of using the compound  $\text{LiBO}_2$  as a flux for the crystal growth of the optical frequency converter  $\beta\text{-BaB}_2\text{O}_4$  (1). A peritectic reaction between the phases  $\text{LiBO}_2$  and  $\text{BaB}_2\text{O}_4$  that occurs at  $930^\circ\text{C}$  to form the pentaborate precludes in practice the use of  $\text{LiBO}_2$  as a flux.

From an attempt to grow single crystals of a new, complex barium borate with the flux  $\text{LiBO}_2$ , we isolated several small single crystals of the compound  $\text{Ba}_2\text{LiB}_5\text{O}_{10}$ . In this report we describe the structure of this material, as determined from these crystals by X-ray diffraction.

## Experimental

Crystals of the title compound were isolated from an attempt to grow single crystals of the new pyroborate  $\text{BaCuB}_2\text{O}_5$  (2) with the flux  $\text{LiBO}_2$ . The excellent results obtained from subsequent X-ray analysis of these crystals obviated the need for the growth of additional crystals from a single-phase powder and a different flux.

A crystal with dimensions 0.20 x 0.12 x 0.10 mm was chosen for the structure determination. Unit cell parameters were derived from a least-squares analysis of 12 reflections in the range  $30^\circ < 2\theta < 42^\circ$  that were automatically centered on a Rigaku AFC6R X-ray diffractometer. Intensity data in the range of indices  $-7 \leq h \leq 7$ ,  $0 \leq k \leq 26$ , and  $0 \leq l \leq 12$  were collected with the  $\omega$ - $2\theta$  scan technique at a scan speed of  $16^\circ/\text{minute}$  in  $\omega$  and a scan width  $\Delta\omega = (1.55 + 0.3 \tan\theta)^\circ$ . From the 2815 reflections measured to  $2\theta = 80^\circ$ , 2373 unique data having  $F_o^2 \geq 3\sigma(F_o^2)$  were obtained.

All calculations were performed on a microVax II computer with programs from the TEXRAY crystallographic software package. The systematic absence  $0k0$  ( $k = 2n+1$ ) indicates the centric space group  $P2_1/m$  or the acentric space group  $P2_1$ . We favor the centric group  $P2_1/m$  from the statistical distribution of intensities (3) and the statistical equivalence of the refinements in each group. The position of the Ba atom was determined from analysis of the Patterson map; B and O positions were determined from analysis of subsequent difference electron density syntheses. The Li atom was positioned from inspection of drawings of the unit cell with all other atoms in

place. The resulting Li-O bond distances and O-Li-O angles agree well with expected values (Table 8.2). Following refinement with isotropic thermal parameters the data were corrected for absorption with the computer program DIFABS. Final least-squares refinement on  $F_o$  with those data having  $F_o^2 \geq 3\sigma(F_o^2)$  and anisotropic thermal factors for each atom resulted in the residuals  $R = 0.021$  and  $R_w = 0.042$ . The largest peak in the final difference electron density map corresponds to 0.28% of a Ba atom. Crystal data and final atomic parameters are summarized in Table 8.1.

A powder sample of the pentaborate was prepared by grinding a stoichiometric ratio of  $\text{LiNO}_3$  (reagent grade, Mallinckrodt),  $\text{Ba}(\text{NO}_3)_2$  (reagent grade, Mallinckrodt), and  $\text{B}_2\text{O}_3$  (99.99%, Morton Thiokol) under hexane and then heating the mixture in an alumina crucible at  $600^\circ\text{C}$  for 24 hours; the heating was interrupted several times for additional grinding of the sample. The powder X-ray diffractogram of the product compares well to that calculated with the computer program LAZY-PULVERIX (4) and the results of the single-crystal structure analysis. An X-ray trace of the sample quenched from  $875^\circ\text{C}$  also compares well to the calculated pattern.

Thermal analysis of the powder sample was performed over the temperature range  $600^\circ\text{C}$  -  $1000^\circ\text{C}$  with a Harrop model DT-726 differential thermal analyzer. The unit is interfaced to a personal computer through a Metrabyte DAS-8 A/D converter and a Series M1000 signal conditioner. The sample and reference ( $\text{Al}_2\text{O}_3$ ) were enclosed in platinum cups.

Table 8.1 Crystal data for Ba<sub>2</sub>LiB<sub>5</sub>O<sub>10</sub>.

space group P2<sub>1</sub>/m, Z = 2, formula wt. 495.6 amu,  $\mu = 94.16 \text{ cm}^{-1}$

$\underline{a} = 4.414(1)$ ,  $\underline{b} = 14.576(2)$ ,  $\underline{c} = 6.697(2) \text{ \AA}$ ,  $\beta = 104.26(2)^\circ$

2373 unique reflections, 88 variables, R = 0.021, R<sub>w</sub> = 0.042

Atom	x	y	z	B <sub>eq</sub>		
Ba	0.33616(3)	0.41151(1)	0.19724(2)	0.753(5)		
Li	0.991(1)	1/4	0.477(1)	0.7(2)		
B(1)	0.7688(9)	1/4	0.0029(6)	0.81(9)		
B(2)	0.0492(6)	0.0794(2)	0.6782(4)	0.70(6)		
B(3)	0.5562(5)	0.3363(2)	0.6750(4)	0.61(5)		
O(1)	0.6195(6)	1/4	0.5825(4)	0.66(6)		
O(2)	0.9506(8)	1/4	0.1941(4)	1.51(8)		
O(3)	0.1700(4)	0.4871(1)	0.8099(2)	0.85(5)		
O(4)	0.2192(4)	0.3549(1)	0.6056(3)	0.79(4)		
O(5)	0.6670(5)	0.3322(1)	0.9029(3)	0.92(4)		
O(6)	0.7225(4)	0.0867(1)	0.6020(3)	0.75(4)		

Atom	U <sub>11</sub>	U <sub>22</sub>	U <sub>33</sub>	U <sub>12</sub>	U <sub>13</sub>	U <sub>23</sub>
Ba	0.0095(1)	0.0096(1)	0.0095(1)	-0.0007(1)	0.0024(1)	-0.0003(1)
Li	0.010(2)	0.006(2)	0.012(2)	0	0.004(2)	0
B(1)	0.013(1)	0.008(1)	0.010(1)	0	0.003(1)	0
B(2)	0.0097(8)	0.0082(8)	0.0086(8)	-0.0003(6)	0.0020(6)	-0.0010(6)
B(3)	0.0072(7)	0.0068(7)	0.0093(8)	-0.0011(6)	0.0025(6)	-0.0006(6)
O(1)	0.0114(8)	0.0055(8)	0.0088(8)	0	0.0034(6)	0
O(2)	0.023(1)	0.020(1)	0.009(1)	0	-0.0041(9)	0
O(3)	0.0108(7)	0.0074(6)	0.0138(7)	-0.0014(4)	0.0023(5)	-0.0043(5)
O(4)	0.0077(5)	0.0080(6)	0.0144(6)	0.0000(4)	0.0028(5)	-0.0035(5)
O(5)	0.0181(7)	0.0072(6)	0.0082(6)	0.0014(5)	0.0007(5)	-0.0009(5)
O(6)	0.0064(6)	0.0089(6)	0.0127(7)	-0.0013(4)	0.0017(5)	-0.0012(5)

From symmetry constraints  $U_{12} = U_{23} = 0$  for atoms Li, B(1), O(1), and O(2).

## Discussion

Selected interatomic distances and angles are listed in Table 8.2. A drawing of the structure is provided in Figure 8.1.

The structure is a new type, exhibiting a one-dimensional polyborate anion  $[B_5O_{10}]^{5-}$  that extends in the [100] direction. The anion is comprised of two crystallographically independent trigonal  $BO_3$  groups approximately centered by atoms B(1) and B(2) and one distinct tetrahedral  $BO_4$  group. A double strand of alternating  $BO_3$  and  $BO_4$  groups sharing vertices results from the sharing of atom O(1) by adjoining tetrahedral groups (Figure 8.2). The apices of the tetrahedra, O(5), are further bridged by the additional  $BO_3$  group centered by atom B(1) to complete the anion (Figure 8.3). As seen from inspection of Table 8.2, the anion is metrically quite regular. The average B-O distance, 1.37(2) Å, in the trigonal  $BO_3$  groups compares to the expected value, 1.365 Å; likewise, the average B-O distance, 1.48(1) Å, in the tetrahedral  $BO_4$  group compares to the expected value, 1.475 Å (5).

The chains are interconnected by a Li atom in a distorted tetrahedral site and a Ba atom located in an irregular eight-coordinate site. The vertices of the Li-centered tetrahedron derive from three atoms O(1) and O(4)  $\times$  2 on one chain and the apex atom O(2) of the bridging  $BO_3$  group on another chain (Figure 8.3). The average Li-O distance, 1.91(2) Å, compares with that, 1.95 Å, calculated from crystal radii (6). The eight O atoms about the Ba atom are positioned over the range of distances 2.644(2) - 3.020(2) Å.

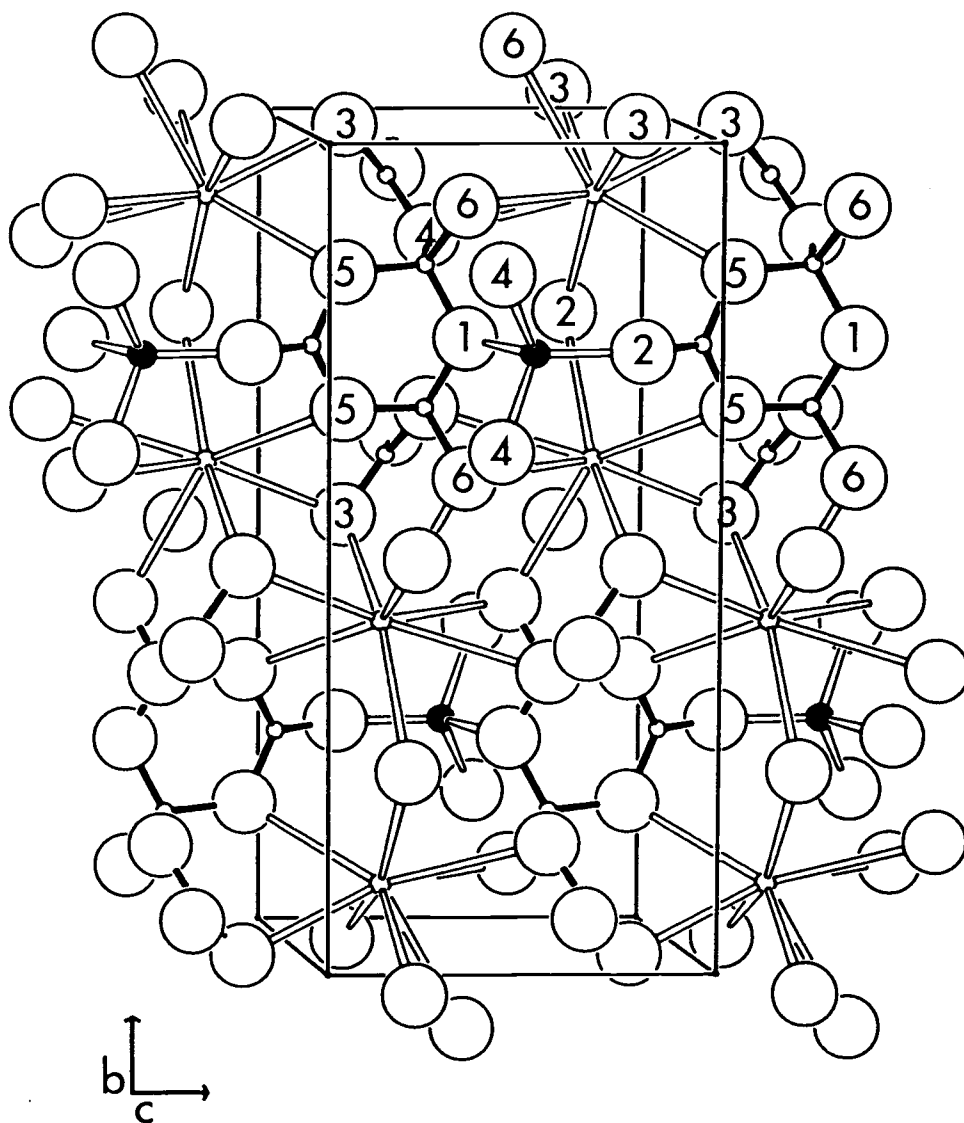


Figure 8.1 Drawing of the structure of  $\text{Ba}_2\text{LiB}_5\text{O}_{10}$ .  
The largest open circles represent O atoms  
and the filled circles represent Li atoms.  
B-O interactions are designated by shaded bonds.

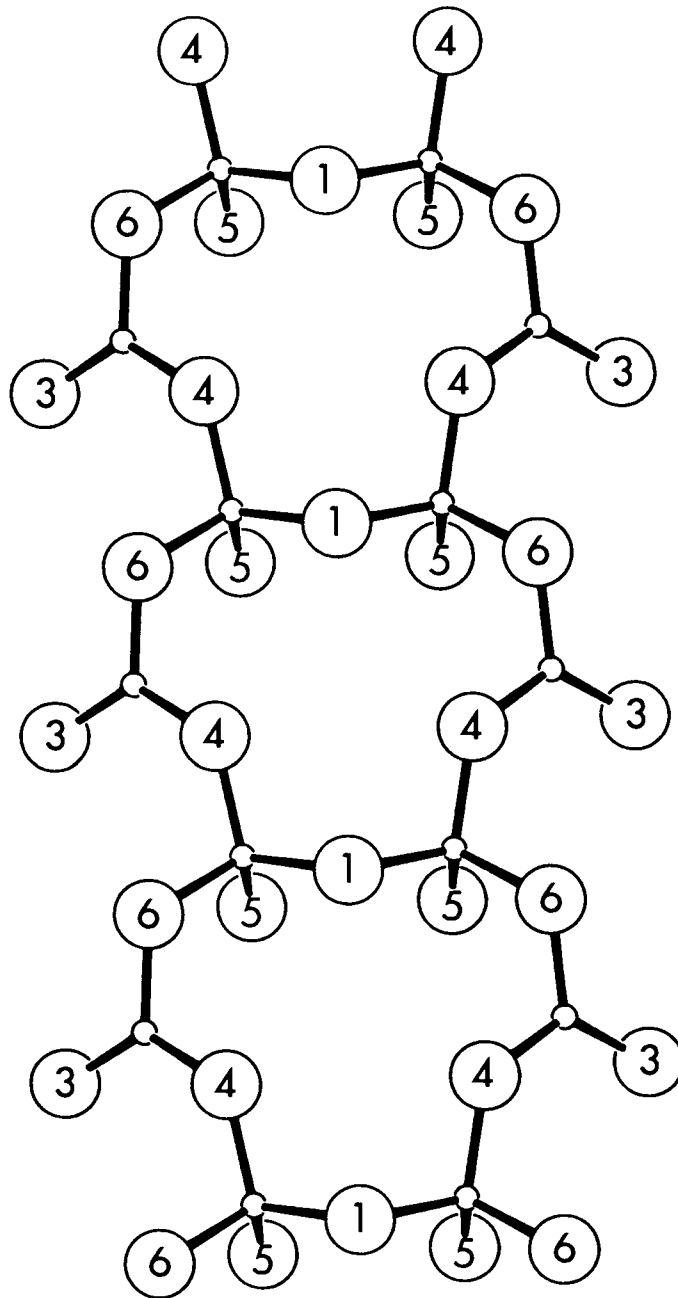


Figure 8.2 Double strands of  $BO_3$  and  $BO_4$  groups in the anion  $[B_5O_{10}]^{5-}$ .

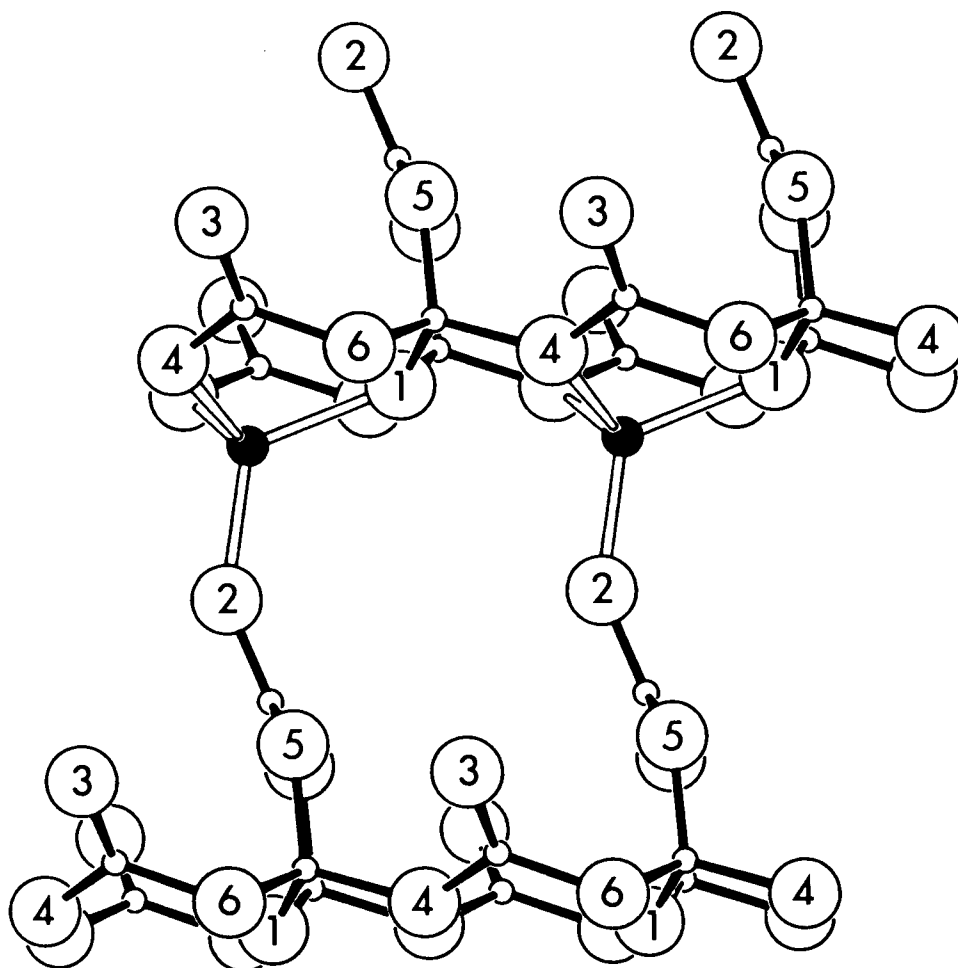


Figure 8.3 The polyanion  $[B_5O_{10}]^{5-}$   
bridged by Li atoms.

Table 8.2 Selected distances (Å) and angles (°) for Ba<sub>2</sub>LiB<sub>5</sub>O<sub>10</sub>.

Atoms	Distance		Angle
Li-0(1)	1.939(7)	0(1)-Li-0(2)	119.7(4)
Li-0(2)	1.856(7)	0(2)-Li-0(4)	111.5(2)
Li-0(4)	1.917(4) × 2	0(4)-Li-0(4)	105.8(3)
Ba-0(3)	2.644(2)	0(3)-Ba-0(3)	77.8(1)
Ba-0(3)	2.669(2)	0(3)-Ba-0(6)	50.0(1)
Ba-0(3)	2.746(2)	0(3)-Ba-0(2)	107.4(1)
Ba-0(6)	2.825(2)	0(6)-Ba-0(2)	103.2(1)
Ba-0(2)	2.902(2)	0(2)-Ba-0(5)	93.6(1)
Ba-0(6)	2.927(2)	0(6)-Ba-0(3)	92.9(1)
Ba-0(5)	2.962(2)	0(5)-Ba-0(3)	70.2(1)
Ba-0(4)	3.020(2)	0(4)-Ba-0(6)	48.0(1)
B(1)-0(2)	1.333(5)	0(2)-B(1)-0(5)	120.5(2)
B(1)-0(5)	1.392(3) × 2	0(5)-B(1)-0(5)	118.9(3)
B(2)-0(3)	1.330(3)	0(3)-B(2)-0(4)	125.2(2)
B(2)-0(4)	1.377(3)	0(4)-B(2)-0(6)	114.7(2)
B(2)-0(6)	1.411(3)	0(6)-B(2)-0(3)	120.1(2)
B(3)-0(1)	1.460(3)	0(1)-B(3)-0(4)	108.0(2)
B(3)-0(4)	1.470(3)	0(4)-B(3)-0(5)	112.6(2)
B(3)-0(5)	1.485(3)	0(5)-B(3)-0(6)	107.7(2)
B(3)-0(6)	1.488(3)	0(6)-B(3)-0(1)	110.4(2)

The average Ba-O distance, 2.84(5) Å, is somewhat longer than those, 2.79 Å and 2.80 Å, observed for the eight-coordinate Ba sites in  $\text{Ba}_2\text{Cu}(\text{BO}_3)_2$  (7) and that, 2.80 Å, predicted from crystal radii. The long Ba-O distances and their irregularity certainly contribute to the thermal instability of the material.

The compound may be classified as a metaborate from consideration of the formula as  $\text{Ba}_2\text{Li}(\text{BO}_2)_5$ . Such a classification, however, provides no information on the structural aspects of the polyborate ion  $[\text{BO}_2]_n^{n-}$ . The great structural diversity associated with this notation may be readily appreciated by considering the presence of one-dimensional chains of vertex-sharing  $\text{BO}_3$  groups in the compounds  $\text{LiBO}_2$ -I (8) and  $\text{Ca}(\text{BO}_2)_2$ -I (9), boroxine rings  $(\text{B}_3\text{O}_6)^{3-}$  in the compound  $\text{Ba}(\text{BO}_2)_2$  (10), and a network of tetrahedral  $\text{BO}_4$  groups in the compound  $\text{LiBO}_2$ -II (11). And in compounds isostructural to the meta- (penta-) borate  $\text{SmCo}(\text{BO}_2)_5$  the polyborate anion is built from three independent  $\text{BO}_4$  groups and two independent  $\text{BO}_3$  groups that condense by sharing only vertices to form a two-dimensional sheet (12,13).

Huang *et al.* reported the discovery of the title compound from an analysis of the phase line  $\text{BaB}_2\text{O}_4$ - $\text{LiBO}_2$  (1); they also reported for it a peritectic temperature of 930(2)°C. This decomposition point is in agreement with the value, 930(5)°C, that we obtain from analysis of our DTA data. They, however, indexed the powder X-ray diffraction pattern of the phase with an orthorhombic cell of dimensions  $\underline{a} = 13.033$ ,  $\underline{b} = 14.360$ , and  $\underline{c} = 4.246$  Å. Analysis of their reported X-ray data indicates that application of a zero-point

adjustment of  $+0.05^\circ$  in  $2\theta$  (for Cu  $K\alpha$  radiation) affords complete agreement with the lattice parameters reported here.

We attempted to prepare the Sr analog of the pentaborate by heating a mixture of the reagents  $\text{Sr}(\text{NO}_3)_2$ ,  $\text{LiNO}_3$ , and  $\text{B}_2\text{O}_3$  and by heating the precipitates formed by addition of oxalate to an aqueous solution of the nitrates and  $\text{B}_2\text{O}_3$ . The products of each synthesis as determined from powder X-ray diffraction are the compounds  $\text{SrB}_2\text{O}_4$  and  $\text{LiBO}_2$ . This result is consistent with the smaller crystal radius of the Sr atom as compared with the Ba atom and its inability to support the large eightfold site at high temperatures.

### Acknowledgements

This research was supported by the US Department of Energy and Lawrence Livermore National Laboratory under contract no. 2143103.

## References

1. Q. Huang, G. Wang, and J. Liang, Acta Phys. Sinica **33**, 76 (1984).
2. R. W. Smith and D. A. Keszler, results to be published.
3. E. R. Howells, D. C. Phillips, and D. Rodgers, Acta Crystallogr. **3**, 210 (1950).
4. K. Yvon, W. Jeitschko, and E. Parthe, J. Appl. Cryst. **10**, 73 (1977).
5. A. F. Wells, "Structural Inorganic Chemistry, 4th ed.," p. 862, Clarendon Press, Oxford (1975).
6. R. D. Shannon and C. T. Prewitt, Acta Crystallogr., Sect. B **25**, 925 (1969).
7. R. W. Smith and D. A. Keszler, Acta Crystallogr., Sect. C , in press.
8. A. Kirfel, G. Will, and R. F. Stewart, Acta Crystallogr., Sect. B **39**, 175 (1983).
9. M. Marezio, H. A. Plettinger, and W. H. Zachariasen, Acta Crystallogr. **16**, 390 (1963).
10. D. Eimerl, L. Davis, S. P. Velsko, E. K. Graham, and A. Zalkin, J. Appl. Phys. **62**, 1968 (1987).
11. M. Marezio and J. P. Remeika, J. Chem. Phys. **44**, 749 (1966).
12. B. Saubat, M. Vlasse, and C. Fouassier, J. Solid State Chem. **34**, 271 (1980).
13. G. K. Abdullaev, Kh. S. Mamedov, and O. Aliev, Zh. Neorgan. Khim. **25**, 364 (1980).

## BIBLIOGRAPHY

- G. K. Abdullaev, Kh. S. Mamedov, and O. Aliev, Zh. Neorgan. Khim. **25**, 364 (1980).
- G. K. Abdullaev, P. F. Rza-Zade, and Kh. S. Mamedov, Zh. Neorgan. Khim. **27**, 1037 (1982).
- A. B. Anderson and R. Hoffmann, J. Am. Chem. Soc. **98**, 7240 (1976).
- S. P. S. Andrew, "Catalyst Handbook," Wolfe Scientific Texts, New York (1970).
- K. Aoki, N. Nagano, and Y. Iitaka, Acta Crystallogr., Sect. B **27**, 11 (1971).
- M. Arjomand and D. J. Machin, J. Chem. Soc., Dalton Trans., 1061 (1975).
- W. H. Baur and E. Tillmanns, Z. Krist. **131**, 213 (1970).
- J. G. Bednorz and K. A. Müller, Z. Phys. B **64**, 189 (1986).
- H. Behm, Acta Crystallogr., Sect. B **38**, 2781 (1982).
- S. V. Berger, Acta Chem. Scand. **4**, 1054 (1950).
- S. Block, G. Burley, A. Perloff, and R. D. Mason Jr., J. Res. Nat. Bur. Stand. **62**, 95 (1959).
- E. A. Boudreaux and L. N. Mulay, "Theory and Applications of Molecular Paramagnetism," Wiley, New York (1976).
- O. A. Chaltykyan, "Copper Catalytic Reactions," Consultants Bureau, New York (1966).
- C. Chen, Y. Fan, R. C. Eckardt, and R. L. Byer, SPIE Laser and Non-linear Optical Materials **681**, 12 (1986).
- C. Chen and G. Liu, Ann. Rev. Mater. Sci. **16**, 203 (1986).
- C. Chen, B. Wu, A. Jiang, and G. You, Sci. Sin. B **28**, 235 (1985).
- C. Chen, B. Wu, A. Jiang, Y. Wu, R. Li et al., Nonlinear Opt. Mat. Symp., Boston (1985).
- G. C. Chinchin, P. J. Denny, J. R. Jennings, M. S. Spencer, and K. C. Waugh, Appl. Catal. **36**, 1 (1988).

- G. C. Chinchin, P. J. Denny, D. G. Porter, G. D. Short, M. S. Spencer, K. C. Waugh, and D. A. Whan, Prepr. Pap.-Am. Chem. Soc., Div. Fuel Chem. **29**, 178 (1984).
- C. F. Dewey Jr., Appl. Phys. Lett. **26**, 714 (1975).
- D. Eimerl, L. Davis, S. P. Velsko, E. K. Graham, and A. Zalkin, J. Appl. Phys. **62**, 1968 (1987).
- A. Farrand, A. K. Gregson, B. W. Skelton, and A. H. White, Aust. J. Chem. **33**, 431 (1980).
- S. Garcia-Blanco and S. Block, Z. Krist. **127**, 145 (1968).
- G. J. Gilmore, "MITHRIL: A Computer Program for the Automatic Solution of Crystal Structures from X-Ray Data," University of Glasgow, Scotland (1983).
- R. M. Hazen, L. W. Finger, R. J. Angel, C. T. Prewitt, N. L. Ross, C. G. Hadidacos, P. J. Heaney, D. R. Veblen, Z. Z. Sheng, A. El Ali, and A. M. Hermann, Phys. Rev. Lett. **60**, 1657 (1988).
- P. C. Healy and A. H. White, J. Chem. Soc., Dalton Trans., 1913 (1972).
- G. Heller, Topics in Current Chemistry **131**, 39 (1986).
- E. R. Howells, D. C. Phillips, and D. Rodgers, Acta Crystallogr. **3**, 210 (1950).
- Q. Huang, G. Wang, and J. Liang, Acta Phys. Sinica **33**, 76 (1984).
- I. L. Karle and J. Karle, Acta Crystallogr. **17**, 835 (1964).
- D. A. Keszler and H. Sun, Acta Crystallogr., Sect. C **44**, 1505 (1988).
- A. Kirfel, G. Will, and R. F. Stewart, Acta Crystallogr., Sect. B **39**, 175 (1983).
- V. H. König and R. Hoppe, Z. Anorg. Allg. Chem. **439**, 71 (1978).
- H. P. Klug and L. E. Alexander, "X-Ray Diffraction Procedures," Wiley, New York (1974).
- J. Krogh-Moe, Acta Chem. Scand. **18**, 2055 (1964).
- N. I. Leonyuk and A. A. Filimonov, Krist. Tech. **9**, 63 (1974).

- M. Marezio, H. A. Plettinger, and W. H. Zachariasen, Acta Crystallogr. **16**, 390 (1963).
- M. Marezio and J. P. Remeika, J. Chem. Phys. **44**, 749 (1966).
- M. Martinez-Ripoll, S. Martinez-Carrera, and S. Garcia-Blanco, Acta Crystallogr., Sect. B **27**, 672 (1971).
- M. Martinez-Ripoll, S. Martinez-Carrera, and S. Garcia-Blanco, Acta Crystallogr., Sect. B **27**, 677 (1971).
- S. K. Mazumdar and R. Srinivasan, Z. Krist. **123**, 186 (1966).
- S. K. Mazumdar, K. Venkatesan, H. -C. Mez, and J. Donohue, Z. Krist. **130**, 328 (1969).
- Molecular Structure Corporation, "TEXRAY," 3200A Research Forest Drive, The Woodlands, TX 77381, USA (1985).
- S. B. Monaco, L. E. Davis, S. P. Velsko, F. T. Wang, and A. Zalkin, J. Cryst. Growth **85**, 252 (1987).
- G. Moretti, G. Fierro, M. Lo Jacano, and P. Porta, Surface and Interface Analysis **14**, 325 (1989).
- A. Mosset, J. -J. Bonnet, and J. Galy, Z. Krist. **148**, 165 (1978).
- L. N. Mulay and E. A. Boudreaux, "Theory and Applications of Molecular Diamagnetism," Wiley, New York (1976).
- E. Otsuka, T. Takahashi, N. Hashimoto, and F. Matsuda, Chem. Econ. Eng. Rev. **7** (4), 29 (1975).
- A. Pabst, Am. Mineral. **59**, 353 (1974).
- A. Perloff and S. Block, Acta Crystallogr. **20**, 274 (1966).
- G. Petrini, A. Bossi, and F. Garbassi, Studies in Surface Science and Catalysis **16**, 735 (1983).
- K. R. Poepeimeier and D. O. Kipp, Inorg. Chem. **27**, 766 (1988).
- L. Richter and F. Müller, Z. Anorg. Allg. Chem. **467**, 123 (1980).
- B. Saubat, M. Vlasse, and C. Fouassier, J. Solid State Chem. **34**, 271 (1980).
- K. I. Schaffers and D. A. Keszler, J. Solid State Chem., submitted.

- R. D. Shannon and C. T. Prewitt, Acta Crystallogr., Sect. B 25, 925 (1969).
- G. M. Sheldrick, "Crystallographic Computing 3," Eds. G. M. Sheldrick, C. Krüger, and R. Goddard, pp.175-189, Oxford University Press, Oxford (1985).
- Z. Z. Sheng and A. M. Hermann, Nature 332, 55 (1988).
- R. W. Smith and D. A. Keszler, J. Solid State Chem. 81, 305 (1989).
- R. W. Smith and D. A. Keszler, Acta Crystallogr., Sect. C, in press.  
Stauffer Chemical Company, British Patent 1,306,191.
- R. H. Summerville and R. Hoffmann, J. Chem. Phys. 60, 4271 (1974).
- H. Sun and D. A. Keszler, Inorg. Chem., submitted.
- C. L. Teske and H. Müller-Buschbaum, Z. Anorg. Allg. Chem. 371, 325 (1969).
- C. L. Teske and H. Müller-Buschbaum, Z. Anorg. Allg. Chem. 379, 234 (1970).
- P. D. Thompson and D. A. Keszler, Solid State Ionics 32/33, 521 (1989).
- C. C. Torardi, M. A. Subramanian, J. C. Calabrese, J. Gopalakrishnan, K. J. Morrissey, T. R. Askew, R. B. Flippen, U. Chowdhry, and A. W. Sleight, Science 240, 631 (1988).
- J. M. P. J. Verstegen, J. Electrochem. Soc. 121, 1631 (1974).
- N. Walker and D. Stuart, Acta Crystallogr., Sect. A 24, 214 (1968).
- A. F. Wells, "Structural Inorganic Chemistry, 4th ed.," Clarendon Press, Oxford (1975).
- D. J. Williams, Angew. Chem. Int. Ed. Eng. 23, 690 (1984).
- M. K. Wu, J. R. Ashburn, C. J. Torng, P. H. Hor, R. L. Meng, L. Gao, Z. J. Huang, Y. Q. Wang, and C. W. Chu, Phys. Rev. Lett. 58, 908 (1987).
- D. Xu, M. Tiang, and Z. Tan, Acta Chim. Sinica 2, 230 (1983).
- D. J. C. Yates, N. E. Zlotin, and J. A. McHenry, J. Catal. 117, 290 (1989).

X. Yin, Q. Huang, S. Ye, S. Lei, and C. Chen, Huaxue Xuebao 43 (9), 822 (1985).

K. Yvon, W. Jeitschko, and E. Parthe, J. Appl. Cryst. 10, 73 (1977).

W. H. Zachariasen, Acta Crystallogr., Sect. A 24, 214 (1968).

A. Zalkin, D. Eimerl, and S. P. Velsko, Acta Crystallogr., Sect. C 45, 812 (1989).

A. Zletz, US Patent Application 709, 790, 11 March 1985.

## APPENDIX

## APPENDIX A

## MOLECULAR ORBITALS OF THE ORTHOBORATE AND PYROBORATE ANIONS

MO of the  $[\text{BO}_3]^{3-}$  Anion

To fully appreciate the bonding characteristics of the simple trigonal-planar orthoborate anion,  $[\text{BO}_3]^{3-}$ , it is necessary to construct the molecular energy level diagram. From this diagram we can describe both the symmetry and energy levels of bonding, antibonding, and nonbonding electron pairs. Nonbonding electron pairs are important because they are available for bonding to associated cations in the three-dimensional crystal structure. The calculations reported in this appendix were done by the extended Hückel method using the parameters given in Table A.1 (1,2). Mulliken symbols and energy levels for the calculated molecular orbitals are listed in Table A.2.

Each orthoborate anion contains 24 electrons derived from the valence atomic orbitals of the constituent atoms and the three electrons from the anionic charge. The Lewis dot structure of the orthoborate anion consists of three  $\sigma$  bonds, one  $\pi$  bond, and eight lone electron pairs. Molecular orbital calculations reveal essentially the same electronic configuration. Drawings of selected molecular orbitals are shown in Figure A.1. The three  $\sigma$  bonds are associated with the lowest energy orbitals,  $A'_1$  and  $E'$ , the  $\pi$  bond is the  $A''_2$  orbital, and the remaining orbitals may be associated with lone

Table A.1 Extended Hückel parameters.

	$\chi_{\mu}$	$\zeta_{\mu}$	$H_{\mu\mu}$ , eV
B	2s	1.3	-15.5
	2p	1.3	-8.5
O	2s	2.275	-32.3
	2p	2.275	-14.8

Table A.2 Molecular orbital energies (eV).

MO	Energy	MO	Energy
$A_1'$	-34.750	$E'$	-32.859
$A_1'$	-15.832	$A_2''$	-15.435
$E'$	-15.226	$E''$	-14.748
$A_2'$	-14.544	$E'$	-14.521
$A_2''$	-5.587	$A_1'$	22.237
$E'$	26.742		

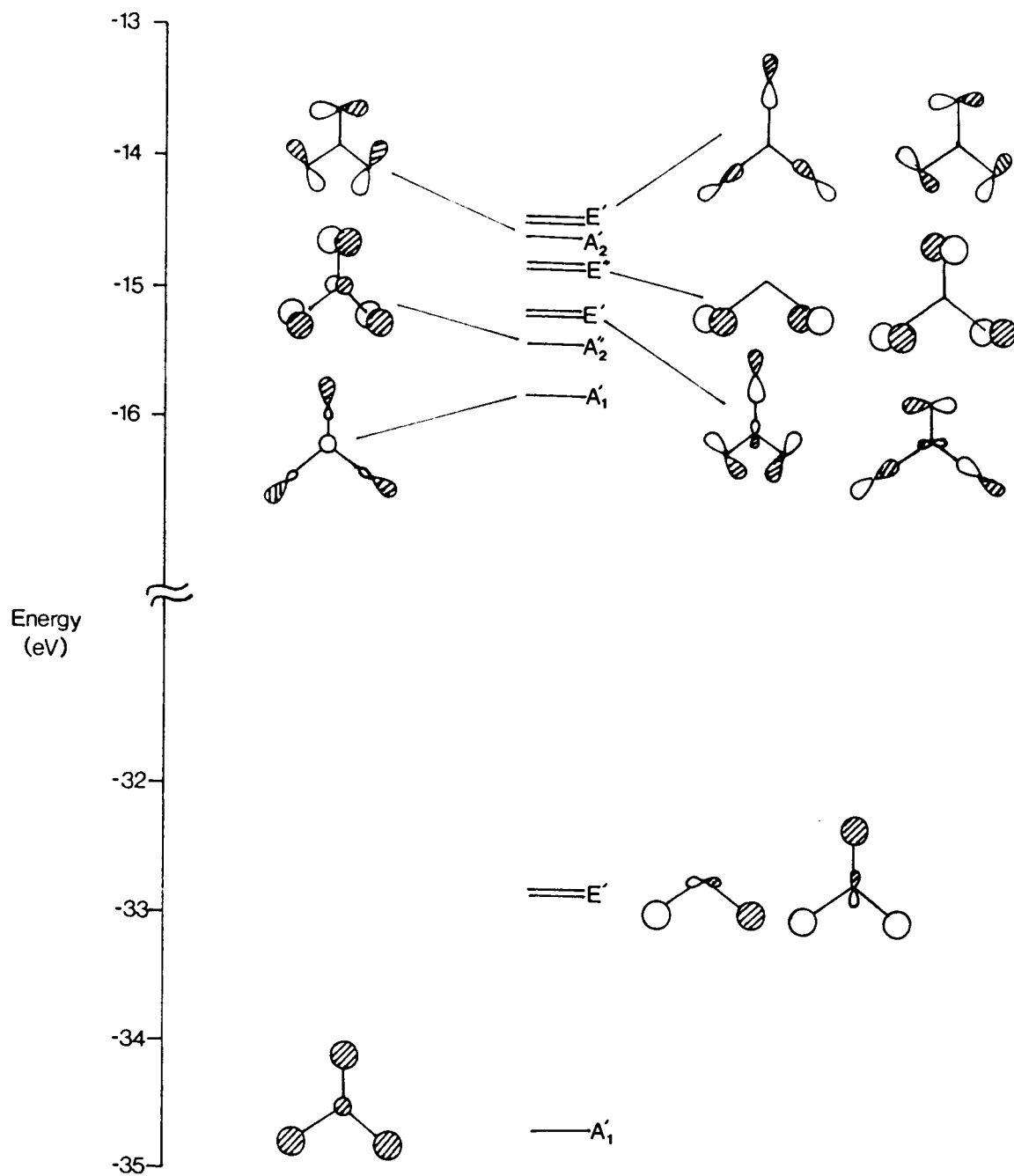


Figure A.1 Energy level diagram for the orthoborate anion.

electron pairs. The lone pairs are identified by the electron density that is directed outward from the oxygen vertices. The HOMO is an  $E'$  MO, which corresponds to a lone pair, though association with cations in a crystal structure would significantly lower the energies of all the nonbonding levels and leave the  $A_2'' \pi$  level as the HOMO. The LUMO (not shown in Figure A.1) is the  $A_2'' \pi^*$  MO at -5.587 eV. This results in a HOMO-LUMO gap of approximately 9 eV; consequently, orthoborates are expected to be electrical insulators.

The  $\sigma$  bonds are primarily of oxygen 2s character as expected by the relative energies of the oxygen and boron 2s energy levels and by the electronegativity differences of the two atoms. While the orthoborate anion is nonpolar, having  $D_{3h}$  symmetry, its individual bonds are polar with the negative charge directed toward the oxygen atom. Similarly, the lone electron pairs have primarily oxygen 2p character as expected from the energy levels of the constituent atomic orbitals.

#### MO of the $[B_2O_5]^{4-}$ Anion

The pyroborate anion  $[B_2O_5]^{4-}$  was known to adopt only the geometry that was described in the introduction to this work, *i.e.*, double-triangles that are oriented approximately parallel to each other. Recently, two mixed orthoborate, pyroborates  $A_2Sc_2B_4O_{11}$  where  $A = Sr$  and  $Ba$  have been discovered in this lab (3). Each compound exhibits a unique pyroborate geometry. The Sr analog displays a  $B_2O_5$  group with a B-O-B angle of  $180^\circ$  while the Ba analog displays a  $B_2O_5$  group with a twist of approximately  $75^\circ$  between the two triangular

portions of the group. Normally, the B-O-B angle and twist are similar to the values  $140^\circ$  and  $14^\circ$ , respectively, observed in the compound  $\text{Co}_2\text{B}_2\text{O}_5$  (4). In order to fully understand geometrical preferences, it is necessary to construct the correlation diagram of the pyroborate anion for its geometrical extremes.

MO energy levels were determined for each geometry from the extended Hückel calculations of the type described above. Starting from the geometry in which the  $\text{B}_2\text{O}_5$  group is planar and the B-O-B angle is  $180^\circ$  ( $D_{2h}$  symmetry) the group was successively closed to afford a B-O-B angle of  $120^\circ$  ( $C_{2v}$  symmetry) then the triangles were twisted in opposite directions to afford an interplanar angle of  $90^\circ$  ( $C_2$  symmetry). MO energy levels were calculated for every  $10^\circ$  iteration.

The calculations reveal that the correlation diagram is relatively flat for all the orbitals. The energies of all orbitals change by less than 0.3 eV and the majority change by less than 0.15 eV through the entire range of investigated geometries. A portion of the correlation diagram for selected MO's is illustrated in Figure A.2.

Cursory consideration of the bonding scheme led me to believe that the  $\pi$  system delocalized through the central O atom would present a barrier to twisting the two triangular portions since delocalization of electron pairs over all the  $p_z$  orbitals would be prevented by the loss of the nodal plane orthogonal to the principal axis of the  $p_z$  orbital. (The delocalization of the  $\pi$  system is unaffected by perturbing the group from  $D_{2h}$  to  $C_{2v}$  symmetry since the

$p_z$  nodal plane would be maintained.) However, examination of Figure A.2 reveals that the  $\pi$  system MO's shown ( $B_1$  and  $A_2$ ) do not increase appreciably in energy upon reduction of symmetry from  $C_{2v}$  to  $C_2$ . The explanation for the lack of a barrier to rotation by the  $\pi$  system involves the hybridization and charge density of the central O atom. If the central O atom has no electron density (as in the  $A_2$  MO), then the  $\pi$  system is localized around the periphery of the  $B_2O_5$  group and twisting the triangular portions of the group does not disrupt the  $\pi$  system interactions. If the central O atom has significant electron density (as in the  $B_1$  MO), then reducing the symmetry from  $C_{2v}$  to  $C_2$  allows  $p_y$  orbital contributions to mix with the  $p_z$  orbitals on the central O atom; thus, the central O atom may interact with the  $\pi$  systems of both triangular portions of the  $B_2O_5$  group. Idealized sketches of the MO's for the  $B_1 \rightarrow B$  perturbation are illustrated in Figure A.3. Hence, one should not be surprised to observe a variety of geometries for the  $B_2O_5$  group as the geometry adopted will be primarily dictated by the packing and bonding requirements of the associated cations.

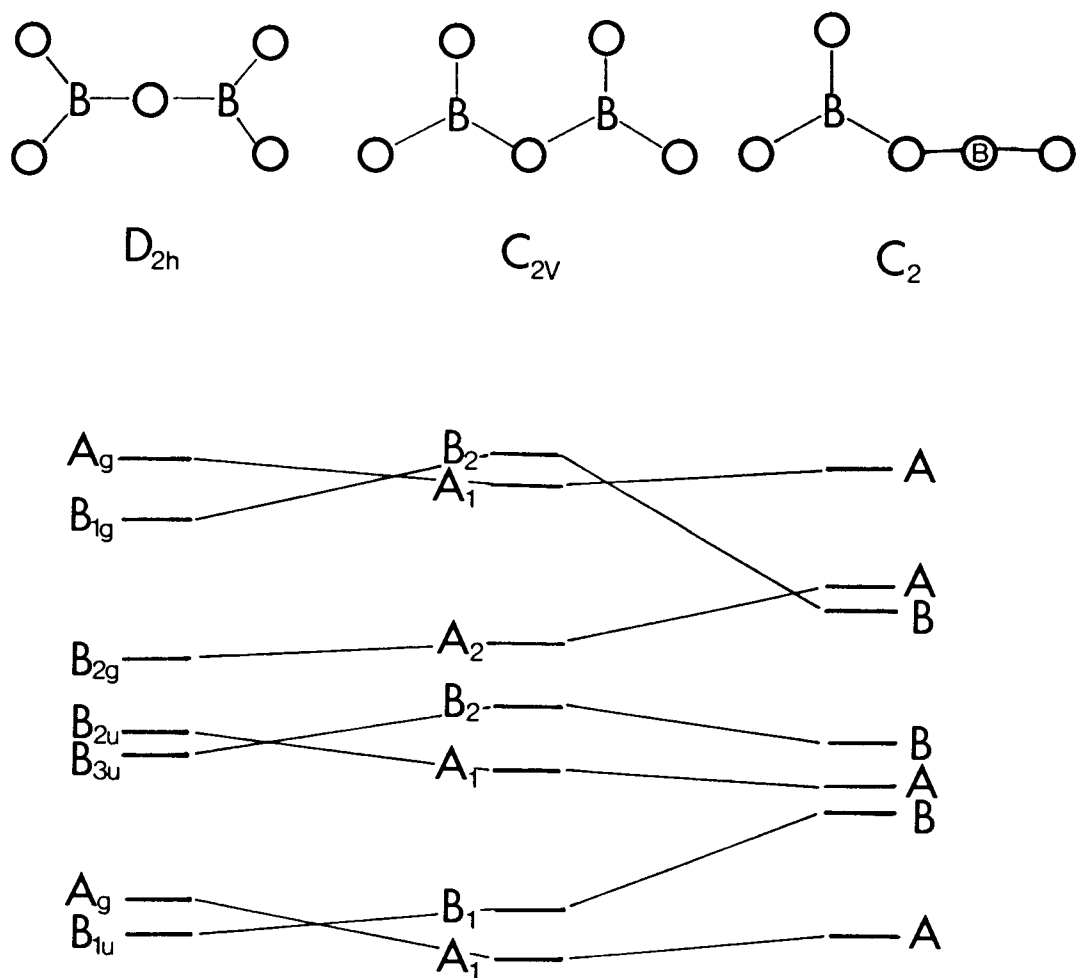


Figure A.2 Correlation diagram of selected MO's between  $D_{2h}$  (left),  $C_{2v}$  (center), and  $C_2$  (right)  $[B_2O_5]^{4-}$  geometries.

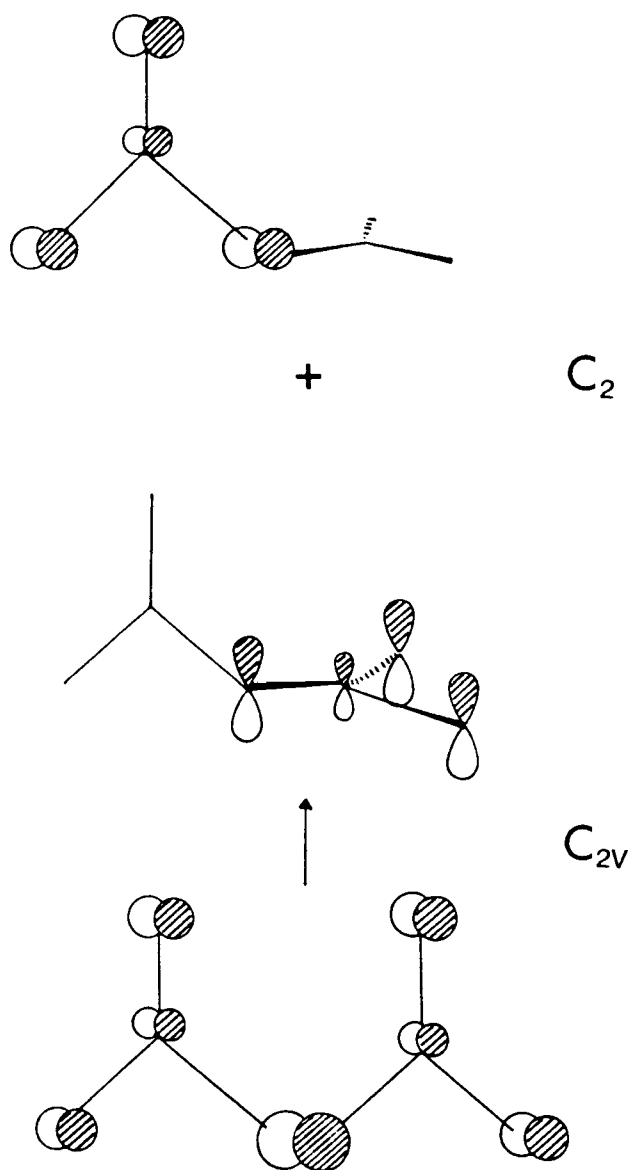


Figure A.3 Sketches of idealized  $\pi$  system MO's in  $C_{2v}$  and  $C_2$  symmetry.

### References

1. R. H. Summerville and R. Hoffmann, J. Am. Chem. Soc. **98**, 7240 (1976).
2. A. B. Anderson and R. Hoffmann, J. Chem. Phys. **60**, 4271 (1974).
3. P. D. Thompson, J. Huang, R. W. Smith, and D. A. Keszler, results to be published.
4. S. V. Berger, Acta Chem. Scand. **4**, 1054 (1950).